ADVANCED MATERIALS
www.advmat.de

Micro-Bio-Chemo-Mechanical-Systems: Micromotors, Microfluidics, and Nanozymes for Biomedical Applications

Jawayria Mujtaba, Jinrun Liu, Krishna K. Dey, Tianlong Li, Rik Chakraborty, Kailiang Xu, Denys Makarov, Roman A. Barmin, Dmitry A. Gorin, Valeri P. Tolstoy, Gaoshan Huang, Alexander A. Solovev, and Yongfeng Mei**

Wireless nano-/micromotors powered by chemical reactions and/or external fields generate motive forces, perform tasks, and significantly extend short-range dynamic responses of passive biomedical microcarriers. However, before micromotors can be translated into clinical use, several major problems, including the biocompatibility of materials, the toxicity of chemical fuels, and deep tissue imaging methods, must be solved. Nanomaterials with enzyme-like characteristics (e.g., catalase, oxidase, peroxidase, superoxide dismutase), that is, nanozymes, can significantly expand the scope of micromotors' chemical fuels. A convergence of nanozymes, micromotors, and microfluidics can lead to a paradigm shift in the fabrication of multifunctional micromotors in reasonable quantities, encapsulation of desired subsystems, and engineering of FDA-approved core–shell structures with tuneable biological, physical, chemical, and mechanical properties. Microfluidic methods are used to prepare stable bubbles/microbubbles and capsules integrating ultrasound, optoacoustic, fluorescent, and magnetic resonance imaging modalities. The aim here is to discuss an interdisciplinary approach of three independent emerging topics: micromotors, nanozymes, and microfluidics to creatively: 1) embrace new ideas, 2) think across boundaries, and 3) solve problems whose solutions are beyond the scope of a single discipline toward the development of micro-bio-chemo-mechanical-systems for diverse bioapplications.

1. Introduction

The field of micromotors has recently experienced rapid and unprecedented growth—nano-/micromotors possess remarkable physical, mechanical, chemical, and biological properties, which can offer exceptional opportunities for bioapplications.[1] Catalytic and/or externally-driven nano-/micromotors with tunable size, shapes, controllable speed, position, and propulsion modes (i.e., self-electrophoresis, self-diffusiophoresis, bubble recoil, surface tension, external fields) can be applied as wireless micromachines to perform specific tasks including biosensing,[2] delivery of cargo,[3] minimally invasive surgery,[4] capture of pathogens,[5] the isolation of cancer cells,[6] and related potential applications. For instance, thermobiochemically actuated microgrippers,[7] powered by an external magnetic field, can locally respond to capture bio-materials and even take biopsies. Today, the development of biocompatible fuels is a hot topic, including glucose,[8] urea,[9] and carbon dioxide[10] as sources of energy. Ideally, both fuels and reaction products are parts of metabolic pathways. Micromotors wirelessly steer themselves and they can significantly expand short-range dynamic stimuli responses of biomedical microcarriers.[11] Microfluidics can solve multiple challenges of micromotors for direct translation into clinical uses, including desired biocompatibility, biodegradability, bio-physicochemical

Dr. J. Mujtaba, J. Liu, Prof. K. L. Xu, Prof. G. S. Huang, Prof. A. A. Solovev, Prof. Y. F. Mei
Department of Materials Science
Fudan University
Shanghai 200433, P. R. China
E-mail: solovev@fudan.edu.cn; yfm@fudan.edu.cn

Prof. K. K. Dey, R. Chakraborty
Discipline of Physics
Indian Institute of Technology Gandhinagar
Gandhinagar, Gujarat 382355, India

Dr. T. Li
State Key Laboratory of Robotics and System
Harbin Institute of Technology
Harbin, Heilongjiang 150001, P. R. China

The ORCID identification number(s) for the author(s) of this article can be found under https://doi.org/10.1002/adma.202007465.

Prof. K. L. Xu
School of Information Science and Technology
Fudan University
Shanghai 200433, P. R. China

Dr. D. Makarov
Helmholtz-Zentrum Dresden-Rossendorf e.V.
Institute of Ion Beam Physics and Materials Research
Bautzner Landstraße 400, 01328 Dresden, Germany

R. A. Barmin, Prof. D. A. Gorin
Center of Photonics and Quantum Materials
Skolkovo Institute of Science and Technology
3 Nobelya Str, Moscow 121205, Russia

Prof. V. P. Tolstoy
Institute of Chemistry
Saint Petersburg State University
26 Universitetskii Prospect, Petergof, St. Petersburg 198504, Russia

DOI: 10.1002/adma.202007465

properties, and mass-production. Moreover, microfluidic methods used to prepare micromachines with required softness, stiffness, flexibility, and shape adaptability have triggered a high interest for in vivo and in vitro bioapplications.[12]

Enzymes are vital components of biological reactions and living organisms. Enzymes display remarkable specificity and they are capable of enhancing the rate of biochemical reaction, on some occasions nearly by 10^{12} times than that of the uncatalyzed reactions. This extraordinary phenomenon occurs due to the juxtaposition of chemically reactive groups within the binding pockets of the enzyme (active sites) and complementary groups from the substrates (the reactants), lowering the activation energy barrier and facilitating the conversion of the substrates into the reaction products. However, drawbacks of natural enzymes include rapid denaturation, difficulty in preparation, and laborious recycling. Nanozymes are catalytic nanomaterials with enzyme-like properties, tunable size, shape, structure, composition, surface area, and selective catalytic reactions responsive to temperature and external stimuli. As alternatives to natural enzymes, highly stable and low-cost "artificial enzymes",[13] have been synthesized using functional nanomaterials such as cyclodextrin, metal complexes, porphyrins, polymers, dendrimers, and other molecules.[14] The term "nanozymes" was used to describe thiol monolayer protected gold clusters, which showed RNase-like activity.[15] Ferromagnetic nanoparticles (Fe_3O_4) were reported to mimic the activity of peroxidases,[16] which paved the way for a completely new area of investigation involving design, synthesis, and applications of nanomaterials with "enzyme-like activities". As per the study, there are currently more than 200 research groups worldwide working actively on nanozymes.[14]

Drop-based microfluidics is actively used to fabricate drops/microdrops and capsules, providing capabilities for very precise mixing of fluids to form new materials, high throughput screening on the target of interest, encapsulation, and controlled release of a wide variety of active materials.[17] Microfluidics enable the preparation of microdrops, which carry out vast numbers of reactions in short times using minimal quantities of reagents. Owing to their high water content, shells of stimuli-responsive microcapsules can be made of hydrogels. Hydrogels have structures and bio-physicochemical properties similar to extracellular matrices. Capsules as "microreactors" containing an aqueous core and permeable shell possess unique properties including controllable reaction, diffusion, separation, and delivery of molecular species for water cleaning,[18] regenerative, precision,[19] targeted[20] medicine, drug/cell delivery, tissue engineering, wound dressings, and anti-tumor treatments, to name a few examples. Moreover, a gaseous core encapsulated in protein-/lipid-/polymer-shells can have programmable stability and solubility for intravenous uses. Such microbubbles can be visualized in arteries using super-resolution ultrasound (US) tissue imaging methods. At the same time, shells of microbubbles can include additional optical, magnetic, chemical, mechanical properties for theranostics.

Herein, we discuss a potential convergence of previously independent disciplines: micromotors, nanozymes, and microfluidics to develop versatile μ-BCMS (**Figure 1**), previously inspired by the micro-chemo-mechanical-systems.[21] Ultimate goals are core–shell engineering, nanozymes encapsulation, and design of power/control methods (Figure 1a–c). Subsequently, dynamic bio-microcarriers can self-propel over long distances, react/respond locally, and be tracked in tissue using state-of-the-art super-resolution imaging methods (Figure 1d–f). Such a combinatorial approach can enable a controllable reaction, separation and delivery of molecular species (e.g., using hydrogel micromotors), minimally-invasive surgery, potential clots removal from arteries, isolation of pathogens, and deactivation of cancer cells, to name a few examples. Moreover, microcarriers with stimuli-responsive dynamic properties can also respond to variations in pH,[22] temperature,[23] light,[24] electric[25] and magnetic[26] fields, leading to a subsequent release of therapeutic agents. Catalytic nanoparticles with various enzyme-like properties (e.g., peroxidase, catalase, oxidase, and superoxide dismutase) can manipulate biological pathways and open new horizons of μ-BCMS.

Many excellent reviews exist about emulsions/microemulsions, capsules, and bubble techniques.[27–29] Here, we limit our discussion to fabrication, properties, applications of catalytic micromotors, nanozymes, and core–shell structures: nanoparticle/-protein shelled microbubbles, layer-by-layer (LbL) assembly methods for the subsequent integration with tissue imaging methods and applications in theranostics. Today, the biomedical micromotors field faces challenges (toxic fuels, reaction products, difficulty to obtain biocompatible materials). Microfluidics can be used to prepare and mass-produce FDA-approved biocompatible microcarriers, which can integrate micromotors' motion control methods. Nanozymes utilize catalytic reactions, which can be applied in medicine and subsequently, discovered biocatalytic fuels could help to replace toxic fuels of nano-/micromotors. Moreover, since conventional optical microscopy (widely used in nano-/micromotors research) cannot be used to imaging micromachines in the human body—powerful super-resolution deep tissue biomedical imaging methods (e.g., ultrasound) are desperately needed. There are multiple excellent reviews already available for each of our discussed emerging topics: nanozymes,[14,30] nano-/micromotors,[2,31] and microfluidics.[32–35] By cultivating interdisciplinarity as a habit of mind, our review discusses integration or interconnectedness of these emerging topics by focusing on i) generation of new ideas, ii) discussions across disciplinary boundaries (overlap of emerging topics allows looking at the problem from a variety of viewpoints—the same questions can be asked in different ways), and iii) solutions to complex problems, which are beyond the scope of a single discipline.

2. Man-Made Micromotors

Biological nano-/micromotors like the flagellum, motor proteins, and cilia demonstrate high sophistication and efficiency—they convert chemically stored energy into highly efficient motion and perform tasks, transporting cells searching for nutrients, and delivering biomolecules to support viable cellular functions. Recent achievements in the field of synthetic nano-/micromotors led to demonstrations of autonomously and remote controlled micromachines to perform specific tasks, such as "on-the-fly" delivery and assembly of cargo,[39] detection of DNA hybridization,[40] removal/drilling of cancer cells,[41] the isolation of pathogens[6] in

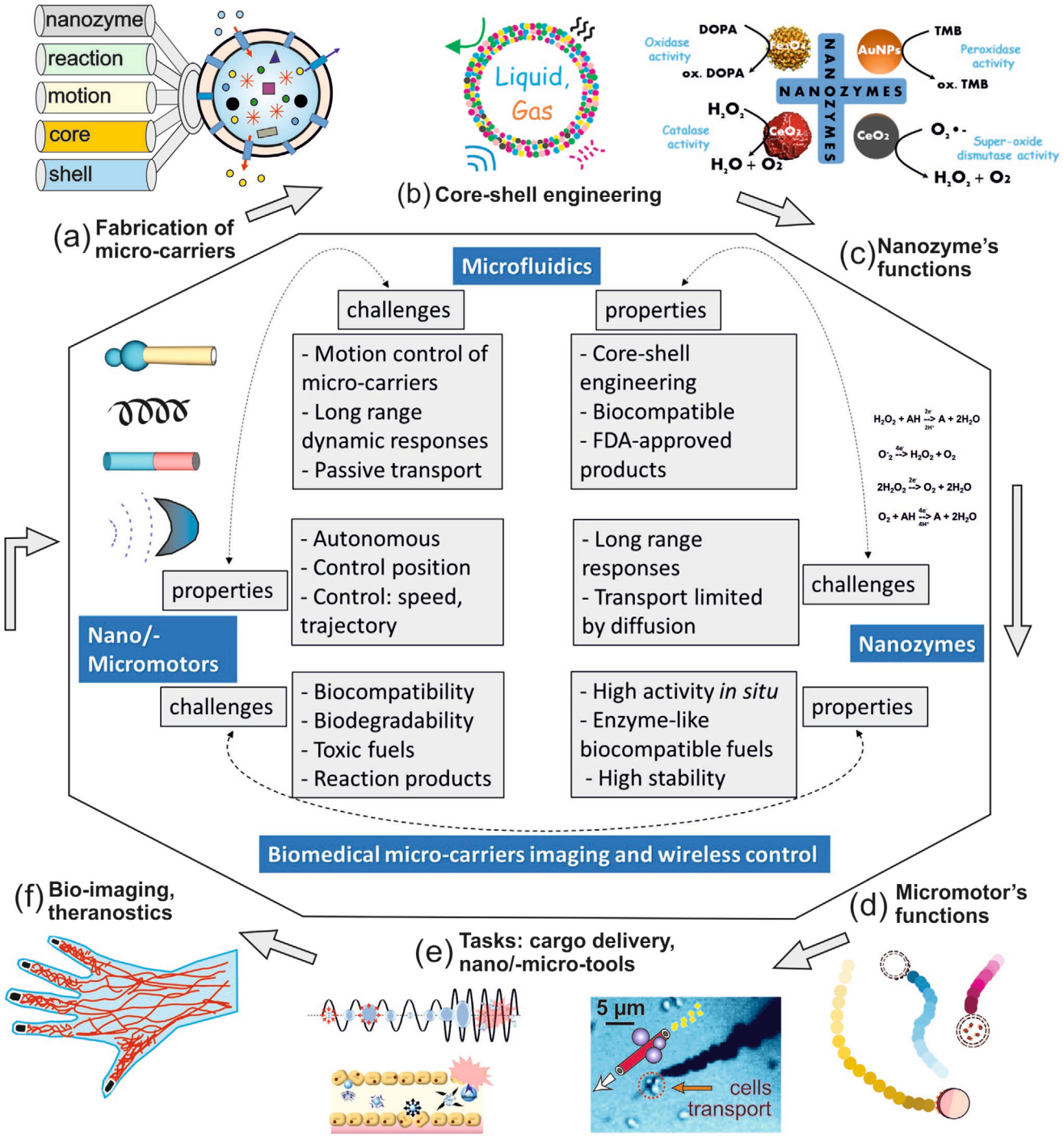

Figure 1. Integration of micromotors, nanozymes, and microfluidics toward the construction of biomedical µ-BCMS. a) Schematic image of a microfluidic generation of drops/microdrops, capsules, and bubbles with controllable shell, core, catalytic, and dynamic motive functions. b) Core–shell engineering includes the desired fabrication of gaseous or liquid core with encapsulated sub-systems and compositions. The shell can include magnetically, optically, chemically, and ultrasound-responsive nanomaterials. c) Example of nanozymes with oxidase, catalase, peroxidase, and superoxide dismutase activities based on FeO_4, Au, and CeO_2 catalytic nanoparticles, which can be potentially encapsulated in the fluidic core or solid/polymer shell of biomedical microcarriers. d) Schematic of microparticles/capsules with catalytic segments, which obtain motive functions and self-propel autonomously in chemical fuels. e) An example of an autonomous catalytic nanotube-based nanomotor transporting yeast cells in hydrogen peroxide solution (right side image). Application of ultrasound to visualize biological capillaries using microbubbles. Subsequently, microbubbles can be destructed on-demand using high-intensity focused ultrasound (left side image). f) Application of state-of-the-art tissue imaging methods, such as ultrafast ultrasound and microbubbles below 10 µm, allowing observation of blood flow in the smallest capillaries. Image in (c): Reproduced with permission.[37] Copyright 2012, American Chemical Society. Right-hand-side image in (e): Reproduced with permission.[36] Copyright 2017, The Author, published by Symbiosis Online Publishing. Left-hand-side image in (e): Reproduced with permission.[38] Copyright 2014, Ivyspring International Publisher.

complex media. Miniaturization leads to multiple advantages of mechanical devices, such as negligible inertia, ultra-fast relative motion, the ability to control tetherless micromotors' speed and location very precisely.[42] Moreover, micromotors with size below 10 µm can successfully navigate through the smallest capillaries of the human body, potentially deliver drugs,[43] arrest/isolate pathogens,[5] and perform cleaning of clogged arteries[44] and related micromechanical minimally-invasive operations.

2.1. Mechanisms of Autonomous Propulsion

Micromotors represent miniaturized devices that achieve autonomous movements powered by chemical reactions.[45] The propulsion mechanisms of catalytic nano-/micromotors can be divided into self-electrophoresis, self-diffusiophoresis, interfacial tension, and gas/bubble recoil.[46] Depending on the nano-/microparticle's shape, size, catalytic part, materials' combinations, concentration, and composition of chemical fuels—various non-biological motion mechanisms have been reported to power micromotors.[47] First, the size of the micromotors is optimized to overcome Brownian diffusion. A growing body of literature has examined different shapes, sizes, materials of micromotors,[48] compositions,[31] and concentrations.[49] Mechanisms of catalytic reactions have been elucidated to achieve higher motive forces, ultra-fast propulsion,[50] ultraprecise positioning,[51] develop accurate control methods, and test swarming/collective behaviors of micromotors.[52,53]

2.1.1. Micromotors Motion by Self-Diffusiophoresis

Particles in fluids can self-propel autonomously by creating concentration gradients of solutes; a phenomenon referred to as "self-diffusiophoresis."[54] During self-diffusiophoresis, the solutes generated during catalytic oxidation–reduction reactions on nano-/micromotor segments induce osmotic pressure on the nano-/microparticles. Self-diffusiophoresis can be divided into two categories: nonelectrolyte-based self-diffusiophoresis and electrolyte-based self-diffusiophoresis. The latter mechanism generates lower magnitude forces, but has higher ionic tolerance. The first mechanism generates stronger motive forces but fails in high-ionic-strength solutions.[47] **Figure 2**a,b[55,56] shows schematic images of non-electrolytic self-diffusiophoresis and electrolytic self-diffusiophoresis, respectively. Figure 2a illustrates micromotors prepared by the modified Grubbs' ring-opening metathesis polymerization catalyst on the silica side of Au–SiO_2 Janus particles. The asymmetric catalyst consumes monomers on the SiO_2 side, creating a low monomer concentration area, and the net fluid flows from the side (SiO_2) with a lower monomer concentration to the side (Au) with a higher concentration. Subsequently, the micromotor self-propels in the opposite direction. Figure 2b demonstrates the dielectric-AgCl Janus micromotor moving away from the AgCl side during illumination by UV light, driven by the electrolytic self-diffusiophoresis. When the micromotors are exposed to UV light, AgCl reacts with H_2O, and the produced protons (H^+) diffuse faster than chloride ions (Cl^-). Due to the formed inward electric field, the near-field slip flows from the uncoated to the coated particle's side, leading to a motion direction away from

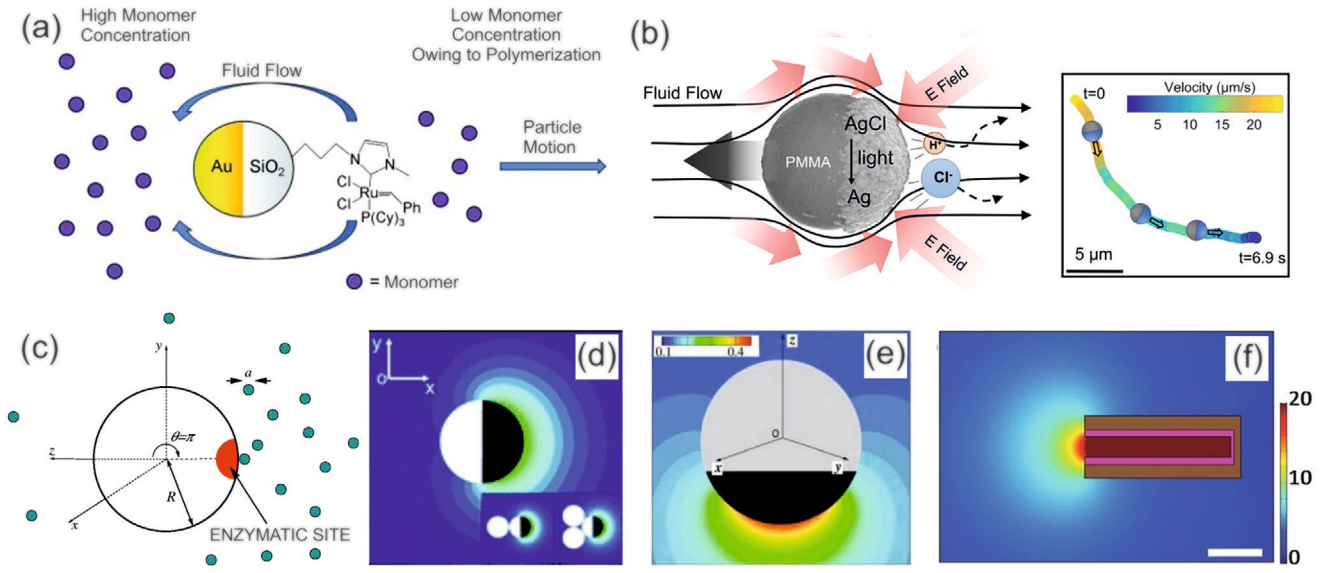

Figure 2. Nano-/micromotors driven by self-diffusiophoresis and model. a) Schematic of Au–SiO_2 Janus sphere attached with Grubbs' catalyst, caused by nonelectrolyte self-diffusiophoresis. b) Schematic of AgCl–PMMA micromotor's motion driven by electrolyte self-diffusiophoresis. c) Model for a spherical motor with an enzyme reaction site. d)The simulated steady-distribution of reaction products of a Pt-capped polystyrene Janus sphere, a translational motion along the axis will be performed if the symmetry axis of the micromotor coincides with the in plane concentration distribution. e) The simulated solute distributions of spherical particles to show shape effect on the phoretic velocity. f) The simulated oxygen concentration distribution produced by a tubular bilayer nanorocket undergoing self-diffusiophoresis. a) Reproduced with permission.[55] Copyright 2011, Wiley-VCH. b) Reproduced with permission.[56] Copyright 2018, American Chemical Society. c) Reproduced with permission.[57] Copyright 2005, American Physical Society. d) Reproduced with permission.[58] Copyright 2012, The Royal Society of Chemistry. e) Reproduced with permission.[59] Copyright 2010, Springer Nature. f) Reproduced with permission.[60] Copyright 2017, Wiley, VCH.

the AgCl side. Multiple theoretical models have been developed to understand better self-diffusiophoresis based on an asymmetric release of reaction products. For example, one model describes a molecule machine with an enzymatic site that can propel in the blood channels by the asymmetric release of reaction products (Figure 2c).[57] The motor is considered a diffusive equivalent of the jet engine that releases the reaction products asymmetrically to gain an inertial thrust force. Based on the Pt-catalyzed decomposition of H_2O_2, a distribution of catalytic reaction products around the Pt-capped polystyrene Janus spheres is calculated (Figure 2d).[58] The model predicts that if the symmetry axis of the micromotor coincides with that of the in plane concentration distribution, the motion should involve a translational motion along the axis only; and the complex dynamics of various active micromotor-cargo composites were also investigated. The solute distributions of three spheroidal particles with different shapes (prolate, spherical, and oblate) are qualitatively analyzed and the effect of the shape on the phoretic velocity is discussed (Figure 2e).[59] Bilayer nanotube with a diameter as small as 10 nm undergoes motion by self-diffusiophoresis, leading to more efficient propulsion than achieved by cylindrical and spherical catalytic nanomotors (Figure 2f).[60]

2.1.2. Micromotors Motion by Generated Microbubbles

The bubble propulsion mechanism leads to efficient propulsion, high speeds, and robust performance,[61] regardless of the ionic strength of solutions. Different geometries of bubble propelled micromotors have been investigated: rod, tube, and sphere and the mechanisms of motion are discussed in detail.[46,62,63] Understanding of gas nucleation/generation on catalytic surfaces plays an important role in the design of microbubble-propelled motors. For example, during the decomposition of H_2O_2, molecular oxygen diffuses from the surface of the catalyst. Depending on surface curvature and particle size, bubbles are nucleated and continuously generated from the surface. Bubbles grow, recoil, and replace the mass of fluid near/at the particles providing a "jet" force, which propels the micromotors forward.[64] For instance, Au–Ni nanorods are prepared by template-assisted electrochemical deposition. As shown in **Figure 3**a, in H_2O_2 solution, O_2 is produced at the Ni surface, which provides the driving force for the nanorod.[62] Figure 3b shows the bubble-propelled tubular micromotor made of rolled-up Ti/Fe/Au/Ag nanomembranes.[46] H_2O_2 decomposes in the catalytic microtube inner interior, causing the ejection of gas bubbles and pumping of fluid into the tube. Subsequently, the tube motion is in the opposite direction. Later, a Pt-coated SiO_2-microsphere-based micromotor was demonstrated (Figure 3c).[63] H_2O_2 is decomposed into water and O_2 bubble on the surface of Janus microparticle, leading to a detachment of the bubbles and achievement of motion. Other materials and fuels have also been investigated to power the micromachines, such as tubular polyaniline (PANI)/Zn micromotors fabricated by template-assisted electrodeposition.[65] As shown in Figure 3d, such a micromotor works in the acidic media, taking advantage of H_2 bubbles, which originates from the redox reaction of H^+ in contact with Zn. Another micromotor materials' choice used Pt coated on the surface of Mg spheres.[66] Figure 3e illustrates the Mg–water reaction mechanism that continuously generates H_2 bubbles (in the presence of $NaHCO_3$) to propel micromotors. Likewise, a partially coated Al–Ga alloy spherical motor has been demonstrated (Figure 3f).[67] Al reduces water to hydrogen, and liquid Ga is used to remove the reaction-hindering aluminum oxide film to promote the Al–water reaction, making it feasible to propel the particle by the Al–water reaction. Another example demonstrates Ag and MnO_2 micromotors self-propelled at a low concentration of H_2O_2 (Figure 3g).[61] Moreover, artificial enzyme-powered micromotors immobilized with biocatalytic catalase are fabricated using a template-based electrodeposition method (Figure 3h).[68] The biocatalytic catalase enzyme decomposes H_2O_2. Subsequently, an oxygen bubble recoil leads to efficient propulsion. Recently, a hydrophobic/hydrophilic phase-shifting polymer is used to retain/expel gas bubbles from the micromotors (Figure 3i),[22] resulting in buoyancy-controlled descending or ascending vertical motion that results in directional/vertical propulsion of micromotors.

2.1.3. Micromotors Motion by Self-Electrophoresis

Charged objects can migrate if located in an external electric field, a phenomenon that is referred to as "electrophoresis." If the charged object generates an electric field by itself and move, this is termed as "self-electrophoresis." The first demonstration of self-propelled nanomotor driven by self-electrophoresis is shown in **Figure 4**a.[69,70] In solutions, H_2O_2 generates H^+ on the Pt part during the oxidation process, and the H^+ is consumed at the Au part during the reduction of H_2O_2. Subsequently, the electrons are generated at the Pt end and consumed in the Au end. The resulting ion flux from the Pt to Au parts induces an electric field, propelling the particle by the Pt end forward. Pt/PS micromotors have been studied experimentally and theoretically, demonstrating that electrokinetic effects play an important role in the motion of non-conducting spherical Janus micromotors (Figure 4b).[71,72] A catalytic reaction pathways showed the competing reactions responsible for Pt/PS micromotors' motion and consisted of a combination of diffusiophoresis and electrophoresis.

2.2. External Control of Micromotors

Micromotors' control using external fields (e.g., US, magnetic field, light, electrical field, chemical gradient) can be used both to power motion of microparticles and guide the position of catalytically driven autonomous particles to a specific location. External control can also be used to program specific dynamic patterns of motion of micromotors. External control can be used to deliver and release specific cargo during targeted therapy. Particularly, external control is important for biomedical applications for micromachines, which can operate in blood vessels, tissues, and organs. Moreover, external control enables the realization of tiny mechanical tools, like nano-/microsurgeons capable of performing minimally invasive mechanical operations. For instance, nano-/micromotors with

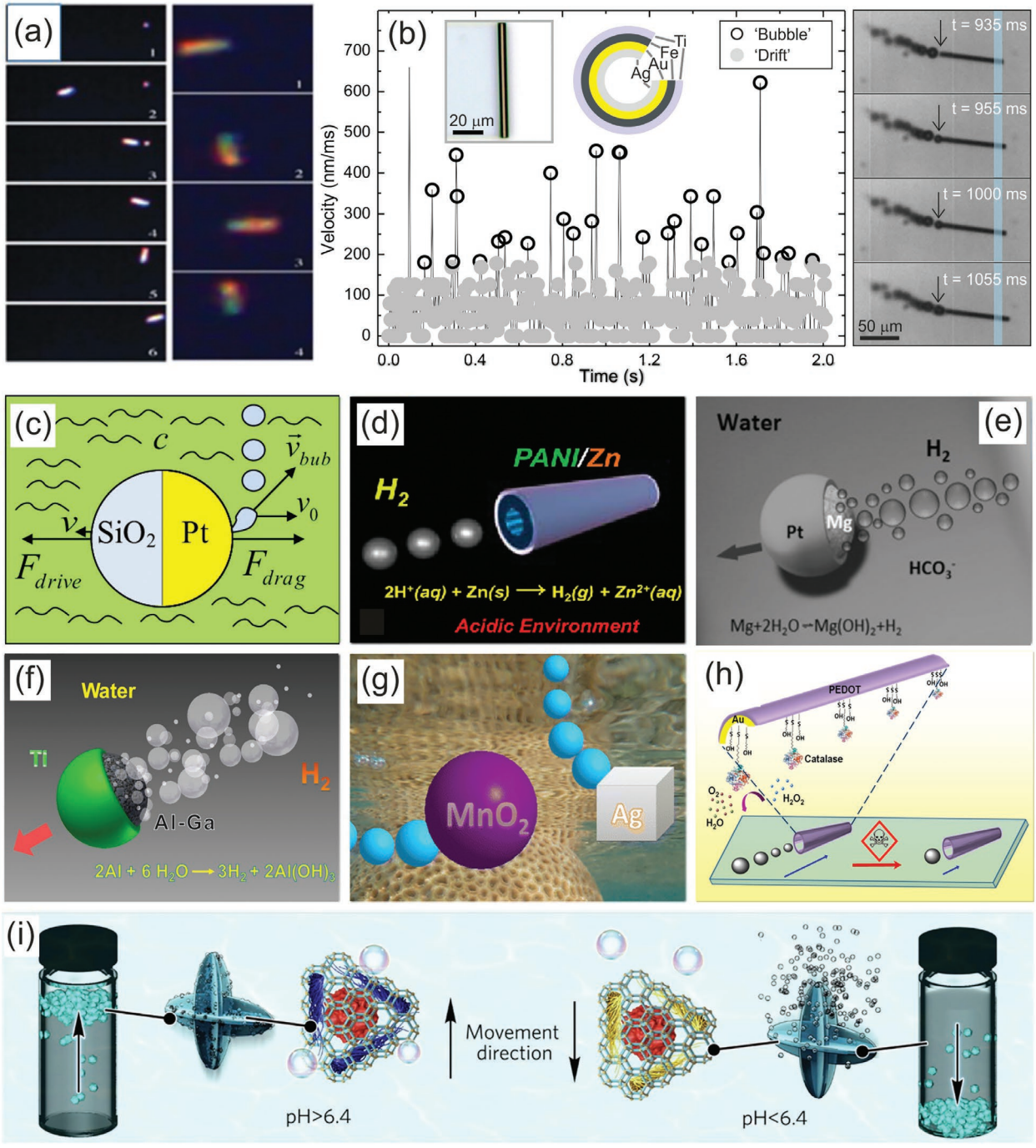

Figure 3. Micromotors self-propelled by bubble ejection. a) Schematic of Au–Ni nanorods propelled by produced O_2 at the Ni surface. b) Motion of rolled-up Ti/Fe/Au/Ag tubular micromotor propelled by ejection of gas bubbles generated in the inner interior of the tube. c) Schematic of Pt–SiO_2 sphere micromotor in H_2O_2 propelled by O_2 bubbles generated on the surface of Pt. d) Schematic of PANI–Zn tubular micromotor propelled by H_2 bubbles originating from the redox reaction of H^+ in contact with Zn. e) Schematic of Mg–Pt micromotor propelled by continuously generated H_2 bubbles in the presence of $NaHCO_3$. f) Schematic of Al–Ga/Ti micromotor propelled by the H_2 bubbled generated from Al–water reaction. g) Schematic of Ag and MnO_2 micromotors driven by O_2 bubbles from decomposition of H_2O_2. h) Schematic of tubular micromotor with catalase biocatalytic layer in the inner interior driven by O_2 bubbles from the catalase-enhanced decomposition of H_2O_2. i) Schematic illustration showing the motion mechanism of submarine-like micromotor, that is, by shifting its hydrotropism using solution adjusted pH: the structure can retain or expel O_2 bubbles to perform a buoyancy-controlled descending or ascending vertical motion. a) Reproduced with permission.[62] Copyright 2005, The Royal Society of Chemistry. b) Reproduced with permission.[46] Copyright 2008, Wiley-VCH. c) Reproduced with permission.[63] Copyright 2009, AIP Publishing. d) Reproduced with permission.[65] Copyright 2012, American Chemical Society. e) Reproduced with permission.[66] Copyright 2013, Wiley-VCH. f) Reproduced with permission.[67] Copyright 2012, American Chemical Society. g) Reproduced with permission.[61] Copyright 2014, American Chemical Society. h) Reproduced with permission.[68] Copyright 2013, American Chemical Society. i) Reproduced with permission.[22] Copyright 2019, Elsevier Ltd.

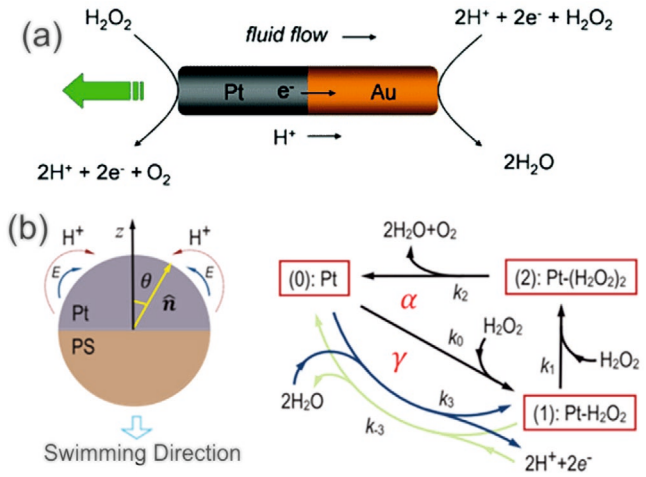

Figure 4. Micromotors swimming by self-electrophoresis. a) Schematic illustration of self-propelled Pt–Au nanorod motor driven by self-electrophoresis. b) Schematic image of Pt–PS spherical micromotor and competing catalytic reactions. a) Reproduced with permission.[70] Copyright 2006, American Chemical Society. b) Reproduced with permission.[71] Copyright 2014, European Physical Society.

sharp tools can be designed to remove blood clots caused by atherosclerosis. External fields (magnetic field, US, light, electric field, electrochemical potential, etc.) can also be applied to induce self-propulsion in micromotors.

2.2.1. Magnetic Control of Micromotors

The magnetic field provides a strategy to drive micromotors wirelessly. Magnetic control suits various applications because it can penetrate deep into the body. In the scope of this paper, the magnetically propelled micromotors[73] are not taken into account. We concentrate on the micromotors, which are controlled by the magnetic field.[74] By embedding the ferromagnetic layer into the motors, the motors will attempt to align their magnetization direction with the field vector; remote navigation can thus be accomplished. In 2005, a nickel-contained metallic nanomotor was reported.[75] It is a catalytic self-electrophoresis-driven mechanism and the magnetic field only changes the direction of motion, but it does not influence the motor's speed. A rotating magnetic field has also been applied to control and localize the strain-engineered tubular micromotors' trajectories.[76] Subsequently, selective loading, transportation, and delivery of microobjects were accomplished.[39] The motion of micromotors through flowing fluidic microchannels can be precisely navigated in a controllable manner,[77] followed by biomaterials' delivery.[78] During the early stage of research, magnets were used to navigate the micromotors,[79] which cannot offer precise positioning. With the help of an automated control system—closed-loop control of micromotors have been realized. In 2013, a magnetic-field-controlled closed-loop system was demonstrated.[80] Tubular micromotors could align along the controlled field lines in 3D space, and move point-to-point using the electromagnetic system. Further, an advanced autonomous navigation system with visual feedback and an artificial intelligence (AI) planner was introduced to realize closed-loop control of micromotors, which navigated the Ti/SiO_2 microsphere in diverse environments in a collision-free manner. With the help of visual recognition, the micromotor can be oriented toward its predetermined targets autonomously, thus enhancing the intelligence of micromotors toward practical applications in complex environments.[81]

2.2.2. Motion Control of Micromotors Using Temperature

The thermal stimulus is a convenient strategy to modulate the speed of the motors.[82] Because the oxidation and reduction kinetics of the H_2O_2 can be modulated by temperature, Au–Pt nanorod motors were reversibly accelerated and slowed down by adjusting the solution temperature first in 2009.[83] Temperature stimulus was employed to modulate the speed of tubular micromotors, while reducing the amount of H_2O_2 needed simultaneously.[50] The same group proved that the tubular micromotors could self-propel in ten times diluted blood samples at 37 °C while being inactive at 25 °C due to the high viscosity of the blood.[84] The abovementioned strategy takes advantage of the temperature influence on the H_2O_2 reaction rate, while the other used the temperature-induced geometrical deformation to adjust the speed. A thermoresponsive polymer formed a tubular micromotor, and it could reversibly fold and unfold by applying changes of solution temperature.[85] The micromotor compressed at temperatures below low critical solution temperature (LCST) and expanded above LCST. The radius of the tubular micromotor defines the speed, leading to the in situ modulation of speeds.[23]

2.2.3. Motion Control of Micromotors Using Light

Light is one of the most common external physical stimuli to drive nano-/micromotors.[86] Light can induce many phenomena such as photocatalysis, photolysis, photothermal phenomenon, photochromism, photoisomerization, which can be used to drive or control the motors. TiO_2–SiO_2 Janus nanotrees were fabricated by wet silicon etching followed by TiO_2 nanowire hydrothermal growth. They can be employed as phototactic micromotors in a programmable manner. The micromotors contained nanoscale photocathode and photoanode at opposite ends that release photogenerated cations and anions to propel the micromotors, this so-called light-induced self-electrophoresis provide a way to sense and orient the illumination direction to steer the micromotors.[24] In addition to light-induced self-electrophoresis,[87] there are also many light-induced self-diffusiophoresis[88] and bubble propulsion[89] originate from photocatalytic reactions. Researchers also used photolysis to generate electrolyte gradient, which can induce self-diffusiophoresis to the AgCl micromotors under UV light exposure.[90] There are also many interesting non-photocatalytic mechanisms like photothermal,[91] photochromism,[92] and photoisomerization[93] effects, which are not in the scope of this review.

2.2.4. Motion Control of Micromotors Using Ultrasound

In recent years, the US has attracted significant attention to power and control motion of micromotors. It was first reported that the US can propel metallic rods autonomously in solution. The metallic rods have an asymmetry shape, leading to an uneven distribution of acoustic pressures in the fluid that is stronger at the concave end, propelling the micromotors with the other end forward.[94] Further studies were performed to confirm the asymmetry effects experimentally and theoretically.[95] For external control of bubble-propelled nano-/micromotors, the US was reported to be able to tune their speed. When a US field is applied, the bubble evolution will be disrupted due to Bejerkn's force, leading to a significant speed decrement. This kind of reversible motion control can be used to regulating the movement remotely and instantaneously.[51] For external control of catalytic nanorod motors, US is used to restrict their motion as and when needed. Metallic microrod motors are self-propelled by self-electrophoresis in the presence of H_2O_2. When the US is applied, micromotors are assembled into a swarm in the pressure nodes' location.[96] Besides, the US triggered separation of different kinds of catalytic motors is accomplished according to density variation, offering a new approach for on-demand isolation of motors at small scales.[53]

2.2.5. Motion Control of Micromotors Using Chemical Gradients

Chemotaxis is the ability of living creatures to sense chemical gradients in their surroundings and react accordingly. Inspired by the chemotactic bacteria, researchers made an effort to externally control the motors using a similar bioinspired strategy. Pt–Au microrod motors can move up an H_2O_2 fuel gradient, providing a novel way to direct particles motion toward specific targets. The process is explained by random walk physics using diffusion coefficient gradient.[97] Two types of catalytic micromotors (tubular micromotors and Janus particles) showed chemotactic behavior in microfluidic channels, both oriented toward higher H_2O_2 concentrations. Particles are governed by the diffusion process that induces random reorientations of catalytic particles.[98] A novel kind of stoma-shaped nanomotors loaded with Pt nanoparticles was demonstrated to move toward a fuel gradient. This directional movement is due to the nanomotors travel longer distances in the presence of higher fuel concentration, resulting in a movement up the H_2O_2 gradient.[3] Calcium carbonate Janus micromotor moves in extremely light acid solutions, even in acid environments in situ generated by HeLa cells, enabled by diffusioosmotic flows.[99] Chemical gradients are a facile, but efficient method to orient the motors, holding a bright future in the drug delivery.

3. Biomedical Applications

The micromotors offer controllable locomotion of active particles, capable to deliver cargo payloads, perform biomedical surgery operations, isolate pathogens, and biodetoxify solutions. Micromotors can complete diverse bio-tasks using autonomous motion and external control. However, most of performed experiments represent first demonstrations of dynamic micromachines' capabilities with procedures, which are not yet medically approved.

3.1. Drug Delivery Enabled by Micromotors

Typically, micromotors depend on non-biocompatible materials and toxic hydrogen peroxide fuel was used during the early stage research.[102] Alternative ways have been found, such as biodegradable chitosan–sodium alginate–Pt motors, fabricated using template-assisted LbL assembly.[103] Using external magnetic field, the micromotor partially penetrated the HeLa cell, and doxorubicin (DOX) was released in situ under ultrasonic treatment. In recent years, using advantages of biocompatible materials, drug delivery applications using micromotors are conceptually demonstrated. For instance, the template-assisted electrodeposited Zn-based micromotors could efficiently self-propel in the stomach acid, which demonstrated their in vivo operation for the first time.[104] The micromotors could self-propel during 10 min to complete drug delivery operations and self-dissolve. Mg-based micromotors were encapsulated in enteric protective capsules to protect micromotors from degradation in the stomach. With the help of photoacoustic (PA) computed tomography, the micromotors can be guided through the stomach to the intestine, where drugs can be released in the targeted areas (**Figure 5**a).[100]

3.2. Nano-/Microsurgery by Micromotors

Micromotors can self-propel to access deep tissue locations, facilitating microsurgery at a small scale. Compared to the magnetic-actuation[41,105] or US-triggered[106] nano-/micromotors, additional apparatus for providing magnetic fields or the US is not required for catalytic micromotors. For instance, the fabricated InGaAs/Ga/Cr/Pt rolled-up micromotor can self-propel a corkscrew-like trajectory. The micromotors are autonomously embedded themselves into a fixed HeLa cell, leading to cells' drilling (Figure 5b).[37] The Ti/Cr/Fe microdriller with a sharp tip could drill a hole in a pig liver under the control of the magnetic field, which suggests feasibility of the minimally invasive surgery. (Figure 5c).[4] Magnetic nanorod-based motors fabricated by the angular deposition method was used to enhance thrombolysis in vitro and in vivo.[44] It is demonstrated that compared to passive nanocarriers, nanomotors' active locomotions accelerate the thrombolysis by improving the mass transport of tissue plasminogen activator. Subsequently, the drug agitation nanosurgery by nanomotors could be used as a proof-of-concept for other disease treatments.

3.3. Biodetoxification Using Micromotors

The unique advantage of fluid mixing provided by micromotors can enhance the diffusion process, which facilitates the motor-based biodetoxification. The cell-derived red blood cell membrane-coated Mg Janus micromotor could absorb and neutralize toxins (Figure 5d).[107] This Janus micromotor can self-propel efficiently by Mg-water reaction-induced H_2 bubble.

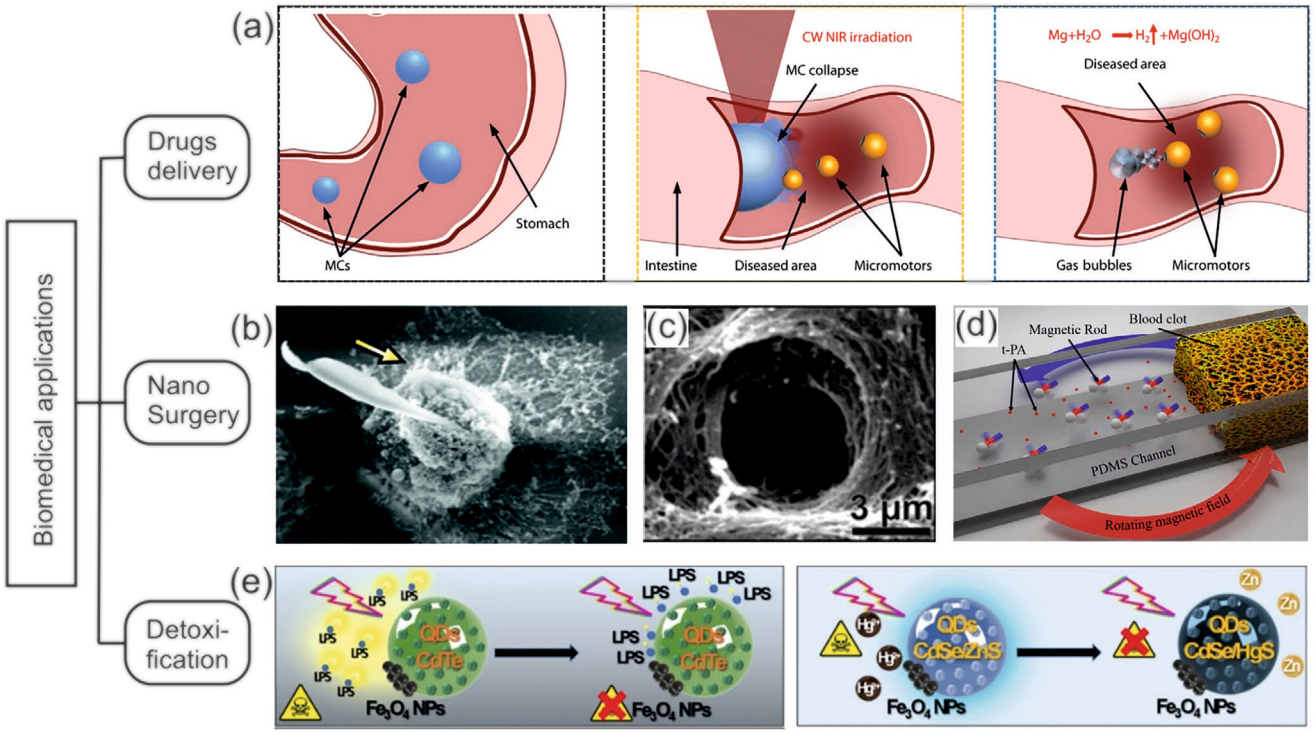

Figure 5. Biomedical applications of micromotors in the three directions: drug delivery, minimally invasive surgery and detoxification. a) Schematic of micromotors passing through the stomach with enteric coating. Motors are activated by NIR irradiation on-demand to complete drug delivery. b) SEM image of asymmetrically rolled-up tubes drilled and embedded themselves into biological tissue. c) SEM image of a drilled hole in a pig liver after extracting the microdriller. d) Schematic image of nanomotor enhanced thrombolysis treatment in the fluidic channel, showing a potential to remove clots in vessels. e) Schematic showing the cell-derived red blood cell membrane-coated Mg Janus micromotor absorption and neutralization of toxins. a) Reproduced with permission.[100] Copyright 2019, The Authors, published by American Association for the Advancement of Science. b) Reproduced with permission.[37] Copyright 2012, American Chemical Society. c) Reproduced with permission.[4] Copyright 2013, The Royal Society of Chemistry. d) Reproduced with permission.[44] Copyright 2014, American Chemical Society. e) Reproduced with permission.[101] Copyright 2019, Wiley-VCH.

The cell membrane coating protected the motor from protein fouling effects when operated in a biological fluid, holding great promise for biodetoxifications. A new kind of micromotors assembled by polycaprolactone, photoactive quantum dots and Fe_3O_4 have been demonstrated (Figure 5e).[101] The light-induced self-diffusiophoresis propelled the biocompatible micromotor in peroxide, glucose, and human blood serum. The micromotors can remove bacterial endotoxins, and heavy metals, leaving only a low toxic by-product, demonstrating a high potential of light-driven detoxification.

4. Nanozymes

Nanozymes are composed of nanoparticles of inorganic materials possessing intrinsic enzymatic activities. Nanozymes have been developed with nanoparticle forms of Fe_3O_4,[16] platinum,[108] gold,[109,110] copper oxide,[111] $CoFe_2O_4$,[112] graphene oxide,[113] carbon,[114] among others. Besides classifying the nanozymes based on the type of enzymatic reactions they mimic,[115] they may also be categorized based on their atomic composition, which largely determine their catalytic activity and specificity in operation.[116] As reviewed[116] based on the atomic composition of their core and surface, nanozymes may be distributed into three different categories—metal oxide-based, metal-based, and carbon-based nanozymes. A variety of metal oxide-based nanozymes have been reported to mimic catalytic activities of peroxidase, catalase, and superoxide dismutase (SOD). Since metal oxide nanoparticles are usually chemically and biologically inert, additional surface engineering and conjugation are required to endow these structures with desired functionalities.[116] Metal oxide nanozymes have found wide application in fabricating amperometric and colorimetric detection systems.[117]

Metal-based nanozymes may be further classified as Type I and Type II, depending on the part of their structure participating in catalysis. The activities of Type I nanozymes are entirely from the assembled monolayer onto a metallic core, while for Type II, the nanozymes' activities are largely due to the metallic part.[118] Metal based nanozymes have been reported to possess catalytic activities of SOD, peroxidase, and catalase. Composite structures of metal[119] and metal oxide[120] nanozymes have also been found to function as a distinct class of nanozyme having enhanced catalytic activity.

Carbon-based nanozymes are usually found to behave as peroxidase[113] and SOD-mimics,[121] which due to their unique electrical, optical, thermal, and mechanical properties can offer a variety of multifunctional platforms for biomedical applications.[122] Material selection for nanozymes may also be dependent on their envisaged functionalities or specific

application requirements. TiO_2 nanoparticle is a commonly used nanozyme for photocatalysis and environmental remediation.[123] Graphite carbon nitride (g-C_3N_4),[124] graphene oxide (GO),[125] black phosphorus (BP),[126] carbon quantum dots,[127] metal–organic frameworks (MOFs),[128] and thin chromium thiophosphate ($CrPS_4$)[129] are nanozymes that exhibit remarkable photocatalytic properties. Magnetic nanozymes, such as mussel-inspired nanoflower (PDA-Cu NFs) are considered as antibacterial agents for biosensing applications.[130] Another group reported laccase-like active magnetic nanozyme which can be used for efficient removal of toxic phenolic pollutant like *o*-phenylenediamine (OPD).[131] Optically active plasmonic nanozymes (AuNPs) exhibits enhanced peroxidase-mimicking activity.[132] Nanozymes can also be endowed with multifunctional capability. Recently, experimentally derived multifunctional nanozyme based on MOFs, which contains catalytic Cu^{2+} and luminescent Tb^{3+} ions are also reported. This nanozyme not only possessed excellent catalytic activity comparable to horseradish peroxidase but also could indicate the real time concentration of H_2O_2 through its fluorescence.[133] Recently, biocompatible nanozymes were developed for in vivo sensing and drug-delivery applications. Notably among them was citrate-capped palladium nanozyme that exhibited efficient antioxidant properties within the cellular environment.[134]

Noble metal nanoparticles such as Au, Pd, and Pt demonstrate remarkable catalytic activities and intrinsic antioxidant properties.[135,136] Functionalizing these nanomaterials with various ligands can greatly improve their biocompatibility and broaden their biomedical application potentials. To this end, efforts have been made to adjust the size and morphology of Pt nanoparticles (NPs) with a protective layer of sodium alginate to enhance their dispersibility, stability, and possibility of infusing additional surface features, nanogel preparation, and diverse applications in other fields.[137] Similar studies have also been demonstrated with citrate-coated Pd NPs, which displayed enhanced biocompatibility and stability, while functioning as reactive oxygen species scavengers.[134] Another group used BSA-stabilized Pt nanozyme in developing a rapid, sensitive, and selective Hg^{2+} sensing system.[138] Poly(amidoamine) (PAMAM) encapsulated platinum nanoparticles were used as efficient catalase mimic.[139] Platinum nanoparticles anchored metal–organic frameworks were further shown to display enhanced electrocatalytic property in detecting the activity of telomerase, a ribonucleoprotein.[140] Therefore, the unique physicochemical properties of metal nanoparticles can greatly be enhanced by functionalizing their surfaces with different ligands and functional moieties. This further facilitates development of multifunctional nanocarriers and sensing platforms, where the metal nanoparticles, besides their inherent enzymatic activity can be further endowed with magnetic, fluorescent, and self-propulsion capabilities. With appropriate conjugation and surface charge, hydrodynamic radii of nanozymes may also be optimized for their complete elimination from the body after use[141] and minimum nonspecific tissue/organ uptake during in vivo operations.[142]

Natural enzymes are characterized by a high degree of selectivity and catalytic activity. But, they are often expensive and have limited chemical and biological stability. Functional materials like nanozymes have enzyme-like activity, and possess greater stability and application potentials due to their simpler preparation technologies. Nanozymes offer size and composition-dependent activity, which facilitates design of materials with a broad range of catalytic activity—by varying their shape, structure, and composition.[143] Natural enzymes are mostly proteins and can be considered as soft materials, whereas nanozymes are hard with porphyritic nuclei.[144] Compared to natural enzymes, nanozymes have large surface areas, which facilitate their modification and conjugation with other functional groups. The catalytic efficiencies of nanozymes in most cases are lower than that of natural enzymes. For example, CeO_{2-x} nanorods,[145] can act as an efficient green urease mimics that catalyzes the hydrolysis of urea under ambient conditions with a turnover number k_{cat} of 9.58×10^1 s^{-1}, which is significantly lower than that of native jack bean urease. In some cases, however, nanozymes have been reported to have catalytic efficiencies comparable to that of natural enzymes. $MnFe_2O_4$ with a nanooctahedron morphology, has been reported to have a turnover number (k_{cat}) and catalytic efficiency (k_{cat}/K_M) in the oxidation of 3,3′,5,5′-tetramethylbenzidine (TMB) of 8.34×10^4 s^{-1} and 2.21×10^9 M^{-1} s^{-1}[146] respectively, which are similar to the catalytic efficiency of their natural counterparts. Surface modification and functionalization may lead to further enhancement of catalytic efficiency of nanozymes. For example, histidine-modified Fe_3O_4 nanoparticles (NPs) exhibited more than 10-fold higher binding affinity (K_M) for H_2O_2 and a 20-fold higher catalytic efficiency (k_{cat}/K_M) compared to unmodified Fe_3O_4 NPs.[147] These results show that with appropriate engineering methodologies, nanozymes can be endowed with fundamental characteristics of natural enzymes such as fast kinetics, high productivity, and high selectivity, under identical reaction conditions—with added advantages of robustness, stability, and ease of synthesis. Recently developed single atom nanozymes (SAzymes), owing to their well-defined electronic and geometric structures, have been reported to have maximum atom efficiency, unique quantum size effect, and excellent substrate selectivity.[148] SAzymes could potentially make nanozyme better alternatives to nature enzymes—accomplishing specific enzyme-based applications easily with higher therapeutic efficiency and biosafety.[142] Nanozymes or synthetic catalytic nanomaterials with enzyme-like functions (e.g., peroxidase, catalase, superoxide dismutase, and oxidase) pave the way toward integration of nano-/micromotors, catalytic reactions, and biological systems. Nanozymes help micromotors' community extend the scope of chemical fuel applications/reactions beyond the motion significantly. Moreover, it is highly interesting in biology and medicine to better understand the dynamics of individual enzymes and nanozymes during catalytic reactions. Recently reported energy transduction by active enzymes and their collective dynamics makes nanozymes promising platforms to understand molecular machine dynamics, substantially improving our knowledge of activity-induced transport and intracellular communication pathways. Nanozymes can also respond to a wide range of stimuli with broad applications in diagnostics, protection against oxidation, immunoassays and biosensing. In comparison to biological enzymes—nanozymes offer size tunability, control over shapes, compositions, and surface area, flexibility

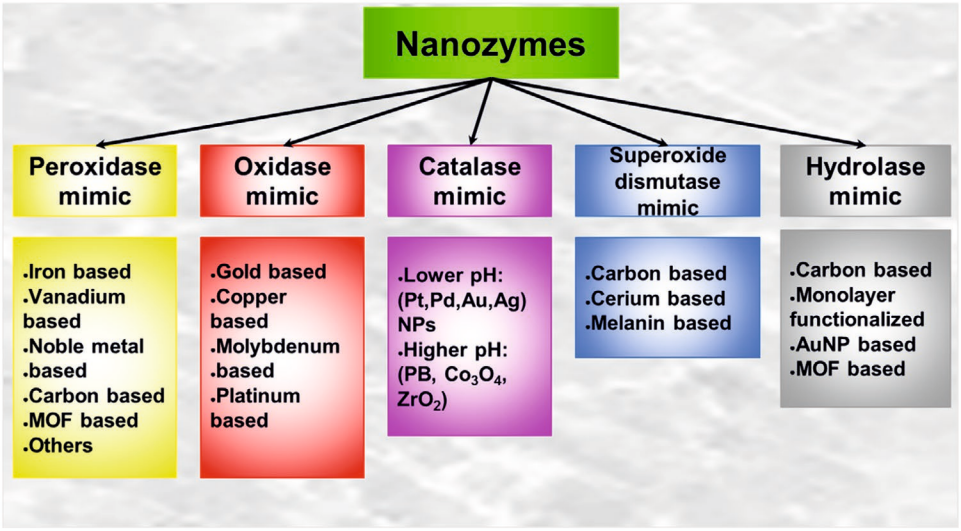

Figure 6. Classification of nanozymes based on the type of enzymatic reaction: peroxidase, oxidase, catalase, superoxide dismutase, and hydrolase mimic.

in bioconjugation, stability, and robust catalytic performance in harsh chemical conditions. Subsequently, nanozymes can be integrated into emulsions/microemulsions, drops, and capsules, forming chemical "microreactors" for controllable biosensing, purification, separation, and reaction product release.

4.1. Classification of Nanozymes

Nanozymes can be categorized into five distinct types (**Figure 6**): a) peroxidase nanozymes, b) oxidase nanozymes, c) catalase nanozymes, d) superoxide dismutase (SOD) nanozymes, and e) hydrolase nanozymes. Each of these types is further categorized depending on the nanomaterials used to replicate the enzymatic functions.

a) Peroxidase nanozymes: Peroxidases are a large group of enzymes typically involved in the break-up of peroxides (a group of compounds with the structure R—O—O—R) and catalyzing the following types of reactions

$$2AH + H_2O_2 \xrightarrow{\text{Peroxidase}} 2A + 2H_2O \quad (1)$$

$$2AH + ROOH \xrightarrow{\text{Peroxidase}} 2A + ROH + H_2O \quad (2)$$

After the discovery of Fe_3O_4 magnetic nanoparticles (Fe_3O_4 MNPs), multiple iron-based alloys are used to synthesize peroxidase mimic nanozymes. Prussian blue (PB, $[Fe_{(III)}Fe_{(II)}(CN)^6]^-$) is an important example among the various compounds investigated that is also referred to as the "artificial peroxidase."[149] It was observed that with 3,3′,5,5′-tetramethylbenzidine [TMB] as a substrate, PB nanoparticles (PB NPs) showed a fourfold higher k_{cat} than that of Fe_3O_4 MNPs.[150] PB has also been reported to show catalase and SOD-like activity under different pH conditions.[151] A study showed monocrystalline vanadium oxide (V_2O_5) nanowires in the presence of glutathione (GSH) were able to catalytically reduce hydrogen peroxide (H_2O_2) and protect cells from oxidative damages.[152] Many noble metals (e.g., Au, Ag, Pt, Pd) based nanoparticles are reported to mimic the activity of peroxidases. The catalytic efficiency of Pd–Ir nanoparticles is found to be 28 times higher than that of horseradish peroxidase (HRP) and has been successfully used in enzyme-linked immunosorbent assays (ELISA) for disease detection.[153] Graphene quantum dots (GQDs),[154] Au nanocluster (Au NC) graphene oxide,[155] carbon nanodots[156] are carbon-based peroxidase-like nanozymes and are widely used due to their large surface area that facilitates substrate diffusion and adsorption. Metal–organic framework (MOF)-based nanomaterials are another kind of enzyme-mimicking structures, which are used extensively for biomedical applications. MOF-based peroxidase nanozymes were constructed using metal ions, nanoclusters (e.g., Fe and Cu),[157] organic ligands (e.g., terephthalic acid [H_2BDC], and 1,3,5-benzenetricarboxylic acid [H_3BTC]). The unique composition, structural diversity, and size tailorability of MOFs have made them the ideal platforms for many novel nanozymes that are used widely in chemical sensing and detection of analytes.[158] Other important constructs such as copper hydroxide ($Cu(OH)_2$) supercages (**Figure 7**a) attracted much attention in recent years as peroxidase nanozymes. The supercages are capable of showing 90% catalytic efficiency under the optimum conditions of pH and temperature (pH 4.5, temperature 25 °C).[159]

b) Oxidase nanozymes: Oxidases are another subclass of oxidoreductase enzymes that catalyze oxidation–reduction reactions and produce H_2O or H_2O_2 along with other products. Oxidases are usually named after their respective substrates such as glucose oxidase (GOx, substrate Glucose), alcohol oxidase (AOx, substrate alcohol), lactate oxidase (LOx, substrate lactate), cholesterol oxidase (COx, substrate cholesterol), and urate oxidase (UOx, substrate

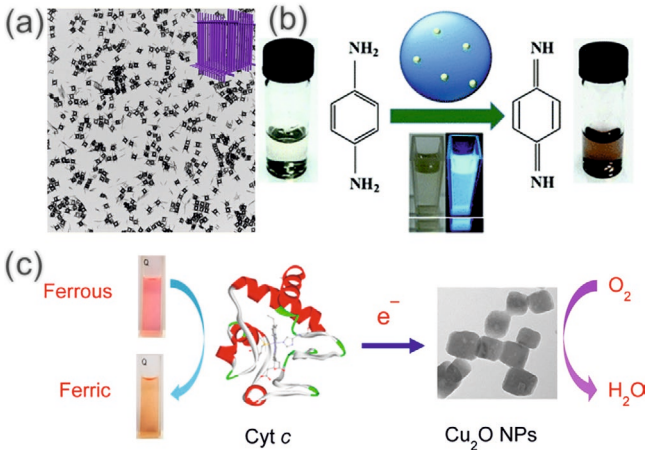

Figure 7. a) A TEM image of $Cu(OH)_2$ supercages. The schematic of the supercage structure has been shown in the inset (right-top corner). b) Schematic illustration of laccase-like catalytic activity of Cu-carbon dots with substrate p-phenylenediamine. c) Schematic illustration of CcO-like activity of Cu_2O NPs. a) Reproduced with permission.[159] Copyright 2015, American Chemical Society. b) Reproduced with permission.[160] Copyright 2015, The Royal Society of Chemistry. c) Reproduced with permission.[161] Copyright 2017, American Chemical Society.

uric acid). The catalytic reactions may be schematically represented as follows

$$AH + O_2 \xrightarrow{\text{Oxidase}} A + H_2O \quad (3)$$

$$AH + O_2 + H_2O \xrightarrow{\text{Oxidase}} A + H_2O_2 \quad (4)$$

Another study demonstrated the use of Au, Pt, Pd, and Cu nanoparticles of diameter 3–5 nm in catalyzing glucose oxidation reaction, wherein bare Au NPs were reported to possess better catalytic efficiency than the rest.[162] Interestingly, various Au based composite materials such as Au/Al_2O_3, Au/TiO_2, and Au/ZrO_2 have also been reported to function as GOx nanozymes.[163] Copper-containing nanoparticles were also found to be efficient oxidase mimics.[164] Fluorescent Cu-carbon dot nanozymes oxidize the laccase substrate PPD (p-phenylenediamine) in the presence of oxygen and are used for hydroquinone detection (Figure 7b).[160] Importantly, Cu with Guanosine 5′-monophosphate (GMP) ligand forms an amorphous MOF material that showed higher catalytic activity compared to laccase, with substantially higher stability over the pH range 3–9, temperature range 30–90 °C, and storage period of 9 days.[165] Moreover, copper oxide (Cu_2O) NPs, exhibited cytochrome c oxidase (CcO)-like activity and catalyze the oxidation of cytochrome c (Cyt c), converting it from the ferrous state to the ferric state under normal atmospheric conditions (Figure 7c).[161] Molybdenum trioxide (MoO_3) NPs also behaved as nanozymes and mimicked the function of sulfite oxidase (SuOx).[166] Similarly, Au/Pt nanostructure behaved as a Pt-based biocompatible nanozyme, mimicking the behavior of ferroxidase,[167] which plays a crucial role in transferring and storing iron in the cellular environment.

c) Catalase nanozymes: Catalase is a common oxidoreductase enzyme found in almost all living organisms, which catalyzes the decomposition of H_2O_2 to H_2O and O_2. Catalase is one of the most important antioxidants, which protects the cell from reactive oxygen species (ROS) (like H_2O_2).

$$H_2O_2 \xrightarrow{\text{Catalase}} O_2 + H_2O \quad (5)$$

There are various metals (Au, Ag, Pt, and Pd), metal oxides (Co_3O_4 and ZrO_2), and PB that exhibit catalase-like activity under certain ranges of pH and temperature. Pt- and Pd-based NPs showed better catalytic activity in this regard compared to Au and Ag based NPs under acidic condition.[168] However, Co_3O_4 NPs,[169] ZrO_2 NPs,[170] and PB NPs[150] rather act as catalase nanozymes at high pH conditions. CeO_2 NPs showed promising catalase-like activity by involving Ce^{4+} in the reduction of H_2O_2 to form Ce^{3+} along with the formation of H^+ and O_2. The subsequent capture of another H_2O_2 molecule was hypothesized to form Ce^{3+} along with H^+ and H_2O, taking the NPs back to their initial state. The proposed mechanism is shown in **Figure 8**a.[171]

d) Superoxide dismutase nanozymes: Superoxide dismutase (SOD) is another important antioxidant that prevents cells from oxidative damage by reactive oxygen species (ROS) like

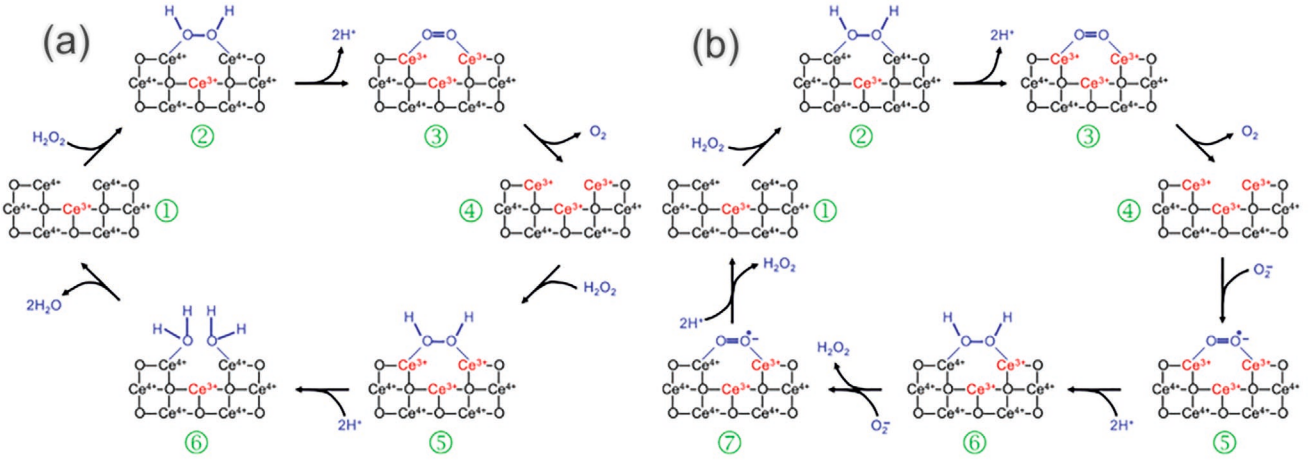

Figure 8. a,b) Proposed mechanisms of CeO_2 NPs functioning as catalase mimics (a) and SOD mimics (b). a,b) Reproduced with permission.[171] Copyright 2011, The Royal Society of Chemistry.

superoxide radicals ($O_2^{\bullet -}$) by catalyzing its dismutation into O_2 and H_2O_2.

$$2O_2^{\bullet -} + 2H^+ \xrightarrow{SOD} H_2O_2 + O_2 \quad (6)$$

There are many carbon-based nanomaterials, such as systems consisting of C_{60} and small carbon clusters (C_{60}–C_3), hydrophilic carbon cluster (HCC), hemin functionalized reduced graphene oxide (H-rGO), which mimic effectively the functions of SOD under different experimental conditions. Nanoceria is a cerium-based nanozyme that was first reported to exhibit SOD-like activities.[172] Unlike other trivalent lanthanides, cerium can exist either in Ce^{4+} or Ce^{3+} states, which allows it to act as SOD-mimic (Figure 8b).[171] Melanin-based nanoparticles (Me NPs), have also been reported to function as useful radical scavengers and could lead to more effective and safer antioxidant therapy, are prepared using dopamine hydrochloride and ammonia by mixing in ethanol–water followed by functionalization with amine-terminated poly(ethylene glycol) (PEG) for better stability.[173]

e) Hydrolase nanozymes: A common but very important enzyme, hydrolase, catalyzes the hydrolysis of chemical bonds in the presence of water and breaks larger molecules into smaller fragments. Hydrolases are classified based on the bonds they act upon, for example, nuclease is a hydrolase that breaks nucleic acids.

$$A-B+H_2O \xrightarrow{Hydrolase} A-OH+B-H \quad (7)$$

Recently, several nanomaterials were developed to imitate the hydrolase activity that was mostly based on carbon (graphene oxide[174] and carbon nanotubes [CNTs] assembled with short peptides[175]), monolayer functionalized Au NPs through Au—S bonds[176] and MOFs.[177] Among the MOF-based hydrolase nanozymes, Zr-based nanomaterials are widely used as phosphotriesterase mimics for cleaving the phosphate ester bond of chemical warfare agents (CWAs).[178]

There are few multi-enzyme-mimicking nanozymes like cerium oxide (CeO_2) NPs, which show SOD and catalase-like activities at neutral or high pH regimes while oxidase-like activity at lower pH condition and can be utilized as a cell protector and cancer cell killer.[179] Similarly, manganese oxide (Mn_3O_4) NPs exhibit SOD, catalase, and glutathione peroxidase (GPx)-like activity simultaneously.[180] Polyoxometalate-based nanozyme acts both as a protease and SOD-mimicking enzyme, which is used for the treatment of Alzheimer's disease.[181]

4.2. Calibration of Activity and Selectivity of Nanozymes

Selectivity of nanozymes is not likely to influence their propulsion, followed by catalytic energy transduction. Selectivity is decided by the functionalization of the nanozyme surface, which is usually chosen depending on their envisaged applications. Propulsion of nanozymes on the other hand is expected to primarily depend on the catalytic activity of the molecules. Functionalization of specific ligands, if somehow, inhibits the intrinsic catalytic activity of the nanozymes, the selectivity may then influence the propulsion. The calibration of activity and selectivity regulations of nanozymes has been achieved by careful manipulation of the intrinsic properties of the nanomaterials used to synthesize the nanozymes. This is schematically exhibited in **Figure 9**. The size is an important parameter in deciding the catalytic efficiency of the nanomaterials as smaller particle size results in a larger surface to volume ratio, which allows more active sites to participate in the catalysis. Among many interesting examples, the flower shaped Mn_3O_4 NPs[180] and 111-faceted Pd octahedra[182] exhibit enhanced catalytic activities compared to their counterparts with different morphology and orientation. The of structures are, therefore, crucial factors that could be manipulated to optimize the catalytic efficiencies of nanozymes.

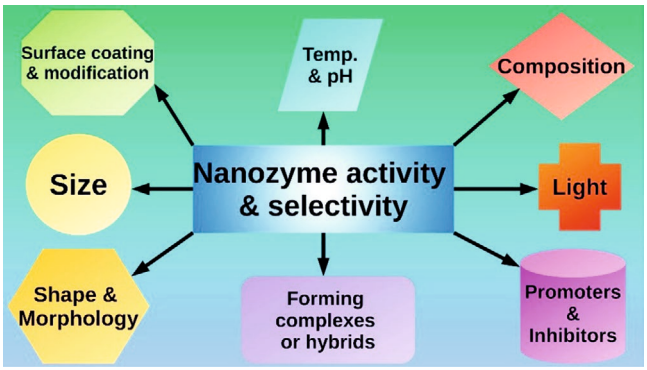

Figure 9. Schematic image of the calibration of nanozymes' activity and selectivity by temperature, pH, surface modification, size, shape, morphology, hybrid complexes, promoters, inhibitors, light, and composition.

Another essential factor is the composition that can control the enhancement of catalytic activity in nanozymes. For example, Pd–Ir cubes exhibited significantly enhanced efficiency, with catalytic constants more than 20- and 400-fold higher than those of only Pd cubes and horseradish peroxidase (HRP), respectively (**Figure 10**a).[183] Furthermore, experimental studies have been performed on nanomaterial conjugations to form interesting complexes and hybrid materials. For example Pt@CuMOFs integrated with hemin/G-quadruplex are reported to show enhanced peroxidase-like catalytic activity.[184] GOx/hemin@ZIF-8 is another interesting example of an integrated nanozyme, where GOx and hemin were added during the assembly of Zn^{2+} and 2-methylimidazole (Figure 10b).[185] Surface modification and coating with extra nanomaterials on nanozymes can also help in increasing significantly the catalytic activity of the latter. The coating of Au nanocrystals with heparin has been shown to enhance their peroxidase-like activity toward 3,3′,5,5′-tetramethylbenzidine (TMB) at neutral pH.[186] Similarly, modification of Fe_3O_4 MNPs with histidine resulted in a 20-fold increase in their catalase-like activity.[147]

Much like the way activators and inhibitors bind and control natural enzyme activity, catalytic efficiencies of nanozymes have been found to get influenced in the presence of various small molecules and ligands. This is illustrated by the incorporation of nucleoside triphosphates to enhance the oxidase-like activity of cerium oxide (CeO_2) nanoparticles.[187] Importantly, nanozymes offer a unique opportunity to selectively control its catalytic efficiency toward particular substrates by a careful choice of activators and inhibitors. An example of this was

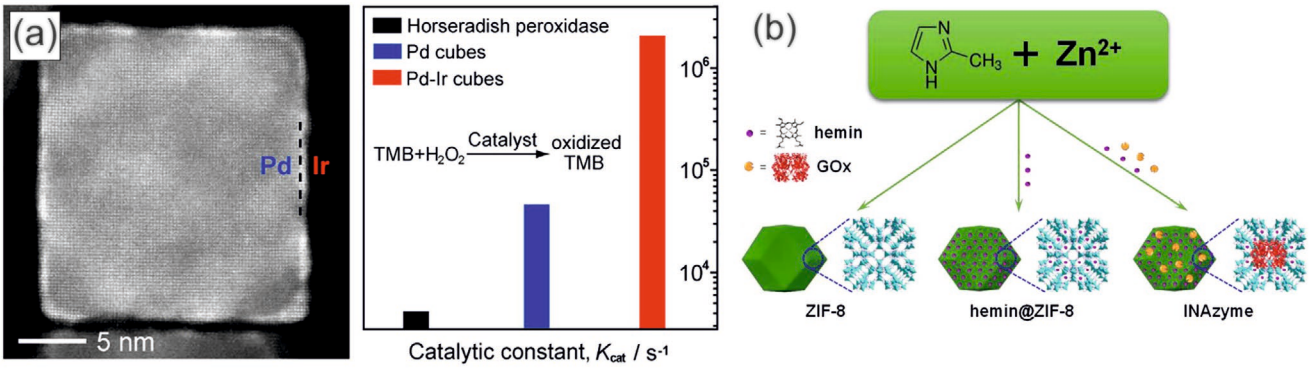

Figure 10. a) Pd/Ir core/shell nanocubes as efficient peroxidase mimics. b) Schematic illustration of the synthesis of GOx/hemin@ZIF-8 integrating nanozymes. a) Reproduced with permission.[183] Copyright 2015, American Chemical Society. b) Reproduced with permission.[185] Copyright 2016, American Chemical Society.

the catalase-like activity of ferritin-Pt nanoparticles, which decreased in the presence of NaN_3, while its catalase and SOD like activities—both became inhibited appreciably in the presence of 3-amino-1,2,4-triazole.[188]

As previously mentioned, pH and temperature are key parameters in the regulation of catalytic activity of nanozymes. For instance, $LaNiO_3$ perovskite nanocubes can be made to function like peroxidase only at pH 4.5 and temperature 55 °C.[189] Au NPs show the highest GOx-like activity at pH 6 and temperature 65 °C.[190] Besides all these factors, light has also been extensively used as an activator for enzyme-like reactions. It has been demonstrated that the peroxidase-like activity of 15 nm Au NPs gets enhanced by the irradiation of visible light of wavelength of 532 nm.[191] Doping with Pt has been found to enhance the photosensitization efficiency of graphite carbon nitride ($g\text{-}C_3N_4$).[192] Similarly, Au and Pd incorporated Bi_2WO_6 ultrathin nanosheets exhibited considerably higher photocatalytic activity compared to their non-doped counterparts.[193]

4.3. Applications and Opportunities

Despite the many advantages of nanozymatic systems such as their low cost, high stability, robustness, and biocompatibility, several challenges are required to be addressed before we realize complete application potentials of these novel nanomaterial systems. The catalytic activity and selectivity of most nanozymes are low compared to the natural enzymes. Surface functionalization, addition of ligands or coating is likely to decrease the catalytic activity further. One should also be careful in fabricating multifunctional nanozymes so that their inherent enzymatic activity does not get compromised, while infusing orthogonal features onto the structures. The surface functionalization techniques for nanozymes therefore need to be optimized for different enzyme mimics, resulting in molecules with robust catalytic activity and specificity. Toxicity of various nanoparticle systems under in vivo operating conditions also needs to be investigated carefully, especially when the molecules are likely to be used for biomedical applications. While traditional research on nanozymes has been performed by random investigation of enzyme-like activities of nanomaterials, it would be better if future research follows a focused and rational study of materials for specific enzyme-like activity and its dependence on their atomic composition and structure.[116] Bioinspired synthesis of nanozymes can also help in designing molecules with minimum or no toxicity, which could be safely recommended for medicine and therapeutic applications, where natural enzymes are often found to become denatured and degraded.

In terms of applications, newer designs of smart nanozyme devices are likely to replace existing enzymatic or inorganic systems. Doping with ions or molecules may enhance nanozyme activity drastically, which would find important applications in sensing and diagnostics. Liu et al. reported one such study recently where binding of fluoride ions has been found to result in 100-fold enhancement in nanoceria activity as oxidase.[194] Heavy metal ions like Hg^{2+} have been detected using tunable peroxidase-like activity of Au NPs. It was also found that in the presence of Hg^{2+} ions, 3,3′,5,5′-tetramethylbenzidine (TMB) peroxidation catalyzed by Au NPs was increased by 25 times.[110] Apart from ions, biomolecules can also be detected by regulated nanozyme activity.[195] In the future, nanozymatic systems are therefore expected to offer many colorimetric, fluorescent, and electrochemical detection platforms, revolutionizing both in vitro and in vivo detection of molecules and toxins under different experimental conditions.[195] Synergistic effects of multifunctional nanozymes would open up newer avenues in biomedical engineering and therapy. In a recent study, it was demonstrated that nanoceria, owing to its cytotoxic and anti-invasive properties, is capable of preventing tumor growth and invasion successfully.[196] Along with therapeutic applications, nanozymes have important prospects in the field tissue engineering. It was demonstrated that CeO_2 nanoparticles in poly(lactic-*co*-glycolic acid) (PGLA) scaffolds could induce aligned growth of stem cells.[197] Inorganic nanozymes consisting of metal oxides,[198] metal,[199] and non-metallic nanomaterials, such as CeO_2,[200] vanadium oxide,[201] Fe_3O_4,[202] TiO_2,[203] Au NPs[204] have been shown to have antibacterial activities. Clinical translation potential of these materials needs to be investigated in the future.

One of the possible applications of nanozymes that is yet to be explored is their potential usage as micro- and nanomotors. Natural enzymes have been found to behave as molecular motors capable of generating forces upon catalysis.[205,206] These systems constitute an important class of molecular active matter and display unusual dynamics such as chemotaxis

and dynamic coupling in solutions.[207,208] With improved biocatalytic activity, nanozymes are expected to constitute a novel class of self-powered systems, the behavior and dynamics of which would be important both from the scientific and technological standpoints. When functionalized over large polymer particles, nanozymes should also be capable of generating enough forces to impart motion into such particles—similar to what has been demonstrated earlier with natural enzymes.[9,209] This would result in active drug delivery strategies, wherein biocatalytic reactions would power molecular drug carriers in fluidic media. Multifunctionality of the carrier would facilitate interaction of the carrier with its surroundings, help it navigate autonomously through complex environments and transport payloads at designed locations without external interventions. Apart from biomedical applications, nanozymes would also find applications in detection of pollutants and environmental remediation, which are already receiving considerable attention. It has been demonstrated that Fe_3O_4 NPs may be used for detection of glucose and organophosphates.[195,210] Application of Pd@Au nanorods and NiO NPs have been shown in detection of contaminants like Malathion[211] and Parathion.[212] Nanozymes such as Fe_3O_4 NPs,[213] $BiFeO_3$ NPs,[214] VO_x nanoflakes have been used in decomposing molecules of Rhodamine B.[215] Decomposition of phenol has been shown using CuO NPs,[216] and FeOOH 2D nanosheets.[217] Nanozymes may also find interesting applications in chemical synthesis, biomedical device fabrication, and realization of logic gates. In a study, researchers prepared poly(DMAA-cross-BIS) hydrogel using peroxidase-mimic CuO NPs.[218] Along with the direct gelation initiated by CuO nanozymes, it has been shown that fluorescent polydopamine can be synthesized via Fe_3O_4 catalysis.[219] With improved physicochemical properties, nanozymes are expected to draw in expertise from diverse disciplines in the future and emerge as a new field of research in nanobiotechnology.[220,221] In recent years, nanozymes have found wide application in diverse areas such as biosensing, therapeutics, and fabrication of electronic devices using functional molecules (**Figure 11**). Numerous in vitro sensing applications have been developed using nanozymes for efficient detection of inorganic and biological molecules. Usage of Fe_3O_4 MNPs have been demonstrated for H_2O_2 and glucose detection.[195] Cerium oxide nanoparticles, also known as nanoceria (CeO_2) become luminescent upon doping it with Eu^{3+}, the fluorescence of which gets quenched in the presence of H_2O_2.[222] TiO_2 nanotube arrays possess intrinsic peroxidase-like activity,

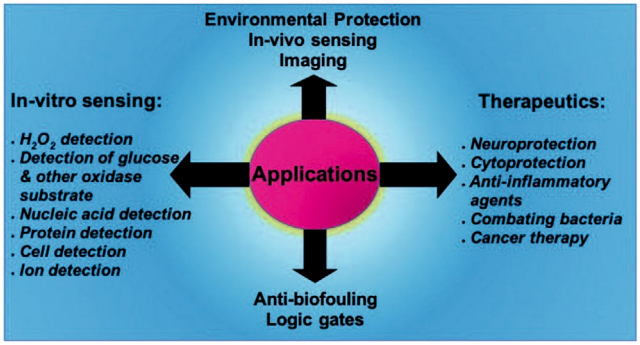

Figure 11. Schematic diagram of the applications of nanozymes in environmental protection, in vivo sensing, imaging, and therapeutics.

making it a simple and inexpensive sensor for both H_2O_2 and glucose.[223] NiPd hollow nanoparticles and GOx, immobilized simultaneously over zeolitic imidazolate framework 8 (GOx@ZIF-8(NiPd)) results in structures in the shape of nanoflowers having peroxidase-like activity and capability to serve as glucose sensors.[224] Graphene oxide@SiO_2@CeO_2 (GSCs) nanosheets showing peroxidase-like activity can be used as colorimetric bioactive paper.[225] MnO_2 nanosheets, which serve as artificial oxidase may be used for glutathione (GSH) detection using colorimetric analysis.[226] Pd@Au nanorod based biosensors may be used to detect malathion, which is an organophosphate insecticide.[211] Fe_3O_4 nanoparticles, owing to their intrinsic enzyme mimetic activity, were used to develop novel immunoassay where antibody modified Fe_3O_4 MNPs could be used in the capture, separation, and detection of molecules. To achieve improved biocompatibility, Fe_3O_4 MNPs were modified with various compounds like SiO_2, 3-aminopropyltriethoxysilane (APTES), polyethylene glycol (PEG), or dextran. Among them, dextran-modified Fe_3O_4 MNPs showed better catalytic activity and were even used for nanozyme-linked immunosorbent assay (NLISA), where it exhibited absorbance signal at 652 nm in the presence of hepatitis B virus surface antigens.[16] Fe_3O_4 MNPs have also been used in local diagnosis of Ebola virus (EBOV) through novel nanozyme-strip.[227] Besides in vivo sensing applications, nanozymes have been vigorously used in many in vitro detection, bioimaging, therapeutics studies such as in neuroprotection,[228] cytoprotection,[135,229] and also as anti-inflammatory[221,230] and antibacterial[218,231] agents. A light-controlled antibacterial hydrogel has been developed by mixing the photothermal nanomaterial graphene oxide (GO), a photobase reagent malachite green carbinol base (MGCB) and CeO_2 nanozyme into the agarose gel matrix as shown in **Figure 12**a.[190] A zinc-based zeolitic-imidazolate framework (ZIF-8) derived Zn–N–C single-atom nanozyme has been shown to be useful for antimicrobial applications (Figure 12b).[148] A self-assembly of MnO_2@PtCo nanoflowers-based nanozymes have been used in cancer therapy.[232] Nanozymes have also found useful applications in environmental protection,[216,233] anti-biofouling,[234] and fabrication of logic gates. Interestingly the color of nanoceria has been found to change from colorless to yellow in the presence of H_2O_2. Harnessing this property, a label-free, resettable, and colorimetric logic network was constructed utilizing biocatalytic reactions powered by CeO_2 nanoparticles (Figure 12c).[235] Likewise, "OR" and "XOR" logic gate operations have also been demonstrated by tuning catalase and oxidase-like activities of Au NPs with various metal ions.[236] Nanozymes have also been proved to have potential applications in UV protection,[237] antithrombosis therapy,[238] and bioorthogonal catalysis.[239]

As discussed, artificial enzymes or nanozymes have received considerable attention in recent years owing to their potential applications in diverse fields of engineering and science. Although much progress has been made in understanding the properties of nanozymatic systems and harnessing their cooperative functions of useful applications, the field is still in its infancy and is expected to lead to a substantial breakthrough in the future.[115,240] One of the major challenges in working with enzymatic systems is the need for very specific working conditions for high operational efficiency. Moreover, enzymes being highly delicate become denatured quite easily. Nanozymes may

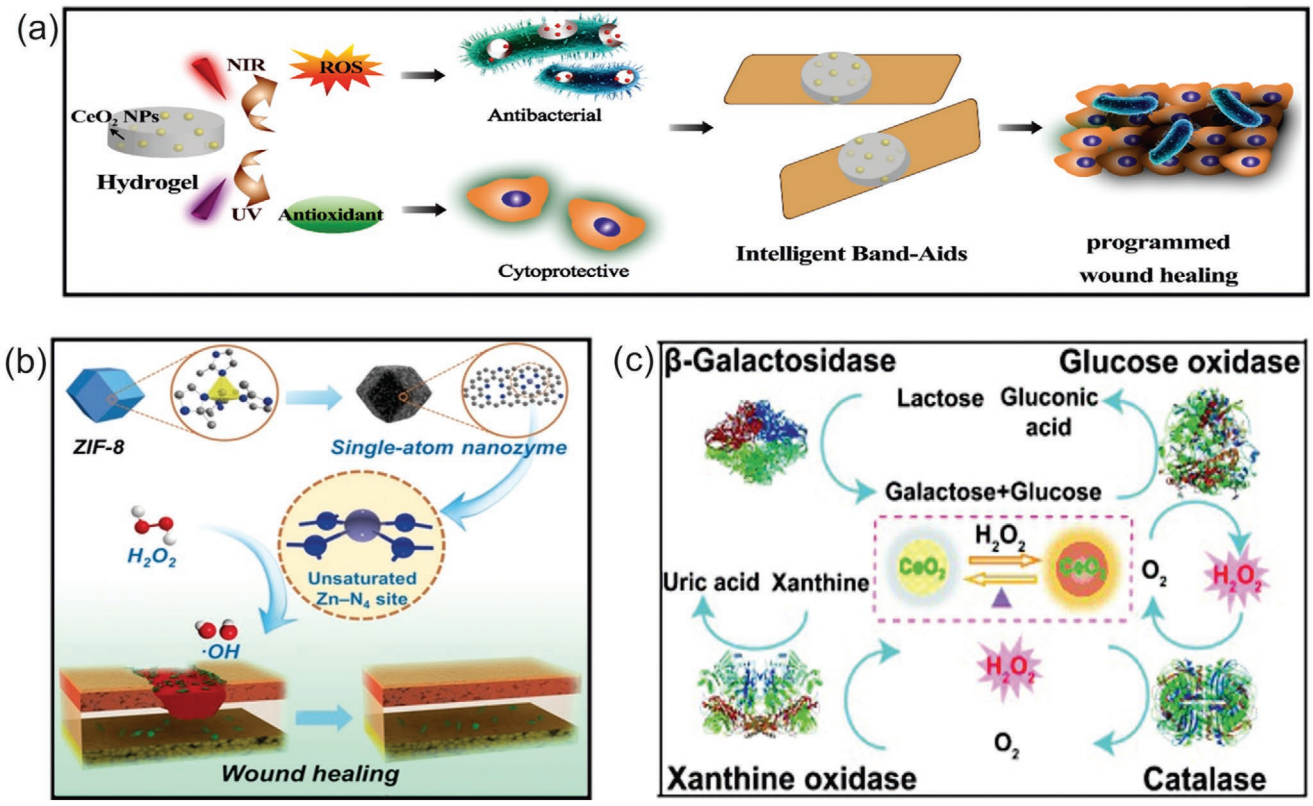

Figure 12. a) Schematic illustration of nanozyme-based light-controlled antibacterial hydrogel for wound healing. b) ZIF-8-derived Zn–N–C single-atom catalyst, which is considered to be an efficient single-atom nanozyme (SAzyme). c) Realization of logic gate operations based on nanoceria's biocatalytic reactions. a) Reproduced with permission.[190] Copyright 2017, American Chemical Society. b) Reproduced with permission.[148] Copyright 2019, Wiley-VCH. c) Reproduced with permission.[235] Copyright 2012, Wiley-VCH.

offer us a more robust system in understanding the catalytic mechanism of various enzymes under different conditions. Nanozymes coupled with functional biomolecules might offer us alternative pathways to study spatiotemporal dynamics of complex systems involving biological catalysts and macromolecules. Careful investigations involving experimental and computational studies are however required to understand the structural features and compositions of nanozymes and their corresponding energetics and catalytic efficiency. A combinatorial approach may be adopted to integrate nanozymes of different functionality or to combine natural and artificial enzymes for enhanced biocompatibility. Nanozyme may also be conjugated with other molecules and ligands to effectively decrease their biotoxicity. Nanozymes may be subjected to surface modifications in order to improve their substrate specificity. Fabrication of organelle and cell mimics with the help of nanozymes could be very useful for biomedical applications.[241] Nanozymes offer great promises to augment our understanding of single enzyme catalysis. It is expected that nanozymes owing to their specificity, biocompatibility, robustness and flexibility in operation would lead to smart technology development in diverse research fields. Much like complex natural enzymes, detailed study of nanozymes functions and their collective dynamics will open up new research directions in nanoscale science and technology. Energy transduction by active enzymes and their collective dynamics in solutions has recently been a focus area of research in molecular biophysics. In a series of experiments, it has been demonstrated that active enzymes, while turning over substrates generate enough mechanical force to enhance their own diffusion in solution.[206,242] The diffusive movement of the enzymes increased with increasing substrate concentration. Moreover, in the presence of an imposed substrate concentration gradient, enzymes collectively moved toward areas of higher substrate concentrations, displaying a novel example of molecular chemotaxis. Enzymes, being operative at very low Reynolds number conditions, has never been previously expected to display directional propulsion and to have energy transduction ability. The non-trivial collective migration of enzymes toward specific targets promised a variety of applications including targeted transport, sensing, and delivery. Besides functioning as a self-powered nanomotor, active enzyme molecules when immobilized over a surface have also been shown to generate enough mechanical forces to cause directional fluid pumping.[243] Although the fluid pumping could be attributed to the heat generated during catalytic reactions, the exact mechanisms behind enzyme diffusion enhancement and chemotaxis however still remain obscure. Repeating diffusion studies with functional nanozymes might shed light on these mechanisms since we will now have opportunities to construct the exact strictures with controllable functionalities, enabling us to understand the effect of various contributing factors independently. Large microscopic structures could be functionalized with nanozymes to realize catalytically drive micromotor assemblies and explore

the nature of physics governing their collective dynamics and interaction.[244] There are therefore immense opportunities to investigate the consequences of biomolecular activities over intracellular dynamics using nanozymes and look for possibilities regarding activity-induced interactions and processes, involving various cellular components.[207] Energy transduction ability of single nanozyme molecules offers ideal experimental platforms in this regard to look for active interaction pathways and emergent dynamics within the cells during catalytic chemical transformations. Nanozymes are, therefore, expected to open up a whole new avenue in active intracellular transport, assembly, and organization of components triggered by controllable catalysis and their influence on various physiological functions as well as the fate of various nanoparticles and therapeutic agents targeted to cells. Moreover, controlled release of encapsulated materials can be achieved using nanozymes, opening up a promising route for novel biomedical applications. Microcapsules degradation by enzymes was demonstrated in a pioneering work, where an external trigger for the capsules decomposition was not necessary.[245] Even shell-in-shell capsules were described as a tool for integrated and spatially confined enzymatic reactions.[246] Recently, encapsulation of the enzyme guanylate kinase on differently shaped calcium carbonate templates was achieved using layer-by-layer assembly.[247] Spatial confinement of nanozymes in silica-based hollow microreactors was previously demonstrated.[248] Diagnostic imaging needs to include non-invasive methods to help determine the causes of an injury or an illness. Since ultrasound is the most widespread imaging tool, it is necessary to integrate core–shell microcapsules with ultrasound imaging capabilities in order to track their motion effectively during cargo transport and delivery.

5. Core–Shell Structures for Biomedical Applications

Novel methods to produce core–shell structures integrating functions of micromotors, nanozymes, and microfluidics are the basis for the development of μ-BCMS. Dynamic bubbles/microbubbles, drops, and capsules can be produced with desirable chemical, mechanical, acoustic, and biological properties at reasonable quantities. Fabrication, properties, and applications of monodisperse capsules/microcapsules and bubbles/microbubbles are discussed using LbL assembly, drop-based microfluidics with examples including nanoparticle-functionalized/shelled microbubbles for US-driven imaging, theranostics, and hydrogel microcapsules for controllable reaction, separation, purification, and release of molecular species. When integrated with catalytic parts core–shell structures self-propel in chemical fuels.

5.1. Basic Principles of Core–Shell Structure Preparation and Functionalization

Core–shell structures are one of the most popular and widely studied objects to meet the current challenges of biomedicine, such as targeted drug delivery. However, researchers envision modern drug delivery systems not only to deliver molecular cargo to the targeted tissues or organs but also to enable us to track their delivery path. Thus, imaging modalities are also essential to consider. We can name two principal components of core–shell structures, such as the core and the shell, where the substance can be found in various phase states. Thus, the shell is represented by a liquid or solid condensed phase, while the core can consist of a different phase, as can be seen in **Figure 13**. Depending on the phase state of the core, we can suppose different functions of such structure.

One can see the direct influence of various nanoobjects included in the structure shell on obtaining the necessary imaging modalities in Figure 13: for example, the presence of magnetite nanoparticles leads to obtain magnetic resonance (MR) modality, the choice of gold nanoparticles or such organic dye as indocyanine green (ICG) provide the photoacoustic (PA) imaging properties; also Indocyanine green (ICG) can be implemented for fluorescent (FL) imaging. The combination of the therapeutic agent and targeting molecules leads us to obtain a successful agent for targeted drug delivery.

Nowadays, theranostics is one of the leading trends in biomedicine, and there are several requirements for such structures that should be considered for further implementation.[249] Thus, these structures should be visualized by one of the methods used in clinical practice, such as US imaging, magnetic resonance imaging (MRI), positron emission tomography

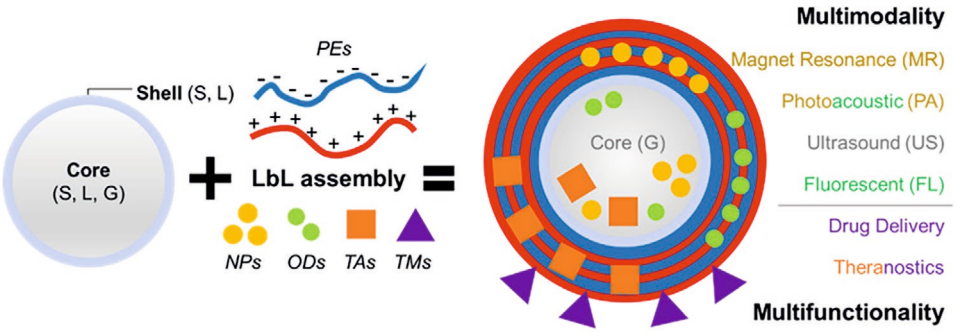

Figure 13. Schematic strategy for multimodal and multifunctional core–shell structures preparation. The core can consist of a solid (S), liquid (L), or gas (G) phase, and the shell can consist of a solid (S) or liquid (L) condensed phase. LbL assembly is used for the functionalization and performed with the use of negatively and positively charged polyelectrolytes (Pes). Functionalization can be obtained with the use of nanoparticles (NPs) (inorganic particles, such as gold, silver, magnetite, and carbon nanotubes [CNTs]), organic dyes (Ods), therapeutic agents (Tas), and targeting molecules (TMs) (such as aptamers, designed ankyrin repeat proteins [DARPins]) to obtain multimodality and multifunctionality as well as targeting.

(PET), computed tomography (CT), and optoacoustic or photoacoustic (PA) imaging modality, which is rapidly evolving for further preclinical and clinical use.[250–252] US imaging is the most popular technique, and the most sensitive structures for such a modality are structures, where the core consists of gas (Figure 13). Market-available contrast agents consist of hollow microcapsules and gas-filled microbubbles are widely used due to their excellent acoustic backscattering properties.

The possibility of performing contrast enhancement with the use of chemicals was reported in 1968: enhanced echogenicity of the aortic root after rapid injection of saline was due to the presence of microbubbles.[253] Nowadays, plenty of compounds are discovered, varying the scale of the object and choice of chemicals for preparation: phase-changing contrast agents (PCCAs), nanobubbles, nanodroplets, protein-coated gas vesicles, echogenic liposomes (ELIPs), still, microbubbles and microcapsules are considered precisely due to variety of promising paths in functionalization and multimodality and the highest proximity in the clinical use.[254] The rise in microbubbles development can be seen from the early 1980s, which lead to the development of the first commercially available agents in Europe and the USA, in 1991 and 1993, respectively.[255,256] Typically, the size of microbubbles varies from 1 to 10 μm, and the structure consists of the gas core (usual filling gases are: air, nitrogen, sulfur hexafluoride, and perfluorocarbons) and the shell made of lipids, polymers, or their combinations. Microbubbles are usually administered into the body by intravenous infusion of such a solution, and then bubbles can be found in the vasculature. The gaseous core is compressible enough, and the shape of bubbles deforms while passing through the capillaries or exposing by the US or PA signal. Under the action of a signal, the bubble shrinks and expands, and the backscattering of occurring radiation or cavitation or even the shell disruption can be observed, which gives the possibility of using these structures as contrast-enhancing agents.

Both the size distribution and mean size are essential for characterization: bubbles with the mean diameter of 2–5 μm (to avoid the risk of embolism bubbles should not exceed 10 μm) and uniform size distribution are usually required for the improvement of acoustic characteristics and dynamic response of bubbles.[29,257] The first generation of clinically available contrast agents are primarily filled with air, and the second generation involves the use of sulfur hexafluoride and perfluorocarbons for filling the core to improve the echogenicity and circulation time of such compounds. With the use of the sonication technique, the dispersion of 5% sonicated human albumin contained air-filled microbubbles were obtained.[256,258] This dispersion is known as Albunex (Molecular Biosystems Inc., San Diego, CA), the example of the first generation of contrast agents, approved by the U.S. Food and Drug Administration (FDA) in 1993. The first available on market contrast agent of the second generation, Optison (GE Healthcare AS, Oslo, Norway) obtained regulatory approval in the USA in 1998 and consisted of the improved formulation of Albunex with octafluoropropane (C_3F_8) gas core instead of air. Still, Optison has only been approved by FDA for left ventricular opacification in echocardiography.[259] The latest agent which have regulatory approval for human use in echocardiography and the first agent approved for use in liver imaging is Sonazoid (GE Healthcare, Oslo, Norway). Still, there is a lack of approval for clinical applications outside cardiology (especially echocardiography) for imaging, drug and gene delivery with relevant opportunities; thus, it is crucial not only to obtain contrast agent for precise imaging modality but to functionalize the structure further to increase the number of possible applications in biomedicine.

Therefore, LbL assembly is a promising approach for core–shell structures preparation and functionalization: self-assembly of the gas microbubbles in aqueous media followed by stepwise LbL deposition of oppositely charged polyelectrolytes onto resulting air core, accomplished in 2005.[260] To the best of our knowledge, the application of polyelectrolyte multilayers for air encapsulation and the formation of polyelectrolyte microcapsules with a gaseous interior in a simple and accessible manner was introduced for the first time. Also, hollow microcapsules produced by LbL assembly method, reported in 1998, are the promising basis for the contrast enhancement as well as obtaining multimodality and multifunctionality.[261] Then, numerous investigations on the use of LbL assembly were described to successfully obtain microcapsules as contrast agents for PA, FL, and MRI modalities with micrometer and sub-micrometer size.[262–266] To the best of our knowledge, there is no commercially available contrast agent based on LbL microcapsules; still, the possibility of multimodal microcapsules preparation is significantly increased with the use of the LbL assembly. Finding a convenient way to produce such contrast agents is one of the most intriguing questions. Also, the monodisperse size distribution and the possibility of targeting for multimodality opportunities are essential points to improve further the microbubbles and microcapsules.

5.2. Application of Ultrasound and Photoacoustic Technologies for Detection, Imaging, and Therapy

Nowadays, imaging is one of the fastest-growing research fields, and there are plenty of imaging modalities, which are used in preclinical and clinical studies: magnetic resonance imaging (MRI), positron emission tomography (PET), single-photon emission computed tomography (SPET), fluorescence tomography (FT), optical coherence tomography (OCT), ultrasound (US), and optoacoustic or photoacoustic (PA) imaging.[267] Thus, several parameters are important to consider for such a modality: deep penetration into tissue (penetration depth should be up to several centimeters), proper resolution (up to micrometers), and high sensitivity to contrast agents (up to $\times 10^{-9}$ M). In this section, US and PA imaging technologies are discussed. US imaging can be described by quantities of frequency, interaction with tissue, and attenuation. Typical medical US devices use sound waves in the range 1–20 MHz where the pulses are a millisecond or so long, and several thousands of pulses are emitted per second.[268,269] It is known that frequencies in the range of 2.0–3.5 MHz corresponds for transesophageal and transthoracic transducers, and frequency of 7.5–8 MHz or higher is used for the epicardial and intravascular probes.[269]

Usually, the US device combines technologies of image production (for example, 2D imaging) with Doppler assessment (continuous and pulse wave as well as color-flow mapping).[269] The most crucial thing in the device is a transducer, device (source and receiver of US), which is coupled to the patient skin accomplished by use of gel to avoid any air gap in between.

Transducers are used to convert electrical energy to mechanical energy and work on the piezoelectric effect: by the stimulation of an electric current, certain crystals in the transducer start to vibrate and produce US, thus, the transducer transmits US into tissue and listens for reflected US from tissue, and, returned echo converts into electrical signals, which are used for image formation.[270] The ideal transducer provides such characteristics as characteristic acoustic impedance, which perfectly matches that of the human body, high transmission efficiency, and high receiving sensitivity, wide dynamic range, and wide frequency response for pulse operation.[271]

In most cases, the initial pulse and returned echo relative intensities are important for imaging, and the amplitude of an echo produced by soft tissues at a boundary is few percent (0.2–1.08%) of the incident ones, in comparison with bones (49%) and air (99%) which limit the ability of imaging. Consequently, scanning at a high frequency can improve axial resolution, but tissue penetration will be lower and vice versa. Hence, there is a need for compromise between resolution and tissue penetration for the versatility of imaging uses.[268] The limitations for contrast resolutions can also be caused by processing speed, monitor resolution, and gray-scale perception of the eye. Since the pioneering research of medical US in the 1950s, including the earliest ultrasonic Doppler systems for measuring the blood flow[272] and the pioneering clinical application of the ultrasonotomography,[273] in the last decades, US imaging has been developed as one of the most promising method for in vivo hemodynamic evaluation with a unique combination of spatiotemporal resolution, sensitivity, and portability.

Behaving as a non-linear oscillator, the microbubble has been applied as an acoustic emitter with the advantage of contrast enhancement in ultrasonic imaging. Regarding the conventional US imaging, the brightness mode image is usually reconstructed after a sequential insonification using focused beams with high local pressure. Recently, instead of the focused emission strategy, a plane-wave imaging method (transmission of a wide-field wavefront and recording of backscattered echoes on the array) has been developed, which achieves the imaging rate typically faster than 1000 frames per second. Plane-wave imaging distributes the emission intensity over multiple excitations, which significantly reduces the peak energy pressure.[276] The advantage allows the continuous monitoring of microbubbles with improved contrast. Recent studies have already confirmed that ultrafast imaging can be used to monitor the moving trajectories of the microbubbles, leading to a super-resolution imaging of the microvessels. As shown in **Figure 14**a, the super-resolution ultrasound localization microscopy (ULM) imaging of the living rat brain vascular was obtained using a 128-element US linear array at a central frequency of 15 MHz and a wavelength of 100 μm. After continuous recording 150 s at a high framerate, the exact positions of the centroid of more than 1 000 000 microbubbles were localized from a stack of 75 000 images. Thus, the rat brain vascular imaging is obtained from the microbubble density maps with a spatial resolution of $\lambda/10 = 10$ μm, which surpasses the diffraction limit with a super-resolution imaging.[277] Similar experiments have been performed for the spinal cord. Figure 14b shows the vascular anatomy of the rat spinal cord using the ultrafast Doppler imaging and the ULM imaging in both sagittal and transverse imaging planes.[275] The recent development of new concepts, such as ultrafast ultrasound,[278] super-resolution ultrasound localization microscopy,[277] paves the way for microvessels imaging in the central nervous tissue with the great potentials for biomedical and neurobiology application, which has facilitated a new research field, so-called functional ultrasound neuroimaging.[279]

Also, it has been described that thermally induced US can be produced by the pulse of light absorption or electromagnetic radiation of microwaves.[271] PA imaging is a hybrid modality that combines the high contrast capabilities and spectroscopic-based sensitivities of optical imaging, and the high spatial resolution and tissue penetration capabilities of the US.[280,281] Here, a pulsed laser can be used for the transient pressure waves generation, which is received by a US transducer and processed for image formation. After the emission of the laser pulse, the generation of the PA signals can be generated by the optical absorbers, caused by thermoelastic expansion, within the field of view and then collected by a transducer.[280] By making measurements of the time at which the PA signal is received, and with the known speed of sound, the depth of the absorbing object can be evaluated, and the image can be formed as with conventional pulse-echo US.[281] For both modalities, the resolution is physically limited by the ultimate inverse relationship between the frequency of the US and the imaging depth. Similarities in the factors affecting on the resolution and in the construction of the devices for a US and PA imaging allows us to modify existing US systems to acquire PA signals and improve imaging capabilities by adding a pulsed laser source, modifying device and software to appropriately time the transmitted and received signals measurement and signal processing. The ability to penetrate tissue in several centimeters is one of the points to improve for PA imaging: a signal attenuation of several orders of magnitude makes the detection of US signals challenging due to their weakness. Current solutions include a careful choice of wavelength, optimization of the light delivery, and, as in US imaging, the use of contrast agents to improve the signal characteristics. The ability to generate robust and unique imaging signals by contrast agents is widely used for further applications. Additionally, multimodal contrast agents can be designed to take place for both US and PA imaging and therapy purposes.

5.3. Methods of Core–Shell Preparation: Bubbles/Microbubbles and Capsules

Plenty of techniques are carried out for obtaining bubbles/microbubbles and capsules: sonication, coaxial electrohydrodynamic atomization (CEHDA), and use of microfluidics chamber approach (T-junction and flow-focusing devices), which are promising approaches in getting uniform size of bubbles. Herein, we discuss only the most widely-used techniques.

5.3.1. Sonication-Assisted Fabrication of Microbubbles

Figure 15a shows the sonification process, where the tip of the ultrasonic generator is located at the interface between

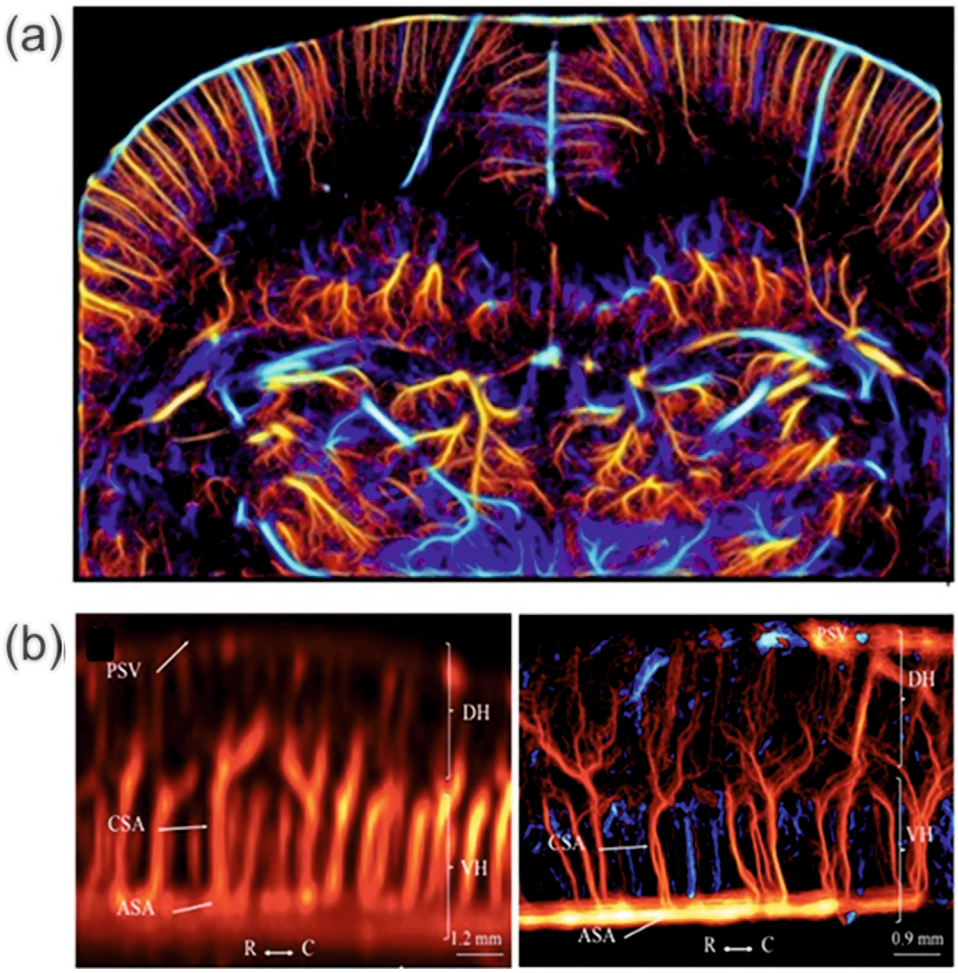

Figure 14. a) Super-resolution ultrasound localization microscopy (ULM) of the living rat brain down to the level of capillaries. b) Vascular anatomy of the rat spinal cord results in sagittal view ultrafast Doppler imaging and ULM imaging. a) Reproduced with permission.[274] Copyright 2018, IEEE. b) Reproduced with permission.[275] Copyright 2020, International Association for the Study of Pain.

the phases of the gas and the liquid future shell. The method allows to obtain bubbles of a wide range of sizes and can negatively affect the further use. As an example, the synthesis of stable and versatile lysozyme microbubbles was performed by high-intensity US-induced emulsification at low frequency (10–100 kHz) and further cross-linking of chemically reduced lysozyme in aqueous solution.[282] The mechanism of air-filled bubbles formation contained two phenomena based on US: emulsification and cavitation. Also to increase the stability of bubbles and to prevent further air dissolution from the bubble it is crucial to control the balance between the hydrophobicity and the number of sulfhydryl units in the solution for the cross-linking process. The flow-through sonication technique was described in 2012 for the synthesis of nano- and microbubbles: here active cavitation zone can be confined by choosing appropriate experimental conditions (for example, the configuration of the ultrasonic horn) and provide control on the size of bubbles.[283] Special attention should be paid to the diameter and type of the horn: the larger the active cavitation zone, the higher the inhomogeneity in power distribution. Lysozyme containing reactive thiol functional groups was used for the preparation of bubbles. Also, thermally denatured bovine serum albumin (BSA) can be used. Due to the covalent links formed between protein molecules by acoustic cavitation generating radicals—bubbles are produced. Microbubbles based on the use of lysozyme can be further functionalized based on the presence of the various functional groups (carboxylic acid, amine, thiol): plenty of compounds such as albumin (due to electrostatic and disulfide interactions), polyelectrolytes (PSS and PAH due to electrostatic interactions), other types of polymers (due to covalent bonding between amine groups in lysozyme microbubbles and aldehyde groups in oxidized dextran), and more.[284] Still, the use of a general ultrasonic synthetic procedure may not be possible for microbubbles and microcapsules synthesis of various shells. The method should be optimized for each case depending on the nature of the chemicals used for the shell preparation, as was clearly shown in the comparison of the physical properties of lysozyme- and BSA-shelled microbubbles.[285] As a way of optimization, sonochemical synthesis of shell-stabilized microbubbles was described: here, bovine serum albumin (BSA) was treated with Traut's reagent to convert primary amines to thiols before the

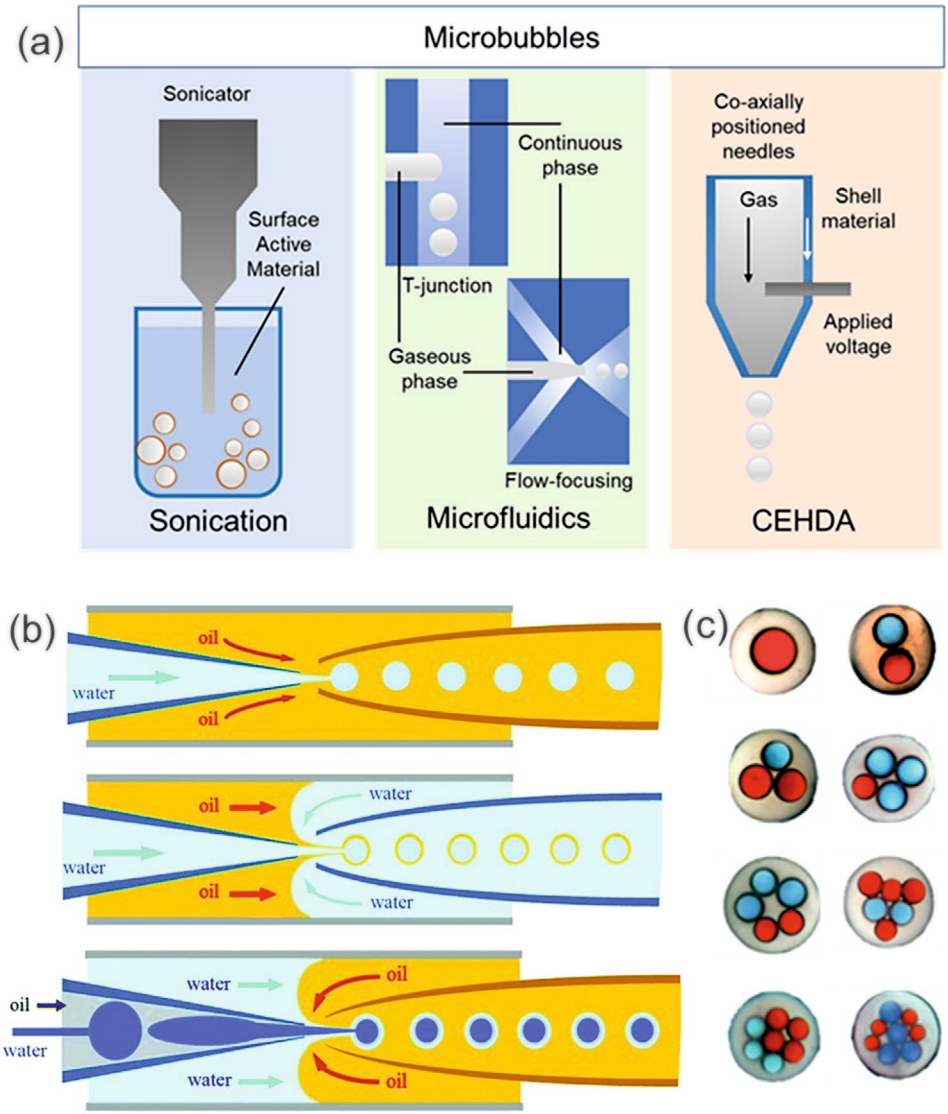

Figure 15. a) Strategies for the microbubbles preparation: sonication, coaxial electrohydrodynamic atomization (CEHDA), microfluidics chamber approach (T-junction and flow-focusing devices). b) Fabrication of emulsions using glass capillary microfluidics. Schematic illustration of the coaxial capillary microfluidic devices for generation of a single (W/O), double (W/O/W), and triple (W/O/W/O) emulsions. c) Optical microscopy images of multi-component double emulsions containing compartmentalized inner microdrops (stabilized by oils with surfactants or a molten wax). Emulsions are prepared using a single emulsification step. b) Reproduced with permission.[35] Copyright 2018, The Royal Society of Chemistry. c) Reproduced with permission.[287] Copyright 2012, The Royal Society of Chemistry.

synthesis procedure.[286] Such treatment leads to improvement in size dispersion of obtained microbubbles: agents were concentrated at median sizes of 0.5 and 2.5 µm, and the presence of free unbound thiols and primary amines on the surface implied the possibility of surface modification—strong gold-thiol bonding effect was examined.

5.3.2. Microfluidics-Assisted Formation of Emulsions

Emulsion represents a mixture of immiscible liquids—one immiscible liquid is dispersed in another liquid. Microfluidic devices assist with fabricating monodisperse drops in co-flow, cross-flow, and flow-focusing configurations. An understanding of droplet breakup depends on forces balance: viscous, inertial, buoyancy, and interfacial tension.[33] Microfluidic channels size and flow rates of the fluid can be used to change the diameter of generated droplets. Weber (We, i.e., the ratio of inertia and surface tension) and capillary (Ca, i.e., the ratio of viscous drag force and surface tension) numbers are dimensionless numbers used to describe the flow in the microfluidic channel. Viscous shear force is used to form drops in dripping mode using flow focusing and co-flow configurations. For example, the co-flow configuration glass capillary is inserted into and aligned with the continuous phase capillary, while the dispersed phase and continuous phase fluids flow in parallel. Figure 15b shows a typical co-flow device consisting of injection, transition, and collection tubes (e.g., two tapered capillaries assembled in

the larger square capillary) for the generation of water-in-oil and oil-in-water emulsion drops. Three capillary pumps are connected to pump fluids through capillaries and interstices between larger and smaller capillary, resulting in the coaxial flow. Capsules with the desired core and shell can be formed. A single drop can be dispersed in a third immiscible phase forming water-in-oil-in-water (W/O/W) or oil-in-water-in-oil (O/W/O) double emulsions. Figure 15c shows optical micrographs of multi-component double emulsions with a compartmentalized inner volume containing multiple drops (stabilized by oils with surfactants or a molten wax). Double emulsions are prepared by the single emulsification technique.[287] During the generation of double emulsions, the middle fluid change from dripping to the jetting regime using dual, triple, and quadruple bore injection capillaries. Subsequently, a thermal stimulus can be applied to melt the inner drops and cause their coalescence.

By fine-tuning the flow of several immiscible fluids, fabrication of various emulsions/microemulsions, drops, and capsules is possible, for example, monodisperse single/double-emulsion drops, emulsions with multiple inner droplets, topological complex emulsions, and Janus particles.[288,289] Although glass capillary-based microfluidics is more chemically inert than PDMS, drawbacks of glass capillary based microfluidics consist in the difficulty to prepare many devices at a time (devices are assembled manually), as well as the technique suffers from reproducibility, that is, precise control of capillaries' diameters and other geometrical parameters. Microdrop generator based on the PDMS is fabricated using standard photolithography/soft lithography and the method allows the creation of highly parallel arrays and devices using replica molding.

5.3.3. Microfluidics-Enabled Fabrication of Bubbles/Microbubbles

The microfluidics approach, where special microdevices are created for obtaining bubbles and capsules, provides precise control over the bubbles' size and the thickness of the shell. However, microfluidics leads to an increase in the cost of production.[290] T-junction devices and flow-focusing devices are the two main classes of microfluidic devices for microbubbles production; both are schematically presented in Figure 15a. Typically, T-junction devices can be obtained by mechanical assembly with the use of capillaries in units, and the flow-focusing technique requires the use of soft lithography.[291] Microbubbles obtained by microfluidic techniques with the flow-focusing approach: by a simple optimization of the channel geometry, lipid-shelled microbubbles with a mean diameter less than 5 μm can be obtained for US imaging.[292] Simultaneously, the T-junction approach is performed to obtain phospholipid-coated air microbubbles that had a mean diameter of 5.1 μm and the possibility to use in diagnostics and therapy.[293] The investigation of the effect on surfactant type and concentration on microbubbles size and stability was described for agents, which were produced by the T-junction device: four different surfactants were chosen, an anionic surfactant sodium dodecyl sulfate (SDS), non-ionic surfactants such as Tween 40 and PEG 40, and a cationic surfactant (CTAB) above the critical micelle concentration (CMC). Microbubbles coated with PEG 40, and Tween 40 had the smallest size, and the PEG 40 coated agents provided the highest stability. Still, for all surfactants, the increase in surfactant concentration leads to significant changes in bubble formation, size, and stability. As discussed in the reported paper, when the solutions containing different surfactants but the same physical properties (for example, approximately similar capillary numbers) are used, the wetting characteristic of the channel wall becomes interestingly important.[294] Recently, by formulating a gas mixture of a low and a high-aqueous solubility gas, highly stable and monodisperse microbubble suspension can be synthesized by the flow-focusing microfluidic chamber at high production rates and clinically relevant concentrations. Moreover, the foam formation was excluded by optimal gas proportion, which allows for the bedside production of readily stable monodisperse agents.[295]

5.3.4. Application of the Electric Field in the Synthesis

Coupled electrophoretic stabilization and electrochemical inflation as a synthesis approach, in which the microfluidic system has incorporated arrays of individually addressable electrodes. The system enabled potentials of 1–3 V to produce high electric fields due to the close inter-electrode spacing within the array.[296] The possibility of microbubbles synthesis was demonstrated with SDS, at concentrations higher than CMC. On the electrode surface, the relatively large micellar structures can be formed and immobilized, then micelles become infused with the electrochemically evolved gas to produce bubbles. The size and quantity of the microbubbles can be manipulated by adjusting the amplitude and duration of the applied potential. Coaxial electrohydrodynamic atomization technique (CEHDA) is a widely-used method of synthesis: an immiscible gas and a suspension for the shell preparation are contained in coaxial needles (inner and outer respectively), and a high electrical potential difference (several kV) is usually applied between the source of the flow (coaxially positioned needles), then a steady dripping stream of bubbles is formed at a stable cone-jet (Figure 15a). As a result, microbubbles and microcapsules are produced with a narrow size distribution between 0.5 and 10 μm and the ability of precise control over their characteristics.[297] For the synthesis process, a range of polymeric materials is used for the shell encapsulation due to their elasticity, electrical insulation, physical strength, and biodegradability.[64]

5.3.5. Microfluidics-Assisted Fabrication of Compound Nanoparticle-Shelled Microbubbles

Drop-based microfluidics can be used to fabricate stable monodisperse nanoparticle- and protein-shelled microbubble with optimal size, core–shell compositions, and desired shell properties (e.g., chemical, magnetic, optical, mechanical).[35] Bubbles coated with water-insoluble surfactants, phospholipids, or biopolymers have been reported to have significantly enhanced stability against dissolution.[288,298] Bubbles stabilized by colloidal particles, referred to as "armored bubbles," also are extremely stable due to the integration of a stiff interfacial material that stabilizes bubbles.[288,298] From these studies, it is

evident that the physicochemical properties of the bubble shell formed at the gas–liquid interface are critical in suppressing bubble dissolution, coalescence, and coarsening. Despite recent progress in the generation of engineered bubbles, and their applications,[288,298] most studies to date have focused on the synthesis and utilization of homogeneously modified bubbles. It is interesting to note that recent advances involving solid particles have shown that asymmetric functionalization of the particle surface leads to novel phenomena that are of fundamental and practical importance. It has been shown, for example, that the assembly of Janus particles—solid particles with polar and apolar hemispheres—leads to the formation of novel colloidal aggregate structures.[288,298] Besides, electrically or magnetically switchable systems based on Janus and patchy particles have been reported for applications in optical devices, self-propulsion, and emulsion stabilization.[288,298] This recent progress based on Janus and patchy particles suggest that asymmetric functionalization of gas bubbles could potentially lead to unique opportunities. Generation of engineered microbubbles and their applications has seen remarkable development in recent years.[299] Bubbles in a fluid tend to dissolve in time due to the high Laplace pressure across the air–water interface, limiting their long-term stability and utilization.[288,298] Stable compound microbubbles can be produced using the air-in-oil-in-water (A/O/W) emulsions (**Figure 16**a). These bubbles consist of hydrophobic silica (SiO_2) nanoparticles with a diameter of 10 nm, dispersed in oil, forming shell structure. In time bubbles are left in an aqueous solution, the oil evaporates and nanoparticles are self-assembled into a stiff shell, stabilizing microbubbles (Figure 16b). Subsequently, metallic/catalytic layers can be evaporated on nanoparticle-shelled bubbles for the demonstration of bubble-based micromotors in hydrogen peroxide solution (Figure 16c).[300] Nanoparticle-shelled microbubbles can withstand drying (SEM image, Figure 16d) and materials evaporation in vacuum (Figure 16e,f). Alternatively, magnetic, catalytic, optical nanoparticles can also be injected along with hydrophobic nanoparticles to form multifunctional bubble shell. However, glass capillary based microfluidics produce too large microbubbles (20-200 µm in diameter) for injection into biological vein/capillaries. Recently, a valve-based PDMS microfluidic chip was used to demonstrate recombinant protein-shelled microbubbles with a tunable diameter in the range from 1 to 10 µm (Figure 16f).[301] Such protein-shelled microbubbles, consisted of a mixture of an amphiphilic oleosin

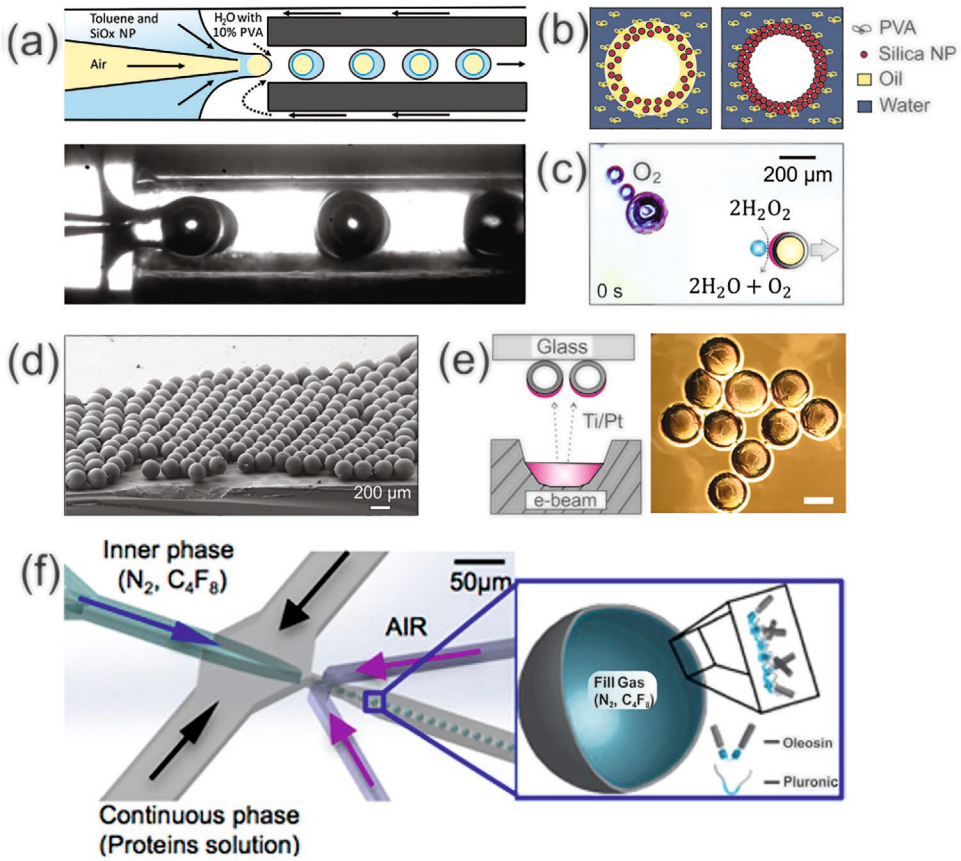

Figure 16. Fabrication of monodisperse compound microbubbles using microfluidic techniques. a) A flow-focusing glass capillary device is used to produce air-in-oil-in-water (A/O/W) emulsions. b) Schematic image of oil core drying and assembly of hydrophobic silica nanoparticles into stable shell. c) Motion of nanoparticle-shelled Janus micromotor (Pt was evaporated on bubble) in solution by the decomposition of hydrogen peroxide into oxygen and water. d) SEM image of dry silica nanoparticle-shelled bubbles. e) Schematic and optical microscopy images of e-beam evaporated metallic/catalytic layer on the surface of microbubbles. f) PDMS microfluidics is used to prepare recombinant protein-shelled microbubbles with tunable diameter. a–e) Reproduced with permission.[300] Copyright 2020, Wiley-VCH. f) Reproduced with permission.[301] Copyright 2014, American Chemical Society.

protein and a synthetic amphiphilic pluronic protein, with tailored echogenic response pave the way toward US-enabled biomedical imaging.[302] Subsequently, by mixing protein/copolymer mixture it was possible to achieve more stable and uniform bubbles than commercially available analogies.

5.3.6. Microfluidics-Assisted Fabrication of Monodisperse Hydrogel Microcapsules

Hydrogel microparticles have advantages over bulk hydrogels due to their properties of the controllable spatio-temporal release of drugs by diffusion, encapsulation of viable cells and injection ability in the desired part of tissue/organ during targeted drug delivery.[303] Soft hydrogel micromotors based on heterogeneous particles and capsules are fabricated using oil-in-water and complex water-in-oil-in-water double emulsion drops using a glass capillary microfluidic device. Thin-shelled hydrogel microcapsules containing aqueous core are prepared using glass capillary microfluidics device (**Figure 17**a).[11,17] Optical images of glass capillary device are shown in Figure 17b,c. Photopolymerization of the double emulsions leads to the formation of poly(methacrylic anhydride) hydrogel capsules with (photo)-catalytic nanoparticles in the aqueous core (Figure 17d).[18] Subsequently, microcapsules are hydrolyzed (at pH = 11) and form a poly(acid) structure of shells. Thin shells of capsules consist

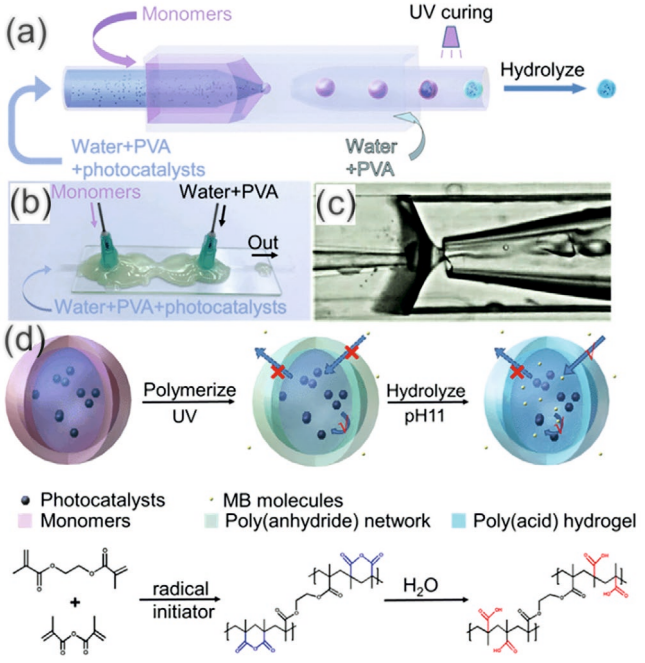

Figure 17. Fabrication of thin-shell hydrogel microcapsules containing aqueous core with encapsulated catalytic nanoparticles. a) Schematic image of glass capillary-based microfluidics with inner, middle, and outer flows. b) Optical image of fabricated glass capillary device. c) Optical microscopy image showing the formation of microcapsules. d) A stable poly(anhydride) network—the capsule's shell is formed upon photo-polymerization of ethylene glycol dimethacrylate and methacrylic anhydride mixture. Subsequently, hydrogel capsules are immersed in pH 11 to hydrolyze and form poly(acid) shells. a–d) Reproduced with permission.[18] Copyright 2020, The Royal Society of Chemistry.

of methacrylic anhydride hydrogels with unique properties, including permeations, separations, purifications, and reactions of molecular species. The microcapsule's shell remains permeable to small molecules capable to uptake nanoparticles/molecules (as cargo) and release them on demand using variation in pH. While nanoparticles larger than hydrogel pores can be encapsulated and remain permanently inside. Catalytic nanoparticles utilization leads to the demonstration of the chemical "microreactor" for controllable reaction, separation, purification, and releases of molecular species, i.e., for water cleaning applications[18] and potentially for biomedical nanozymes encapsulation. Due to diffusion/reaction enabled by ultra-rapid mixing of fluids, adsorbents/catalysts and organic/inorganic pollutants inside the microfluidic volume of microcapsules, it is feasible to enhance degradation, absorption, separation and filtering rates of pollutants. Potentially, a prototype flow microreactor device can be constructed for continuous conversion or removal of molecular species. Moreover, soft hydrogel micromotors containing catalytic nanoparticles in the liquid core or on the outer surface are demonstrated.[11] The balance of forces consisted of the micromotor's buoyancy, weight, motive, and lateral capillary attractive-repulsive interactions lead to specific dynamic behaviors.

5.3.7. Layer-by-Layer Assembly: Preparation and Functionalization of Core–Shell Structures

LbL assembly promises the possibility to create a shell around a particle not only with the use of electrostatic interactions between oppositely charged polyelectrolytes during sequential deposition, but a variety of other chemical interactions, including hydrogen bonding, biomolecule recognition, click chemistry, and sol–gel reactions.[304] Such techniques are often combined for maximum versatility, empowering the user to customize layers with maximum control over thickness, stability, release mechanisms and duration, while simultaneously protecting the functionality of the capsule of interest.

For instance, hollow microcapsules were fabricated by LbL deposition of polyelectrolytes, single-wall carbon nanotubes (SWCNTs), and gold nanoparticles (AuNPs) onto colloidal silica microspheres (**Figure 18**a).[266] After removal of the core, such capsules served as an excellent absorber in the near-infrared region of the spectrum and provided substantial enhancement in PA imaging in both water and blood.

Multilayered nanocomposites with gold nanorods (GNRs) as plasmonic nanoparticles and indocyanine green (IGC) as absorbing dye were obtained with the use of LbL assembly to combine PA and fluorescent modalities (Figure 18b).[305] The average diameter of microcapsules was 4 μm, and the dye was dispersed in a matrix of biodegradable polymers. It was mentioned that undoubted advantages of such capsules as high-loading capacity, the possibility of physical and chemical properties control, and a wide range of possible internal payloads could be taken into consideration. Also, synergetic PA effects for capsules were seen.

Increasing the efficiency of loading of functional nanoparticles or molecular substances into capsules is a vital point to improve and obtain more efficient drug delivery systems based

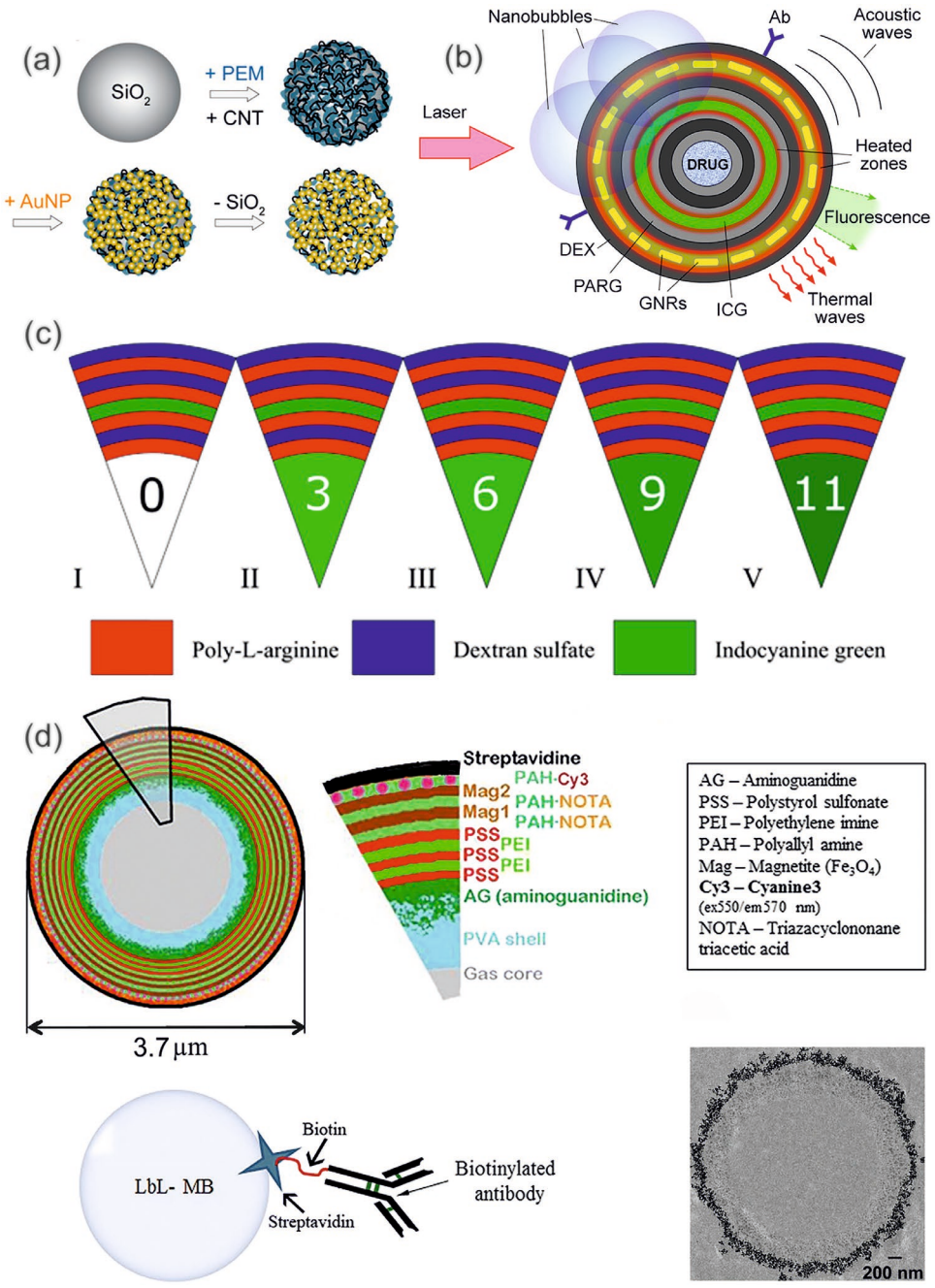

Figure 18. Microcapsules and microbubbles functionalized by LbL assembly. a) Fabrication of hollow microcapsules containing single-walled carbon nanotubes (SWCNTs) and gold NPs (AuNPs) for PA imaging. b) Schematic structure of drug-loaded multilayered nanocomposites (MNCs) as multimodal PA and FL contrast agents, containing antibodies (Ab), dextran sulfate (DEX), poly(L-arginine) (PARG), indocyanine green (ICG), and gold nanorods (GNRs). c) Schematic structures of the obtained bimodal PA and FL contrast agents containing bovine serum albumin (BSA) and indocyanine green (ICG): all samples have the same shell composition, but different numbers of the loading into the cores (I—without loading ICG and BSA into a core, and II, III, IV, V—with 3, 6, 9, and 11 ICG and BSA loading into cores using FIL, correspondingly. d) Schematic structure of microbubbles with potential for multimodal imaging (top). Microbubbles can be coupled to different antibodies via a streptavidin-biotin linkage (bottom left), TEM (bottom right) image of MB with two layers of superparamagnetic iron oxide nanoparticles (SPIONs) is provided. a) Reproduced with permission.[266] Copyright 2016, Wiley-VCH. b) Reproduced with permission.[305] Copyright 2016, Wiley-VCH. c) Reproduced with permission.[264] Copyright 2019, The Optical Society. d) Reproduced under the terms of the CC-BY Creative Commons Attribution 4.0 International License (https://creativecommons.org/licenses/by/4.0/).[306] Copyright 2019, The Authors, published by Springer Nature.

on microcapsules. Freezing-induced loading (FIL) is a method that provides a more efficient and controlled loading, as compared with other traditional approaches, such as adsorption from solution, coprecipitation method, and chemical vapor deposition. FIL method includes several successive steps: addition of microparticle and nanoparticle suspensions to a centrifuge

tube, freezing of samples under gentle mixing, thawing of samples, centrifugation of suspensions, and washing of suspensions with pure water.[307]

A combination of FIL and LbL assembly for the preparation of capsules with a high loading of bovine serum albumin (BSA) and magnetite nanoparticles (MNPs) for sensitivity to high intensity focused US (HIFU) was obtained. For successful in vivo tracking of capsules, BSA was labeled with Cy7. Thus, microcapsules contained near infrared (NIR) fluorescent labels in the shell and exhibited sensitivity to HIFU as well as the possibility of monitoring of the shell degradation by FL tomography: while HIFU destroys the capsule shell into small fragments with low fluorescent intensity, the accessibility of the shell to enzymes is enhanced and as a result, the intensity of fluorescence is increasing. Thus, we can detect remotely by FT the moment when drug release is obtained.[265]

Therefore, a bimodal contrast agent based on the self-quenching of IGC encapsulated in a biodegradable polymer shell was obtained in a similar manner, as can be seen in Figure 18c.[264] Using both FIL and LbL assembly, PA /fluorescent contrast agent achieved an increase in a local ICG concentration.

Air-filled microbubbles can be functionalized using LbL assembly as well as microcapsules, such contrast agents were described for multiple imaging modalities, including US, magnetic resonance, and fluorescence imaging. Poly(vinyl alcohol) (PVA) microbubbles with the diameter 3 μm have a LbL structure with a shell composed of layers of superparamagnetic iron oxide nanoparticles (SPIONs), metal chelating ligands, and a fluorophore-labeled polyelectrolyte, and an outermost layer made of streptavidin (Figure 18d).[306] The streptavidin surface also enabled conjugation of biotinylated ligands (peptides or antibodies) for improving the specificity.

Therefore, core–shell structures, including the microbubbles and the microcapsules obtained with the use of LbL assembly, have perspectives to be explored as promising multimodal and multifunctional contrast agents. Still, surface properties of agents may significantly effect on the stabilization, storage, and further development.

5.3.8. Microfluidic Layer-by-Layer Synthesis of Shells for Core–Shell Structures

As shown in a series of publications, in particular,[308] the use of microfluidics techniques has opened up new opportunities for LbL synthesis. For example, microfluidic layer-by-layer (MF-LbL) synthesis allows applying shells on individual cores with monodisperse sizes (solid nanoparticles, liquid microdrops or gas microbubbles) immediately after their formation in solution. On the other hand, MF-LbL synthesis allows combining microfluidics devices for generating cores and synthesis of shells on their surfaces. One of the undoubted advantages is also the ability to perform multi-stage MF-LbL synthesis in automated mode.

MF-LbL synthesis is based on the multiple and sequential treatment of cores with solutions of reagents and rinsing liquids inside the central device. This device is a unique microfluidics microchip with microchannels, where cores move in the flow of solvent (**Figure 19**a,b). The cores are traveling inside the microchannels, which have different zones filled with solutions of reagents and rinsing liquids. The chemical reactions take place on the surface of cores forming shells. These images show the one cycle of treatment resulting in the assembly of a monolayer of an insoluble compound on the surface. When the cores are moved sequentially through several marked zones, the thickness of such shell increases in proportion to the number of zones. Thus, an automatic synthesis can be obtained by using microfluidics microdevice with multiple processing zones. Advanced designs of microfluidics microdevices are proposed in the literature.[309,310] Thus, the authors[309] (Figure 19c) showed that cores are placed in the special comb withdrawal channel, for example, on the stage of removing reagent excess. It makes this process more effective. The original chip design is shown in Figure 19d. This design demonstrates the process of the multiple and sequential treatment of microparticles with solutions of reagents during their movement in a special array of channels each of which is filled with one of the reagents or a solvent. An important result was obtained in research,[311] where the core (namely the microdrop of water emulsion) inside microfluidics-microchip is placed in the specially shaped cup. Then, the sequential and multiple treatments of core with the reagent (oil–lipid mixture of dioleoylphosphatidylcholine (DOPC) dissolved in squalene) and rinsing liquid (water or squalene) is carried out. Starting from trapped water-in-oil droplets (Figure 19e), each phase-boundary crossing deposits a new monolayer of lipids on the immobilized droplets (Figure 19f–h). Due to the selected sequence of treatment with reagent and solvents a DOPC layer is formed on the surface of the microdrops—cytoplasmic aqueous phase (Q_{cy}) of tris-acetate-EDTA. Interestingly, the authors proposed that the layer can potentially mimic the phospholipid membrane of a living cell.

The original methods of MF-LbL synthesis were considered in the papers.[313,314] To simplify the automation system of the synthesis process, it was proposed to use planar chips with a laminar flow of each of the reagents separated by a laminar flow of the solvent. In the first method of these systems, shells synthesis was performed on the surface of microbeads (**Figure 20**a). Initially, the microbeads are directed into distinct parallel solutions of biotin and avidin (with washes in between) repeatedly building up an extended biological linker. Afterward, the microbeads are directed into the solution of FA, which results in fluorescence on the surface of the microbeads. In the second system, the cores were microdroplets of oil, which move between laminar flows of water solutions of reagents—polyelectrolytes poly(acrylic acid) (PAA), poly(vinylpyrollidone) (PVPON) and rinsing liquids—buffered aqueous solution NaOAc. The authors note that the use of the system, which is shown in Figure 20b allows getting shells after 6 processing cycles.

New opportunities of MF-LbL synthesis are previously proposed[316] using the synthesis on the surface of cores of SiO_2 and $CaCO_3$ of multilayers of polyelectrolytes—poly(styrene sulfonate) (PSS), poly(allylamine hydrochloride) (PAH) and poly(diallyldimethylammonium chloride) (PDADMAC). The authors suggested removing the excess of each of the reagents through the porous walls of a hollow fiber made from polyethersulfone, which is permeable to anions and cations,

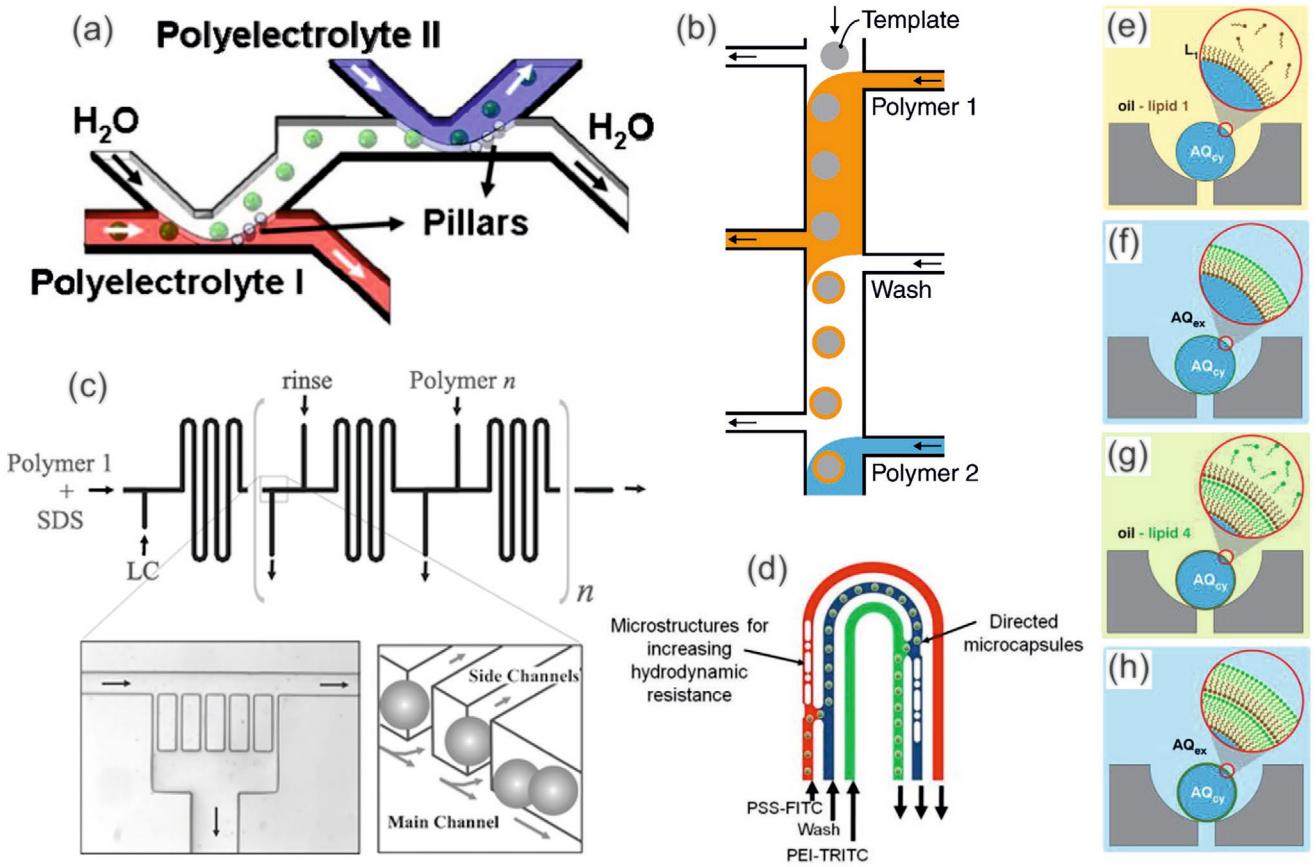

Figure 19. a,b) Microfluidic unit elements for continuous-flow LbL assembly. c) Schematic of the microchip design with images of the comb withdrawal channels. d) Schematic view of the device with capsules being assisted to transfer into adjacent channel due to less hydrodynamic resistance. e–h) Schematics of LbL assembly of phospholipid membrane on microfluidic AQ_{cy} droplets: e,g) Stages of AQ_{cy} droplets treatment with a solution of DOPC in squalene; f,h) Stages of AQ_{cy} droplets treatment with an aqueous buffer solution. a) Reproduced with permission.[312] Copyright 2008, Chemical and Biological Microsystems Society. b) Reproduced with permission.[34] Copyright 2014, Elsevier. c) Reproduced with permission.[309] Copyright 2008, The Royal Society of Chemistry. d) Reproduced with permission.[310] Copyright 2013, Chemical and Biological Microsystems Society. e–h) Reproduced with permission.[311] Copyright 2013, Springer Nature.

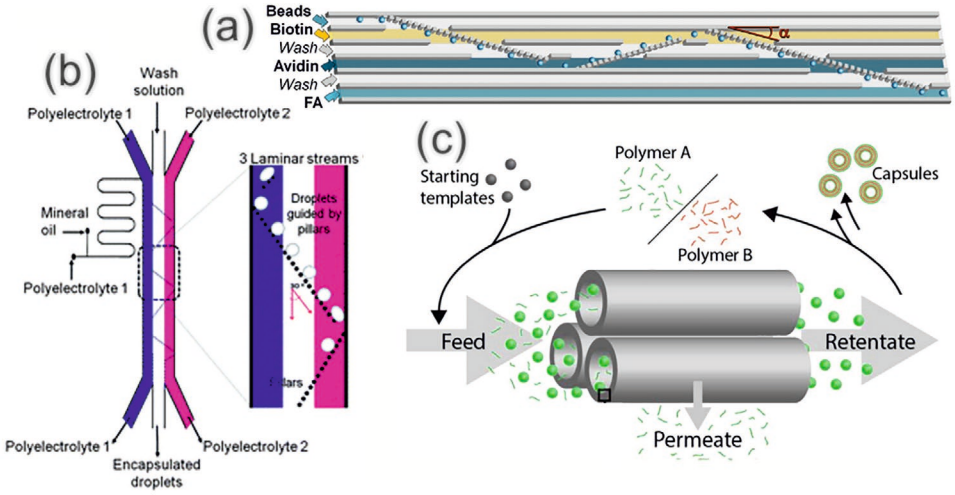

Figure 20. a) Conceptual illustration of the micropillar array railing system for continuous flow LbL microbead functionalization. b) Schematic representing the "microfluidic pinball" approach for generating droplets having six polyelectrolyte multilayers. The zoomed in region presents the droplets guided through three laminar streams along a row of micropillars arranged at an angle of 30. c) Hollow fiber tangential flow filtration LbL assembly of capsules. a) Reproduced with permission.[314] Copyright 2011, IEEE Chemical and Biological Microsystems Society. b) Reproduced with permission.[313] Copyright 2010, Chemical and Biological Microsystems Society. c) Reproduced with permission.[316] Copyright 2015, American Chemical Society.

but impermeable to larger capsules (Figure 20c). This method allows to simplify significantly the synthesis process itself. It is important that this system can be integrated with a device for dissolving the cores and filling the resulting hollow shells with the target substance. Thus, all steps to produce capsules can be performed in one technological cycle. It was suggested that this method has a great potential for practical applications because it can be used to create shells on cores from sub-micrometers to micrometers in diameter. In related work experiments concerning LbL synthesis of coatings on the surface of channels of microfluidics chips are demonstrated.[317] As a result, the contact angles of solvent wetting surfaces are changed, leading to the reduction of hydrodynamic resistance in the microfluidics channels.

5.4. Surface Properties of Core–Shell Structures

Investigations of surface properties may lead to increased stability, storage, and circulation time and further control of monodisperse size distribution and functionalization of such core–shell structures for various applications in biomedicine. The choice of lipids or polymers for the shell obtaining of bubbles or capsules can determine the properties of the surface: if the molecules in a shell are packed loosely or if the shell is not compact enough, the gas core may diffuse through the shell, and it decreases the stability of microbubbles dramatically.

5.4.1. Shell Properties

In the discussion about shell properties, let us start with the consideration of lipids: the elasticity provided by lipids to the microbubbles leads to the widespread use of lipids in their synthesis, which can be seen as a large number of lipids-based clinically-available agents (Definity, Sonovue, etc.). The effect of lipid hydrophobic chain length on dissolution behavior has been reported.[317] The gas permeation resistance monotonically increased with lipid hydrophobic chain length, and the lipid shedding behavior of the shell reveals mechanical effects. Still, it is unlikely to influence the transport of gas from the core if bubbles are immersed in a degassed medium that can be seen. When the process of dissolution occurs, lipids from the shell was shed continuously for the accommodation of the gas core shrinking volume by short-chain lipids. The investigation gives the possibility of controlling the dissolution rate for microbubbles with lipid monolayer shell.[318] A promising way for the obtaining of the compact lipid shell was further described: lipids can be heat-treated above their phase transition temperature and then quenched rapidly to room temperature to produce lipid structures. By this procedure, the lipid molecules are packed in a shell densely. The emulsifier is the essential component here because microbubbles do not form in the pure lipid solution.[319]

For the bubbles with the polymer shell, it was demonstrated that the stiffness and viscosity are mainly determined by the encapsulating shell, not by the air inside.[320] Also, optical observations exemplify that gas bubbles could be extruded and ejected through a shell defect while the shell appears to remain mostly intact. It shows that the behavior of polymer shell and lipid shell of bubbles are different in response to an acoustic pulse.[321]

For each type of microbubbles coating, the amplitude of bubble volumetric oscillation, resonance characteristics, and relative amplitude in tension and compression can be tuned and modified by the presence of the coating on microbubbles.[322] It was shown theoretically that the resonance frequency of microbubbles deviates significantly from the undamped natural frequency over the range of microbubble sizes due to the increased viscous damping coefficient.[323] Interestingly, from an experimental point of view, the viscosity mapping using molecular rotor fluorescence lifetime imaging provides a direct approach to the spatial distribution of viscosity quantification in the microbubble coating. A previously reported work provides direct evidence of a viscosity variation in the microbubbles cohort, which is correlated with their US response variability. These results were obtained with the use of fluorescent dye, BODIPY-C_{10}, which can be incorporated into surfactant coating.[324]

5.4.2. Biofunctionalization: Aptamers and DARPins As a Promising Basis

Both for microbubbles and microcapsules, the functionalization can be applied with the use of targeted ligands (proteins, peptides, antibodies, aptamers, and designed ankyrin repeat proteins (DARPins)) to obtain the selectivity property.

For instance, the microcapsule-based sandwich assay for the detection of proteins and nucleic acids was performed: $(PAH/PAA)_2$ microcapsules were cross-linked and coated with the adaptor proteins (protein A or streptavidin).[325] Such capsules are potent tools in Immunoglobulin G (IgG) antibodies binding, also further attachment of the major histocompatibility complex (MHC) class I proteins could improve the affinity to T cell receptors, and imagine the possibility of observing an immune response. The protocol of polymer capsules biofunctionalization with murine Y3 monoclonal antibodies is also provided in which imaging properties were achieved by loading of fluorescent molecules conjugated with bovine serum albumin (BSA) into the cavity of capsules.[326]

Another study demonstrated that peptides and antibodies could be employed by controlling the capsules surface chemistry: a conjugation of targeted peptide directed against metalloproteinase-2 (MMP2)-degraded collagen IV to the capsule surface by copper click functionalization can be obtained for plaque-targeted in vivo delivery; antibody-modified polymer capsules with the targets on the active form of antiglycoprotein (GP) IIb/IIIa receptors on platelet surface can be obtained for the delivery of thrombolytic agents.[327]

However, aptamers and DARPins are classes of objects of particular interest. Aptamers are single-stranded nucleic acids with tertiary structures for selective binding to a variety of targets. Both aptamers and antibodies demonstrate binding affinity in low nanomolar to picomolar range and act int the same manner by folding into a three-dimensional structure, which is based on their nucleic acid sequence, to bind the target. Therefore, aptamers surpass antibodies in several properties: binding of an aptamer is a highly specific interac-

tion, and aptamers are much smaller than antibodies, that can improve tissue penetration and clearance from the body.[328] Furthermore, from the industrial point of view, the production of aptamers is more comfortable to scale up and more economical. To the date, the only one aptamer gained the FDA approval for the clinical use is Pegaptanib, a pegylated aptamer that binds to human vascular endothelial growth factor (VEGF), for treating age-related macular degeneration (AMD).[329] Nowadays, biomarkers and cellular proteins such as integrins, prostate-specific membrane antigen (PSMA), and nucleolin can be imaged with the use of aptamer-based molecular imaging probes.

Using LbL assembly, functional aptamer films, and then microcapsules were prepared: aptamer-polyelectrolyte microcapsules as the triggered delivery microreactors were prepared from the sulforhodamine B aptamer. Such an aptamer was used due to the ease of detection of target binding by absorbance and fluorescence, and the ability to control the permeation of a target molecule through the capsule's membrane was shown by the use of aptamer.[330,331] Thus, aptamers can serve as molecular recognition agents and have the potential to serve as triggers of controlled release of payloads: with the use of the encapsulation of the aptamer, target-molecule-triggered rupture of $(PDDA/PSS)_5$ microcapsules was described and confirmed with microscopy techniques. One can observe the aptamer's sensitivity with the use of a similar dye, tetramethylrhodamine, which does not have the affinity for sulforhodamine B aptamers. Interestingly, aptamers encapsulation did not change the morphology of capsules, still, during the microcapsule fabrication process, about 30% of aptamers is lost.[332]

Also, the preparation of stimuli-responsive DNA microcapsules consisted of oligonucleotide layers cross-linked by an anti-ATP aptamer sequence is described: in the presence of adenosine triphosphate (ATP), the resulting complex with aptamer fragments the DNA shell and results in the cargoes release of biomolecules and nanoparticles. For this purpose, the release of semiconductor CdSe/ZnS quantum dots or the microperoxidase-11 biocatalyst is reported.[333] Since ATP is overexpressed in certain cells at different diseases (for example, cancer), the ATP-triggered release of loads may present the possibility of combining imaging and cancer treatment.

A computational modeling approach to maximize aptamer-microbubble binding to the target was described with the insight on key parameters for stable binding.[334] The first example of a stimulus-responsive contrast agent with the generation US signal only in response to levels of thrombin found in active blood clots was described.[335] In this study, aptamer-crosslinked microbubbles were designed to show the activation of US only at the level of thrombin represented the formation of the clots, and the binding of thrombin displaced the aptamers from the polymer–DNA complex, it can be useful for molecular imaging of thrombosis. Interestingly, another previous work described microbubbles with a network of cross-linkable oligonucleotides on the shell to create "smart" contrast agents that can be tuned using the properties of the encapsulating shell and control the nonlinear echoes generation.[336]

Unlikely, many aptamers have relatively weak binding affinities to their targets, and the promising strategy is the conjugation of aptamers with nanoparticles should improve the binding avidity and targeting efficacy. The use of A10 aptamer attached to thermally cross-linked superparamagnetic iron oxide performed as the MRI agent and a carrier for doxorubicin for combined prostate cancer imaging and therapy applications.[337] Also, magnetic beads as a captured substrate and gold nanoparticles decorated with aptamers were involved in a surface enhanced Raman spectroscopy (SERS) method for the identification of several sorts of exosomes.[338] To our knowledge, the use of a combination of aptamer and nanoparticles was not performed for a US and PA imaging with core–shell structures including microbubbles and microcapsules.

Also, DARPins are genetically engineered framework residues with the potential to bind any given target protein with high affinity and specificity, are derived from natural ankyrin repeat proteins, which are among the most abundant binding proteins found in the human genome.[339] DARPins, a novel class of non-IgG scaffolds, seems to be ideal ligands for targeting tumor-specific receptors due to their small size (13–20 kD), high solubility in water, stability at different experimental conditions, very high affinity to their protein targets.[340] Thus, DARPins seem to be the solution to the complexity and instability problems.

An experimental demonstration of this has been reported in which the DARPin_9-29, which specifically targets human epidermal growth factor receptor 2 (HER2), binds tightly to gold nanoparticles (GNPs).[340] HER2 is usually overexpressed in ovarian cells and breast cancer and obtained DARPin-GNP conjugate forcefully and specifically binds to the surface of SK-BR-3 cells that overexpress the HER2 receptor, and then internalize into these cells by endocytosis. Interestingly, as many as 35 DARPin_9-29 molecules are connected to the nanoparticle, and binding of the DARPins strongly increase the colloidal stability of the particles. Furthermore, DARPin_9-29 was covalently coupled to the membrane of small (80–90 nm) liposomes through a relatively long enough and flexible linker of 1.7 nm, which allows the DARPin to attain spatial orientation that favors high-affinity binding to HER2 receptor.[341] It is important to note, that electrostatic binding of proteins to the phospholipid membrane for efficient encapsulation is required.

Unfortunately, to the best of our knowledge, there are no contrast agents functionalized with DARPins obtained to the date. Still, more advanced structures included DARPins were synthesized nowadays: for example, the DARPin-PE40 targeted toxin consisted of 40 kDa pseudomonas exotoxin fragment linked with HER2-specific DARPin exhibited its high and selective toxicity against HER2-overexpressing tumor cells realized through apoptosis induction during in vitro studies, the antitumor effect was revealed in vivo.[342] Advanced solution, targeted toxin DARPin-LoPE composed of HER2-specific DARPin and a low immunogenic exotoxin A fragment lacking immunodominant human B lymphocyte epitopes tend to inhibit the growth of HER2-positive human ovarian carcinoma xenografts effectively. Low non-specific toxicity and side effects occurred, such as vascular leak syndrome and liver tissue degradation, as well as low immunogenicity, as was shown by specific antibody titer, still, the potential of use for targeted therapy of HER2-positive tumors was shown.[343]

One of the novel solutions that have not yet been used for core–shell structures like microbubbles and microcapsules to

achieve targeted delivery can be the use of a platform based on SiO_2-binding peptide that binds to the nanoparticle surface and protein adaptor system—Barnase*Barstar pair—serving as a "molecular glue" between the peptide and the attached biomolecule; thus, this method preserved the biological activity of the DARPin9_29 molecules attached to the nanoparticle and selectivity in the labeling of HER2-overexpressing cancer cells even in complex biological fluids as the whole blood.[344] Also, the implementation of magnetite nanoparticle stabilization with simultaneous modification by functionally active protein—Barstar was described.[345] For this purpose, a biocompatible Bs-C-Mms6 fusion protein containing the C-terminal part of the Mms6 (magnetite-binding protein of magnetotactic bacteria) and Barstar (an inhibitor of bacterial ribonuclease Barnase) was developed, and stable modified magnetite nanoparticles were obtained for further self-assembly with a fusion protein of Barnase and DARPin 9.29 through the interaction of high-affinity protein pair Barnase*Barstar. Hence, recent investigations involved the use of DARPins may become a promising direction of research. We are confident that the use of aptamers and DARPins will become the mainstream direction of surface functionalization due to the reasons of economic efficiency and excellent properties for binding with surface and targeting control.

6. Toxicity and Biodistribution Study

In the context of the development of promising contrast agents, toxicity and biodistribution studies are particularly important. Microcarriers (microcapsules, microcapsules, micromotors) are usually manufactured from biocompatible materials (lipids/proteins/polymers shell with gaseous/liquid/hollow core); they can be injected intravenously, and some are approved for clinical use or undergo clinical trials—two targeted microbubble formulations for tumor detection (ovarian/breast cancer) and liver lesion characterization have been clinically tested and found to be safe and promising.[346] Other agents are also currently under development for theranostics applications, such as liquid droplets, gas entrapping nanoparticles, monodisperse agents obtained by microfluidics, and phase-change contrast agents.[28] Herein, we provide recent results of studies of bubbles and capsules taken into considerations, also, interconnections of microfluidics and micromotors in the context of biodistribution will be covered.

6.1. Biodistribution of Microbubbles: Recent Advances

Previous investigations of agents for MRI should be taken into consideration. Such as biodistribution, kinetics, and biological fate of SPION microbubbles were provided in the Sprague–Dawley rats.[347] Microbubbles with PVA–shell consisting of superparamagnetic iron oxide (SPION) nanoparticles trapped with the use of LbL assembly had a diameter of 3.1 μm with narrow size range and were well dispersed. As flow cytometry verified, they were not aggregated and did not contain any debris. The analysis of microscopic tissue samples confirmed rapid uptake in the lungs and their redistribution to the liver and spleen over time. Also, microbubbles could be detected in the liver as early as 10 min post-injection, with the maximum signal detected between 24 h and one week after injection (**Figure 21**). In vivo studies demonstrated that the half-life in the liver was about 31 days (741 ± 219 h), and the presence of clustered bubbles predominantly in the lungs after 10 min was explained by histopathology studies. The loss of iron from microbubbles occurred gradually and had already appeared while the morphological integrity was still preserved. Such bubbles could be used for further multimodal imaging (US and MR combination) as well as a drug delivery carrier.

In situ characterization of microbubble contrast agents for the prediction of their behavior in biological milieu was performed for several types of microbubbles included microbubbles consisted of a shell of cross-linked PVA, and SPION microbubbles as discussed before, both of them were in the size range of 2–4.5 μm and performed similar surface curvature.[348] Flow cytometry was used here for the first time as a high throughput approach in microbubbles characterization dispersion prior and after exposure in different biological fluids: PBS or the biological fluid of choice, such as 6% human plasma, 10% bovine serum, full human plasma, and full human blood. The dose corresponded to a typical injection dose for in vivo imaging. Still, particle size and distribution were not significantly affected by the dispersion medium, and the number of human plasma bubbles withheld good stability. Also, it was

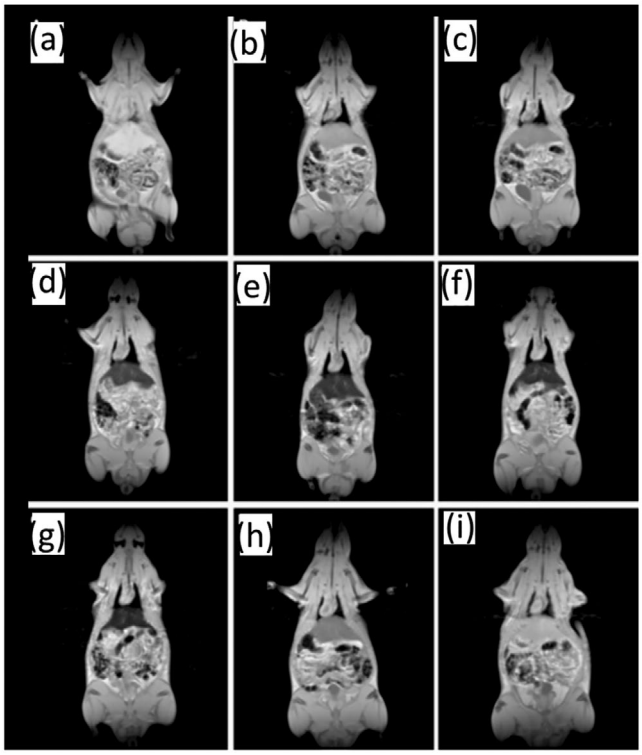

Figure 21. Dynamic MRI of a rat after injection of microbubbles: signal intensity changed mostly in the liver over time from 10 min to 6 weeks comparing with pre-injection. a) Pre-injection and at b) 10 min, c) 1 h, d) 24 h, e) 48 h, f) 1 week, g) 2 weeks, h) 4 weeks, and i) 6 weeks post-injection. a–i) Reproduced with permission.[347] Copyright 2013, The Authors, published by Dove Medical Press.

shown that agents existing in vitro conditions might indicate higher biocompatibility that is performed in vivo.

Nowadays, polysaccharides-functionalized polymer microbubbles were assessed with the ability to target P-selectin in thrombus with in vitro imaging and cytotoxicity investigations, in vivo model of $FeCl_3$-induced thrombosis on rat deep vein and US molecular imaging, and histological evaluations.[349] Polymer microbubbles made of degradable poly(IsoButylCyanoAcrylate) and functionalized with Fucoidan were designed and exhibited a size of 2–6 µm. A higher affinity of Fucoidan-microbubbles than control anionic microbubbles functionalized with CM-Dextran under shear stress conditions was presented in flow chamber experiments on activated human platelets, and in vivo analysis by US and histological results demonstrate that Fucoidan-functionalized bubbles were localized in rat venous thrombotic wall, whereas only a few CM-Dextran-microbubbles were seen. The binding of Fucoidan-microbubbles in a healthy vein is not observed, and it demonstrates the ability of specifically targeting P-selectin, and further applications as an imaging tool for cardiovascular events supported by overexpression of P-selectin, which contributes to the recruitment of leukocytes in areas of inflammation common in tumor vasculature.

Another article described the whole-body biodistribution of tumor-bearing mice for P-selectin targeted streptavidin-coated bubbles functionalized with antibodies.[350] A 3.2-fold enhancement of tumor retention of P-selectin-microbubbles was described in comparison with IgG-control-microbubbles; it confirmed the hypothesis that P-selectin targeting is beneficial for agents delivery to the tumor. At each time point, the lung and liver retention was significantly higher for the IgG-control-microbubble group; still, P-selectin-microbubble retention was more significant than the control group in the blood and tumor during the measurements. Interestingly, the importance of the control group during the whole-body distribution was highlighted due to differences in organs filtration of microbubbles and antibodies.

Also, perfluorocarbon-filled albumin microbubbles were taken into consideration, targeted to vascular endothelial growth factor receptor 2 (VEGFR2) and labeled with *N*-succinimidyl-4-[^{18}F]fluorobenzoate]-radiolabeled antibodies (^{18}F-SFB), evaluation in mice bearing human breast cancer was provided to prove bubbles as a probe for high-frequency ultrasound (microUS) as well as micropositron-emission tomography (microPET).[351] The choice of target supported by the fact that VEGFR is up-regulated on tumor vascular endothelial cells and overexpression of VEGFR1 and/or VEGFR2 is associated with angiogenesis (the growth of new blood vessels) and tumor progression in several tumors. Therefore, the mean tumor-to-muscle tissue ratios in living mice in the microPET image and in the ex vivo biodistribution were about 2.6 and 3.2, respectively, at 5 min, and about 2.4 and 2.7 at 60 min, and the specificity of the binding to the target was validated with the use of microUS. Results of whole-body distribution provided that most of the agents accumulated in the liver (16.31% ID g^{-1}), lung (5.72% ID g^{-1}), and spleen (3.59% ID g^{-1}) at 60 min, still, the peak uptake by the liver was lower than for the lipid-shelled bubbles. The lifetime is 30 min in the blood pool and high tumor-to-muscle tissue uptake ratios prove such agent as a promising probe for US-mediated therapy for breast tumors. To the date, a contrast agent (BR55), where the ligand is targeted to VEGFR2, is underway of clinical trials for prostate cancer treatment; still, there are plenty of angiogenesis markers such as B7-H3 (CD276), thymocyte differentiation antigen 1 (Thy1), E-selectin, and nucleolin.[352] With an F3 peptide targeted to nucleolin, microbubbles were created and compared the performance with non-targeted ones both in vitro and in vivo: the tumor image intensity was enhanced by 4.4-fold targeted agents, and F3-conjugated microbubbles accumulated on tumor vasculature for tumor with the size of 2–8 mm.

One of the most common ways to vary drug targeting is the possibility to vary the polymer material, and the most common polymer material as a shell is PVA. The biological fate of PVA microbubbles in CD1 mice was assessed by coupling a NIR fluorophore on the shell.[353] Thus, microbubbles accumulated mainly in the liver and spleen at 24 h after IV injection. Also, limited ultrastructural alterations were monitored in the kidneys, lungs, and liver 10 min post-injection, but after one month, they were fully recovered.

6.2. Microcapsules (Shells) Biodistribution and Toxicity

While investigating the multilayer composite magnetic microcapsules as targeted delivery systems; in vitro and in vivo studies under conditions of the living organism are provided.[354] A real-time observation of in vivo trapping of the capsules was observed for the first time in conditions, where capsules were injected in rat mesentery microvessels and exposed by the external magnetic field. Intriguingly, for in vitro studies, artificial glass capillary was performed with the wide-field fluorescence microscope employment.[355]

With the LbL assembly, both fluorescence and response to the magnetic field properties were achieved, separating layers with corresponding components by polyelectrolyte bilayers to prevent quenching. The magnetic field can effectively retain the microcapsules, still, in vitro studies explained that the capsules did not attach to the capillary wall, but they remain on the vessel wall after switching the magnetic field off in vivo, in a rat mesentery microvessel. Histological analysis showed the infiltration of capsules into small vessels, while large veins remained unblocked for blood passage. Reported results showed that the potential of multifunctional capsules as delivery systems with remote control, and the multimodality can also be achieved.

One can ask a question: where and when do microcapsules accumulate in organisms? Studies of systemic administration of capsules made of biodegradable polymers and magnetic nanoparticles were provided after IV injection in rats, collecting data of kidney, liver, lung, and spleen.[354] For the liver, the dissolution of the capsules in the Kupffer cells was noted after 24 h of injection, the release of the hepatocytes into the eosinophilic cytoplasm was not marked; the concentration of magnetite dropped sevenfold lower than at the highest value within a week. Maximum changes in lungs were observed after 4 h after injection: clear congestion of large vessels and focal hemorrhages and peribronchial eosinophilic infiltration were observed, still, after 24 h such effects were reduced; the appearance of a large number of lymphocytes was noted after one month after injection, infiltrates had location around bronchus,

and a marked allergic reaction was observed during all time intervals. As for spleen, pronounced congestion and increase in the number of capsules were observed after 4 h after injection, and the most significant accumulation of microcapsules was noted after 24 h—after this interval, the concentration of magnetite was two times higher than in the liver. For kidneys, the maximum changes occurred 24 h after injection, still, capsules passed through the urinary filter, and their contents were reabsorbed from the urine. The maximum changes for heart occurred within 1 h after administration, but most of them reduced after 4 h after injection. Therefore, the absence of marked toxicity in the internal organs was observed: generally, the integrity of capsules was lost over 24 h due to degradation, but traces of nanoparticles can be seen at 7 days in the spleen and liver.

In search of delivery vehicles (core–shell structures) to the respiratory portion of the lung, sub-micrometer vaterite particles can be used: particles with a diameter of 3.15, 1.35, and 0.65 μm were produced with three methods of production and were assessed.[356] All of them were able to enter the lung and deliver the loaded material. Still, the tiniest ones promised mostly as a delivery mechanism due to the possibility of achieving the respiratory portion of the lungs. Also, the time of recrystallization depended on the number of polyelectrolyte layers, which is vital to take into consideration, and a slow-release mechanism for large molecules can be provided by such particles. Investigation of even tiniest capsules was provided recently: polymeric capsules were obtained on a 500 nm template and further compacted down to 250 nm in diameter for the promising use in lung cancer therapy.[357] Delivery of low-molecular-weight drug molecules to lung cancer cells and macrophages was provided, and the internalization of capsules by macrophages and epithelial cells of the lungs and liver was observed with efficacy higher than 75%. Notably, better retainment of small capsules by tumor lungs was demonstrated in comparison with the healthy lung tissue with the use of in vivo mouse model of lung cancer. Such advances and the possibility of obtaining multifunctionality, varying layers number, and composition, must be taken into further consideration. However, further use of capsules with such a diameter for contrast enhancement in imaging is required.

6.3. Microfluidics As a Promising Approach to Achieve Microcarriers Biocompatibility

The microfluidics approach allows the control of the reagents needed for microcarrier production. The ability to produce highly monodispersed and uniform probes remained the most relevant to ensure accurate dosing of a given drug and to maximize delivery efficiency.[291,358] Recent advances significantly improve microfluidics applications: since the use of organic reagents in traditional water-in-oil (W/O) systems-based microfluidics can limit biomedical applications, the use of monodispersed water-in-water (W/W) droplets production approach was recently described.[359] Even materials used for microfluidic device fabrication can be biocompatible: the use of biopolymeric materials (collagen, silk) and polysaccharide hydrogels (chitosan, alginate) enable microfluidic devices with versatile functionalization chemistries, prescribe options of automated valves and drug release systems.[360] Recently, fast bubble-driven micromotors powered by biocompatible fuels (low-concentration fuels, bioactive fluids, and enzymes) were reviewed.[361] Advances of in vivo studies of micromotors were carefully reviewed recently: demonstration of targeted drug delivery, enhanced tissue penetration, and payload retention capabilities were described.[362] Biocompatibility of such carriers was improved in recent years with the use of microfluidics: as an example, the first enzyme-driven gel micromotors based on soft biocompatible materials (oil, PEGDA, and dextran) and obtained by the microfluidic-involved assembly was reported in 2018.[363] Thus, high achieved biocompatibility of microcarriers can be used for their further transition to practice, while microfluidics become a promising production method.

7. Conclusions

μ-BCMS can combine versatile methods of motion control of chemically/externally-powered micromotors, nanozyme-enabled integration with biomaterials using catalytic reactions, high-throughput fabrication using microfluidics, and modern ultrafast super-resolution biomedical imaging methods for a controllable uptake, encapsulation, reaction, diffusion, separation, release, and delivery of molecular species. Microfluidics enables the fabrication of biocompatible, biodegradable, biomedical micromotors with monodisperse size. Instead of searching for biocompatible reactions, nanozymes can be applied as motive power for micromotors. This approach helps to solve the problem of catalytic reactions integration with biomaterials. Several examples of μ-BCMS fabrications are discussed. For example, μ-BCMS can contain a functional gaseous or liquid core with specific functionality, the modality of contrast, and target. Shells of μ-BCMS can consist of functional materials such as a pH-responsive hydrogel, nanoparticles, and proteins. Subsequently, the first demonstration shows that an integration of catalytic nanoparticles in the core or liquid shell helps to achieve self-propelled motion (by decomposition of hydrogen peroxide into oxygen and water) and relevant operations of chemical micromotors. Moreover, control over the encapsulated gaseous core (size, stability, dissolution time) of microcarriers is essential for the biomedical US.[252] For instance, the combination of bubbles containing oxygen with photodynamic dye in the shell is a promising approach for realizing effective photodynamic and sonodynamic therapies.[364] If an additional PA modality is required to contrast the core–shell structure, the chromophore adsorbed light at a defined wavelength can be added. The chromophore role can play inorganic nanoparticles like gold, magnetite nanoparticles, or fluorescent dyes like indocyanine green.[262,264,266,305] It is necessary to remark that indocyanine green is already FDA improved for clinical applications.[365] The presence of magnetite nanoparticle in the shell provides an opportunity to realize the MRI contrast in both T1 and T2 modes, as well as navigation mode obtained by the magnetic field gradient.[262,354] The liquid phase for core preparation is also promising for hydrophobic drug encapsulation.[366] Another advantage of the liquid core is a possible phase transfer from the liquid to the gas using laser

or HIFU induced heating. This phase transfer can drastically increase the US and PA signals from contrast agent or drug delivery system. The shell can be used not only for stabilization or encapsulation of drugs during the continuous release but also for encapsulation of active substances such as photodynamic dyes, cytostatic drugs, and molecular species in gene therapy siRNA, DNA, DNA plasmid.[251] It was described above that promising vectors of core–shell structures are aptamers and DARPins.[330,332,333,335,340] Surface functionalization of core–shell particles by PEG and related vector molecules like aptamers and DARPins provide the methodology to increase the circulation time and realize targeting functions.[329,342] Hence, a combinatorial approach paves the way toward advanced engineering of μ-BCMS with desired properties of core–shell structures, dynamic responses, specific targeting, and optimal contrast imaging modes for diagnostics and therapy.

Acknowledgements

J.M. and J.L. contributed equally to this work. The authors thank the financial support from the National Natural Science Foundation of China grants (51961145108 and 51475093), the Shanghai Natural Science Foundation (No. 19ZR1402700), Science and Technology Commission of Shanghai Municipality, the Program of Shanghai Academic Research Leader (19XD1400600). This work was also supported by the Russian Foundation for Basic Research (RFBR grant 19-53-80047 BRICS_t) and German Research Foundation (DFG) grant MA 5144-1. K.K.D. thanks SERB, India (ECR/2017/002649), DST, India (DST/ICD/BRICS/Pilot Call 3/BioTheraBubble/2019), and IIT Gandhinagar (IP/ IITGN/PH/ KD/201617-10) for financial supports.

Conflict of Interest

The authors declare no conflict of interest.

Keywords

microfluidics, micromotors, nanozymes, optoacoustics, ultrasound

Received: November 1, 2020
Revised: December 27, 2020
Published online:

[1] J. Ou, K. Liu, J. Jiang, D. A. Wilson, L. Liu, F. Wang, S. Wang, Y. Tu, F. Peng, *Small* **2020**, *16*, 1906184
[2] J. Wang, *Biosens. Bioelectron.* **2016**, *76*, 234.
[3] F. Peng, Y. F. Tu, J. C. M. van Hest, D. A. Wilson, *Angew. Chem., Int. Ed.* **2015**, *54*, 11662.
[4] W. Xi, A. A. Solovev, A. N. Ananth, D. H. Gracias, S. Sanchez, O. G. Schmidt, *Nanoscale* **2013**, *5*, 1294.
[5] M. S. Draz, N. K. Lakshminaraasimulu, S. Krishnakumar, D. Battalapalli, A. Vasan, M. K. Kanakasabapathy, A. Sreeram, S. Kallakuri, P. Thirumalaraju, Y. Li, S. Hua, X. G. Yu, D. R. Kuritzkes, H. Shafiee, *ACS Nano* **2018**, *12*, 5709.
[6] M. A. Tabrizi, M. Shamsipur, R. Saber, S. Sarkar, *Biosens. Bioelectron.* **2018**, *110*, 141.
[7] a) E. Gultepe, J. S. Randhawa, S. Kadam, S. Yamanaka, F. M. Selaru, E. J. Shin, A. N. Kalloo, D. H. Gracias, *Adv. Mater.* **2013**, *25*, 514; b) T. G. Leong, C. L. Randall, B. R. Benson, N. Bassik, G. M. Stern, D. H. Gracias, *Proc. Natl. Acad. Sci. USA* **2009**, *106*, 703.
[8] X. Ma, A. Jannasch, U.-R. Albrecht, K. Hahn, A. Miguel-López, E. Schäffer, S. Sánchez, *Nano Lett.* **2015**, *15*, 7043.
[9] a) X. Ma, X. Wang, K. Hahn, S. Sánchez, *ACS Nano* **2016**, *10*, 3597; b) K. K. Dey, X. Zhao, B. M. Tansi, W. J. Mendez-Ortiz, U. M. Cordova-Figueroa, R. Golestanian, A. Sen, *Nano Lett.* **2015**, *15*, 8311.
[10] Y. Zhang, H. Zhu, W. Qiu, Y. Zhou, G. Huang, Y. Mei, A. A. Solovev, *Chem. Commun.* **2018**, *54*, 5692.
[11] H. Zhu, S. Nawar, J. G. Werner, J. Liu, G. Huang, Y. Mei, D. A. Weitz, A. A. Solovev, *J. Condens. Matter Phys.* **2019**, *31*, 214004.
[12] Y. Yu, L. Shang, W. Gao, Z. Zhao, H. Wang, Y. Zhao, *Angew. Chem., Int. Ed.* **2017**, *56*, 12127.
[13] R. Breslow, L. E. Overman, *J. Am. Chem. Soc.* **1970**, *92*, 1075.
[14] H. Wei, E. Wang, *Chem. Soc. Rev.* **2013**, *42*, 6060.
[15] F. Manea, F. B. Houillon, L. Pasquato, P. Scrimin, *Angew. Chem., Int. Ed.* **2004**, *116*, 6291.
[16] L. Gao, J. Zhuang, L. Nie, J. Zhang, Y. Zhang, N. Gu, T. Wang, J. Feng, D. Yang, S. Perrett, X. Yan, *Nat. Nanotechnol.* **2007**, *2*, 577.
[17] J. G. Werner, S. Nawar, A. A. Solovev, D. A. Weitz, *Macromolecules* **2018**, *51*, 5798.
[18] J. Liu, H. Chen, X. Shi, S. Nawar, J. G. Werner, G. Huang, M. Ye, D. A. Weitz, A. A. Solovev, Y. Mei, *Environ. Sci. Nano* **2020**, *7*, 656.
[19] W. X. Song, Q. He, H. Mohwald, Y. Yang, J. B. Li, *J. Controlled Release* **2009**, *139*, 160.
[20] S. Hernot, A. L. Klibanov, *Adv. Drug Delivery Rev.* **2008**, *60*, 1153.
[21] J. S. Randhawa, K. E. Laflin, N. Seelam, D. H. Gracias, *Adv. Funct. Mater.* **2011**, *21*, 2395.
[22] Z. Guo, T. Wang, A. Rawal, J. Hou, Z. Cao, H. Zhang, J. Xu, Z. Gu, V. Chen, K. Liang, *Mater. Today* **2019**, *28*, 10.
[23] V. Magdanz, G. Stoychev, L. Ionov, S. Sanchez, O. G. Schmidt, *Angew. Chem., Int. Ed.* **2014**, *53*, 2673.
[24] B. Dai, J. Wang, Z. Xiong, X. Zhan, W. Dai, C. C. Li, S. P. Feng, J. Tang, *Nat. Nanotechnol.* **2016**, *11*, 1087.
[25] L. Zhang, Z. Xiao, X. Chen, J. Chen, W. Wang, *ACS Nano* **2019**, *13*, 8842.
[26] Z. Ren, W. Hu, X. Dong, M. Sitti, *Nat. Commun.* **2019**, *10*, 2703.
[27] a) Z. Z. Chong, S. H. Tan, A. M. Gañán-Calvo, S. B. Tor, N. H. Loh, N.-T. Nguyen, *Lab Chip* **2016**, *16*, 35; b) T. Ohji, M. Fukushima, *Int. Mater. Rev.* **2012**, *57*, 115; c) M. Sivakumar, S. Y. Tang, K. W. Tan, *Ultrason. Sonochem.* **2014**, *21*, 2069; d) Z. Izadifar, P. Babyn, D. Chapman, *J. Med. Biol. Eng.* **2019**, *39*, 259.
[28] E. Stride, T. Segers, G. Lajoinie, S. Cherkaoui, T. Bettinger, M. Versluis, M. Borden, *Ultrasound Med. Biol.* **2020**, *46*, 1326.
[29] A. Upadhyay, S. V. Dalvi, *Ultrasound Med. Biol.* **2019**, *45*, 301.
[30] J. Wu, X. Wang, Q. Wang, Z. Lou, S. Li, Y. Zhu, L. Qin, H. Wei, *Chem. Soc. Rev.* **2019**, *48*, 1004.
[31] X. Lin, B. Xu, H. Zhu, J. Liu, A. Solovev, Y. Mei, *Research* **2020**, *2020*, 7659749.
[32] R. Seemann, M. Brinkmann, T. Pfohl, S. Herminghaus, *Rep. Prog. Phys.* **2012**, *75*, 016601.
[33] T. Brugarolas, F. Tu, D. Lee, *Soft Matter* **2013**, *9*, 9046.
[34] M. Björnmalm, Y. Yan, F. Caruso, *J. Controlled Release* **2014**, *190*, 139.
[35] W. Li, L. Zhang, X. Ge, B. Xu, W. Zhang, L. Qu, C.-H. Choi, J. Xu, A. Zhang, H. Lee, D. A. Weitz, *Chem. Soc. Rev.* **2018**, *47*, 5646.
[36] S. Singh, *Nanosci. Technol.* **2017**, *5*, https://doi.org/10.15226/2374-8141/5/1/00150.
[37] A. A. Solovev, W. Xi, D. H. Gracias, S. M. Harazim, C. Deneke, S. Sanchez, O. G. Schmidt, *ACS Nano* **2012**, *6*, 1751.
[38] H.-L. Liu, C.-H. Fan, C.-Y. Ting, C.-K. Yeh, *Theranostics* **2014**, *4*, 432.

[39] A. A. Solovev, S. Sanchez, M. Pumera, Y. Mei, O. G. Schmidt, *Adv. Funct. Mater.* **2010**, *20*, 2430.
[40] J. Wu, S. Balasubramanian, D. Kagan, K. M. Manesh, S. Campuzano, J. Wang, *Nat. Commun.* **2010**, *1*, 36.
[41] S. K. Srivastava, M. Medina-Sanchez, B. Koch, O. G. Schmidt, *Adv. Mater.* **2016**, *28*, 832.
[42] T. Xu, L.-P. Xu, X. Zhang, *Appl. Mater. Today* **2017**, *9*, 493.
[43] C. Gao, Y. Wang, Z. Ye, Z. Lin, X. Ma, Q. He, *Adv. Mater.* **2021**, *33*, 2000512.
[44] R. Cheng, W. Huang, L. Huang, B. Yang, L. Mao, K. Jin, Q. ZhuGe, Y. Zhao, *ACS Nano* **2014**, *8*, 7746.
[45] X. K. Lin, Z. G. Wu, Y. J. Wu, M. J. Xuan, Q. He, *Adv. Mater.* **2016**, *28*, 1060.
[46] Y. Mei, G. Huang, A. A. Solovev, E. B. Ureña, I. Mönch, F. Ding, T. Reindl, R. K. Y. Fu, P. K. Chu, O. G. Schmidt, *Adv. Mater.* **2008**, *20*, 4085.
[47] W. Wang, W. Duan, S. Ahmed, T. E. Mallouk, A. Sen, *Nano Today* **2013**, *8*, 531.
[48] a) S. Hermanova, M. Pumera, *Nanoscale* **2018**, *10*, 7332; b) X. Lin, H. Zhu, Z. Zhao, C. You, Y. Kong, Y. Zhao, J. Liu, H. Chen, X. Shi, D. Makarov, Y. Mei, *Adv. Mater. Technol.* **2020**, *5*, 2000279.
[49] A. Panda, A. S. Reddy, S. Venkateswarlu, M. Yoon, *Nanoscale* **2018**, *10*, 16268.
[50] S. Sanchez, A. N. Ananth, V. M. Fomin, M. Viehrig, O. G. Schmidt, *J. Am. Chem. Soc.* **2011**, *133*, 14860.
[51] T. Xu, F. Soto, W. Gao, V. Garcia-Gradilla, J. Li, X. Zhang, J. Wang, *J. Am. Chem. Soc.* **2014**, *136*, 8552.
[52] A. A. Solovev, S. Sanchez, O. G. Schmidt, *Nanoscale* **2013**, *5*, 1284.
[53] T. Xu, F. Soto, W. Gao, R. Dong, V. Garcia-Gradilla, E. Magana, X. Zhang, J. Wang, *J. Am. Chem. Soc.* **2015**, *137*, 2163.
[54] J. L. Anderson, *Annu. Rev. Fluid Mech.* **1989**, *21*, 61.
[55] R. A. Pavlick, S. Sengupta, T. McFadden, H. Zhang, A. Sen, *Angew. Chem., Int. Ed.* **2011**, *50*, 9374.
[56] C. Zhou, H. P. Zhang, J. Y. Tang, W. Wang, *Langmuir* **2018**, *34*, 3289.
[57] R. Golestanian, T. B. Liverpool, A. Ajdari, *Phys. Rev. Lett.* **2005**, *94*, 220801.
[58] L. Baraban, M. Tasinkevych, M. N. Popescu, S. Sanchez, S. Dietrich, O. G. Schmidt, *Soft Matter* **2012**, *8*, 48.
[59] M. N. Popescu, S. Dietrich, M. Tasinkevych, J. Ralston, *Eur. Phys. J. E: Soft Matter Biol. Phys.* **2010**, *31*, 351.
[60] J. Li, W. Liu, J. Wang, I. Rozen, S. He, C. Chen, H. G. Kim, H.-J. Lee, H.-B.-R. Lee, S.-H. Kwon, T. Li, L. Li, J. Wang, Y. Mei, *Adv. Funct. Mater.* **2017**, *27*, 1700598.
[61] H. Wang, G. Zhao, M. Pumera, *J. Am. Chem. Soc.* **2014**, *136*, 2719.
[62] S. Fournier-Bidoz, A. C. Arsenault, I. Manners, G. A. Ozin, *Chem. Commun.* **2005**, *4*, 441.
[63] J. G. Gibbs, Y. P. Zhao, *Appl. Phys. Lett.* **2009**, 94.
[64] M. Enayati, M.-W. Chang, F. Bragman, M. Edirisinghe, E. Stride, *Colloids Surf., A* **2011**, *382*, 154.
[65] W. Gao, A. Uygun, J. Wang, *J. Am. Chem. Soc.* **2012**, *134*, 897.
[66] F. Mou, C. Chen, H. Ma, Y. Yin, Q. Wu, J. Guan, *Angew. Chem., Int. Ed.* **2013**, *52*, 7208.
[67] W. Gao, A. Pei, J. Wang, *ACS Nano* **2012**, *6*, 8432.
[68] J. Orozco, V. García-Gradilla, M. D'Agostino, W. Gao, A. Cortés, J. Wang, *ACS Nano* **2013**, *7*, 818.
[69] W. F. Paxton, K. C. Kistler, C. C. Olmeda, A. Sen, S. K. St Angelo, Y. Y. Cao, T. E. Mallouk, P. E. Lammert, V. H. Crespi, *J. Am. Chem. Soc.* **2004**, *126*, 13424.
[70] P. T. B. Walter F. Paxton, Timothy R. Kline, Yang Wang, Thomas E. Mallouk, Ayusman Sen, *J. Am. Chem. Soc.* **2006**, *128*, 14881.
[71] S. Ebbens, D. A. Gregory, G. Dunderdale, J. R. Howse, Y. Ibrahim, T. B. Liverpool, R. Golestanian, *Europhys. Lett.* **2014**, *106*, 58003.
[72] A. Brown, W. Poon, *Soft Matter* **2014**, *10*, 4016.
[73] a) K. E. Peyer, L. Zhang, B. J. Nelson, *Nanoscale* **2013**, *5*, 1259; b) T. Li, A. Zhang, G. Shao, M. Wei, B. Guo, G. Zhang, L. Li, W. Wang, *Adv. Funct. Mater.* **2018**, *28*, 1706066.
[74] a) L. Baraban, D. Makarov, R. Streubel, I. Mönch, D. Grimm, S. Sanchez, O. G. Schmidt, *ACS Nano* **2012**, *6*, 3383; b) L. Baraban, D. Makarov, O. G. Schmidt, G. Cuniberti, P. Leiderer, A. Erbe, *Nanoscale* **2013**, *5*, 1332.
[75] T. R. Kline, W. F. Paxton, T. E. Mallouk, A. Sen, *Angew. Chem.* **2005**, *117*, 754.
[76] A. A. Solovev, Y. Mei, E. Bermudez Urena, G. Huang, O. G. Schmidt, *Small* **2009**, *5*, 1688.
[77] S. Sanchez, A. A. Solovev, S. M. Harazim, O. G. Schmidt, *J. Am. Chem. Soc.* **2011**, *133*, 701.
[78] S. Sanchez, A. A. Solovev, S. Schulze, O. G. Schmidt, *Chem. Commun.* **2011**, *47*, 698.
[79] J. Burdick, R. Laocharoensuk, P. M. Wheat, J. D. Posner, J. Wang, *J. Am. Chem. Soc.* **2008**, *130*, 8164.
[80] I. S. M. Khalil, V. Magdanz, S. Sanchez, O. G. Schmidt, S. Misra, *Appl. Phys. Lett.* **2013**, *103*, 172404.
[81] T. L. Li, X. C. Chang, Z. G. Wu, J. X. Li, G. B. Shao, X. H. Deng, J. B. Qiu, B. Guo, G. Y. Zhang, Q. He, L. Q. Li, J. Wang, *ACS Nano* **2017**, *11*, 9268.
[82] L. Baraban, R. Streubel, D. Makarov, L. Han, D. Karnaushenko, O. G. Schmidt, G. Cuniberti, *ACS Nano* **2013**, *7*, 1360.
[83] S. Balasubramanian, D. Kagan, K. M. Manesh, P. Calvo-Marzal, G. U. Flechsig, J. Wang, *Small* **2009**, *5*, 1569.
[84] L. Soler, C. Martinez-Cisneros, A. Swiersy, S. Sanchez, O. G. Schmidt, *Lab Chip* **2013**, *13*, 4299.
[85] V. Magdanz, M. Guix, F. Hebenstreit, O. G. Schmidt, *Adv. Mater.* **2016**, *28*, 4084.
[86] a) X. Wang, V. Sridhar, S. Guo, N. Talebi, A. Miguel-López, K. Hahn, P. A. van Aken, S. Sánchez, *Adv. Funct. Mater.* **2018**, *28*, 1705862; b) X. Wang, L. Baraban, V. R. Misko, F. Nori, T. Huang, G. Cuniberti, J. Fassbender, D. Makarov, *Small* **2018**, *14*, 1802537; c) X. Wang, L. Baraban, A. Nguyen, J. Ge, V. R. Misko, J. Tempere, F. Nori, P. Formanek, T. Huang, G. Cuniberti, J. Fassbender, D. Makarov, *Small* **2018**, *14*, 1803613; d) T. Huang, V. R. Misko, S. Gobeil, X. Wang, F. Nori, J. Schütt, J. Fassbender, G. Cuniberti, D. Makarov, L. Baraban, *Adv. Funct. Mater.* **2020**, *30*, 2003851; e) T. Huang, S. Gobeil, X. Wang, V. Misko, F. Nori, W. De Malsche, J. Fassbender, D. Makarov, G. Cuniberti, L. Baraban, *Langmuir* **2020**, *36*, 7091.
[87] C. Chen, S. Tang, H. Teymourian, E. Karshalev, F. Zhang, J. Li, F. Mou, Y. Liang, J. Guan, J. Wang, *Angew. Chem., Int. Ed.* **2018**, *57*, 8110.
[88] R. Dong, Q. Zhang, W. Gao, A. Pei, B. Ren, *ACS Nano* **2016**, *10*, 839.
[89] R. Dong, C. Wang, Q. Wang, A. Pei, X. She, Y. Zhang, Y. Cai, *Nanoscale* **2017**, *9*, 15027.
[90] M. Ibele, T. E. Mallouk, A. Sen, *Angew. Chem., Int. Ed.* **2009**, *48*, 3308.
[91] M. Xuan, Z. Wu, J. Shao, L. Dai, T. Si, Q. He, *J. Am. Chem. Soc.* **2016**, *138*, 6492.
[92] W. Li, X. Wu, H. Qin, Z. Zhao, H. Liu, *Adv. Funct. Mater.* **2016**, *26*, 3164.
[93] S. Palagi, A. G. Mark, S. Y. Reigh, K. Melde, T. Qiu, H. Zeng, C. Parmeggiani, D. Martella, A. Sanchez-Castillo, N. Kapernaum, F. Giesselmann, D. S. Wiersma, E. Lauga, P. Fischer, *Nat. Mater.* **2016**, *15*, 647.
[94] S. Ahmed, W. Wang, L. Bai, D. T. Gentekos, M. Hoyos, T. E. Mallouk, *ACS Nano* **2016**, *10*, 4763.
[95] a) V. Garcia-Gradilla, J. Orozco, S. Sattayasamitsathit, F. Soto, F. Kuralay, A. Pourazary, A. Katzenberg, W. Gao, Y. Shen, J. Wang, *ACS Nano* **2013**, *7*, 9232; b) F. Nadal, E. Lauga, *Phys. Fluids* **2014**, *26*, 082001.

[96] W. Wang, W. Duan, Z. Zhang, M. Sun, A. Sen, T. E. Mallouk, *Chem. Commun.* **2015**, *51*, 1020.
[97] Y. Hong, N. M. Blackman, N. D. Kopp, A. Sen, D. Velegol, *Phys. Rev. Lett.* **2007**, *99*, 178103.
[98] L. Baraban, S. M. Harazim, S. Sanchez, O. G. Schmidt, *Angew. Chem., Int. Ed.* **2013**, *52*, 5552.
[99] M. Guix, A. K. Meyer, B. Koch, O. G. Schmidt, *Sci. Rep.* **2016**, *6*, 21701.
[100] Z. Wu, L. Li, Y. Yang, P. Hu, Y. Li, S.-Y. Yang, L. V. Wang, W. Gao, *Sci. Rob.* **2019**, *4*, eaax0613.
[101] M. Pacheco, B. Jurado-Sanchez, A. Escarpa, *Angew. Chem., Int. Ed.* **2019**, *58*, 18017.
[102] S. Sanchez, A. A. Solovev, Y. Mei, O. G. Schmidt, *J. Am. Chem. Soc.* **2010**, *132*, 13144.
[103] Z. Wu, Y. Wu, W. He, X. Lin, J. Sun, Q. He, *Angew. Chem., Int. Ed.* **2013**, *52*, 7000.
[104] W. Gao, R. Dong, S. Thamphiwatana, J. Li, W. Gao, L. Zhang, J. Wang, *ACS Nano* **2015**, *9*, 117.
[105] R. Mhanna, F. Qiu, L. Zhang, Y. Ding, K. Sugihara, M. Zenobi-Wong, B. J. Nelson, *Small* **2014**, *10*, 1953.
[106] D. Kagan, M. J. Benchimol, J. C. Claussen, E. Chuluun-Erdene, S. Esener, J. Wang, *Angew. Chem., Int. Ed.* **2012**, *51*, 7519.
[107] Z. Wu, J. Li, B. E.-F. de Ávila, T. Li, W. Gao, Q. He, L. Zhang, J. Wang, *Adv. Funct. Mater.* **2015**, *25*, 7497.
[108] W. He, Y. Liu, J. Yuan, J. J. Yin, X. Wu, X. Hu, K. Zhang, J. Liu, C. Chen, Y. Ji, Y. Guo, *Biomaterials* **2011**, *32*, 1139.
[109] W. Luo, C. Zhu, S. Su, D. Li, Y. He, Q. Huang, C. Fan, *ACS Nano* **2010**, *4*, 7451.
[110] Y. J. Long, Y. F. Li, Y. Liu, J. J. Zheng, J. Tang, C. Z. Huang, *Chem. Commun.* **2011**, *47*, 11939.
[111] W. Chen, J. Chen, Y.-B. Feng, L. Hong, Q.-Y. Chen, L.-F. Wu, X.-H. Lin, X.-H. Xia, *Analyst* **2012**, *137*, 1706.
[112] Y. Fan, Y. Huang, *Analyst* **2012**, *137*, 1225.
[113] Y. Song, K. Qu, C. Zhao, J. Ren, X. Qu, *Adv. Mater.* **2010**, *22*, 2206.
[114] Y. Li, Y. Weng, S. Lu, M. Xue, B. Yao, W. Weng, T. Zheng, *J.Nanomater.* **2020**, *2020*, 1363212.
[115] Y. Huang, J. Ren, X. Qu, *Chem. Rev.* **2019**, *119*, 4357.
[116] H. Y. Shin, T. J. Park, M. I. Kim, *J. Nanomater.* **2015**, *2015*, 756278.
[117] a) L. Gao, K. Fan, X. Yan, *Theranostics* **2017**, *7*, 3207; b) A. K. Dutta, S. K. Maji, D. N. Srivastava, A. Mondal, P. Biswas, P. Paul, B. Adhikary, *J. Mol. Catal. A: Chem.* **2012**, *360*, 71.
[118] X. Wang, W. Guo, Y. Hu, J. Wu, H. Wei, *Nanozymes: Next Wave of Artificial Enzymes*, Springer, Berlin/Heidelberg, Germany **2016**.
[119] J. Liu, X. Hu, S. Hou, T. Wen, W. Liu, X. Zhu, J.-J. Yin, X. Wu, *Sens. Actuators, B* **2012**, *166-167*, 708.
[120] a) Y. L. Dong, H. G. Zhang, Z. U. Rahman, L. Su, X. J. Chen, J. Hu, X. G. Chen, *Nanoscale* **2012**, *4*, 3969; b) M. I. Kim, Y. Ye, M.-A. Woo, J. Lee, H. G. Park, *Adv. Healthcare Mater.* **2014**, *3*, 36.
[121] Y. Hu, X. J. Gao, Y. Zhu, F. Muhammad, S. Tan, W. Cao, S. Lin, Z. Jin, X. Gao, H. Wei, *Chem. Mater.* **2018**, *30*, 6431.
[122] H. Ding, B. Hu, B. Zhang, H. Zhang, X. Yan, G. Nie, M. Liang, *Nano Res.* **2021**, *14*, 570.
[123] a) Y. Qu, X. Duan, *Chem. Soc. Rev.* **2013**, *42*, 2568; b) C. Chen, W. Ma, J. Zhao, *Chem. Soc. Rev.* **2010**, *39*, 4206.
[124] H. Wang, S. Jiang, S. Chen, D. Li, X. Zhang, W. Shao, X. Sun, J. Xie, Z. Zhao, Q. Zhang, Y. Tian, Y. Xie, *Adv. Mater.* **2016**, *28*, 6940.
[125] P. Kalluru, R. Vankayala, C.-S. Chiang, K. C. Hwang, *Biomaterials* **2016**, *95*, 1.
[126] Y. Zheng, Z. Yu, H. Ou, A. M. Asiri, Y. Chen, X. Wang, *Adv. Funct. Mater.* **2018**, *28*, 1705407.
[127] J. Zhang, X. Lu, D. Tang, S. Wu, X. Hou, J. Liu, P. Wu, *ACS Appl. Mater. Interfaces* **2018**, *10*, 40808.
[128] Y. Liu, M. Zhou, W. Cao, X. Wang, Q. Wang, S. Li, H. Wei, *Anal. Chem.* **2019**, *91*, 8170.
[129] S. Kim, J. Lee, G. Jin, M.-H. Jo, C. Lee, S. Ryu, *Nano Lett.* **2019**, *19*, 4043.
[130] M. Mohammad, F. Ahmadpoor, S. A. Shojaosadati, *ACS Omega* **2020**, *5*, 18766.
[131] S. Zhang, F. Lin, Q. Yuan, J. Liu, Y. Li, H. Liang, *J. Environ. Sci.* **2020**, *88*, 103.
[132] Y. Zhang, E. Villarreal, G. G. Li, W. Wang, H. Wang, *J. Phys. Chem. Lett.* **2020**, *11*, 9321.
[133] Z. Qi, L. Wang, Q. You, Y. Chen, *Biosens. Bioelectron.* **2017**, *96*, 227.
[134] M. Moglianetti, P. Deborah, G. Udayan, S. F. Retta, D. Debellis, R. Marotta, A. Turco, S. Rella, C. Malitesta, G. Bonacucina, E. De Luca, P. P. Pompa, *Nanomaterials* **2020**, *10*, 99.
[135] M. Moglianetti, E. De Luca, D. Pedone, R. Marotta, T. Catelani, B. Sartori, H. Amenitsch, S. F. Retta, P. P. Pompa, *Nanoscale* **2016**, *8*, 3739.
[136] Z. An, J. Yan, Y. Zhang, R. Pei, *J. Mater. Chem. B* **2020**, *8*, 8748.
[137] S.-B. He, L. Yang, X.-L. Lin, H.-P. Peng, Z. Lin, H.-H. Deng, W. Chen, G.-L. Hong, *Front. Chem.* **2020**, *8*, 654.
[138] W. Li, B. Chen, H. Zhang, Y. Sun, J. Wang, J. Zhang, Y. Fu, *Biosens. Bioelectron.* **2015**, *66*, 251.
[139] X. Wang, Y. Zhang, T. Li, W. Tian, Q. Zhang, Y. Cheng, *Langmuir* **2013**, *29*, 5262.
[140] P. Ling, C. Qian, J. Yu, F. Gao, *Biosens. Bioelectron.* **2020**, *149*, 111838.
[141] Y. Vlamidis, V. Voliani, *Front. Bioeng. Biotechnol.* **2018**, *6*, 6.
[142] M. Liang, X. Yan, *Acc. Chem. Res.* **2019**, *52*, 2190.
[143] N. Stasyuk, O. Smutok, O. Demkiv, T. Prokopiv, G. Gayda, M. Nisnevitch, M. Gonchar, *Sensors* **2020**, *20*, 4509.
[144] J. Golchin, K. Golchin, N. Alidadian, S. Ghaderi, S. Eslamkhah, M. Eslamkhah, A. Akbarzadeh, *Artif. Cells, Nanomed., Biotechnol.* **2017**, *45*, 1.
[145] K. Korschelt, R. Schwidetzky, F. Pfitzner, J. Strugatchi, C. Schilling, M. von der Au, K. Kirchhoff, M. Panthöfer, I. Lieberwirth, M. N. Tahir, C. Hess, B. Meermann, W. Tremel, *Nanoscale* **2018**, *10*, 13074.
[146] a) A. A. Vernekar, T. Das, S. Ghosh, G. Mugesh, *Chem. - Asian J.* **2016**, *11*, 72; b) H. Wang, K. Wan, X. Shi, *Adv. Mater.* **2019**, *31*, 1805368.
[147] K. Fan, H. Wang, J. Xi, Q. Liu, X. Meng, D. Duan, L. Gao, X. Yan, *Chem. Commun.* **2017**, *53*, 424.
[148] B. Xu, H. Wang, W. Wang, L. Gao, S. Li, X. Pan, H. Wang, H. Yang, X. Meng, Q. Wu, L. Zheng, S. Chen, X. Shi, K. Fan, X. Yan, H. Liu, *Angew. Chem., Int. Ed.* **2019**, *58*, 4911.
[149] A. A. Karyakin, E. E. Karyakina, L. Gorton, *Anal. Chem.* **2000**, *72*, 1720.
[150] X.-Q. Zhang, S.-W. Gong, Y. Zhang, T. Yang, C.-Y. Wang, N. Gu, *J. Mater. Chem.* **2010**, *20*, 5110.
[151] W. Zhang, S. Hu, J.-J. Yin, W. He, W. Lu, M. Ma, N. Gu, Y. Zhang, *J. Am. Chem. Soc.* **2016**, *138*, 5860.
[152] A. A. Vernekar, D. Sinha, S. Srivastava, P. U. Paramasivam, P. D'Silva, G. Mugesh, *Nat. Commun.* **2014**, *5*, 5301.
[153] H. Ye, K. Yang, J. Tao, Y. Liu, Q. Zhang, S. Habibi, Z. Nie, X. Xia, *ACS Nano* **2017**, *11*, 2052.
[154] H. Sun, N. Gao, K. Dong, J. Ren, X. Qu, *ACS Nano* **2014**, *8*, 6202.
[155] Y. Tao, Y. Lin, Z. Huang, J. Ren, X. Qu, *Adv. Mater.* **2013**, *25*, 2510.
[156] M. Vázquez-González, W. C. Liao, R. Cazelles, S. Wang, X. Yu, V. Gutkin, I. Willner, *ACS Nano* **2017**, *11*, 3247.
[157] a) H. Yang, R. Yang, P. Zhang, Y. Qin, T. Chen, F. Ye, *Microchim. Acta* **2017**, *184*, 4629; b) S. Wang, W. Deng, L. Yang, Y. Tan, Q. Xie, S. Yao, *ACS Appl. Mater. Interfaces* **2017**, *9*, 24440; c) F. Liu, J. He, M. Zeng, J. Hao, Q. Guo, Y. Song, L. Wang, *J. Nanopart. Res.* **2016**, *18*, 106.
[158] S. Li, X. Liu, H. Chai, Y. Huang, *TrAC Trends Anal. Chem.* **2018**, *105*, 391.

[159] R. Cai, D. Yang, S. Peng, X. Chen, Y. Huang, Y. Liu, W. Hou, S. Yang, Z. Liu, W. Tan, *J. Am. Chem. Soc.* **2015**, *137*, 13957.
[160] X. Ren, J. Liu, J. Ren, F. Tang, X. Meng, *Nanoscale* **2015**, *7*, 19641.
[161] M. Chen, Z. Wang, J. Shu, X. Jiang, W. Wang, Z.-H. Shi, Y.-W. Lin, *Inorg. Chem.* **2017**, *56*, 9400.
[162] M. Comotti, C. Della Pina, R. Matarrese, M. Rossi, *Angew. Chem., Int. Ed.* **2004**, *43*, 5812.
[163] a) I. V. Delidovich, B. L. Moroz, O. P. Taran, N. V. Gromov, P. A. Pyrjaev, I. P. Prosvirin, V. I. Bukhtiyarov, V. N. Parmon, *Chem. Eng. J.* **2013**, *223*, 921; b) Y. Wang, S. Van de Vyver, K. K. Sharma, Y. Román-Leshkov, *Green Chem.* **2014**, *16*, 719.
[164] A. P. Periasamy, P. Roy, W.-P. Wu, Y.-H. Huang, H.-T. Chang, *Electrochim. Acta* **2016**, *215*, 253.
[165] H. Liang, F. Lin, Z. Zhang, B. Liu, S. Jiang, Q. Yuan, J. Liu, *ACS Appl. Mater. Interfaces* **2017**, *9*, 1352.
[166] R. Ragg, F. Natalio, M. N. Tahir, H. Janssen, A. Kashyap, D. Strand, S. Strand, W. Tremel, *ACS Nano* **2014**, *8*, 5182.
[167] J. Liu, X. Jiang, L. Wang, Z. Hu, T. Wen, W. Liu, J. Yin, C. Chen, X. Wu, *Nano Res.* **2015**, *8*, 4024.
[168] J. Li, W. Liu, X. Wu, X. Gao, *Biomaterials* **2015**, *48*, 37.
[169] W. Zhang, J. Dong, Y. Wu, P. Cao, L. Song, M. Ma, N. Gu, Y. Zhang, *Colloids Surf., B* **2017**, *154*, 55.
[170] K. Sobańska, P. Pietrzyk, Z. Sojka, *ACS Catal.* **2017**, *7*, 2935.
[171] I. Celardo, J. Z. Pedersen, E. Traversa, L. Ghibelli, *Nanoscale* **2011**, *3*, 1411.
[172] Y. Li, X. He, J.-J. Yin, Y. Ma, P. Zhang, J. Li, Y. Ding, J. Zhang, Y. Zhao, Z. Chai, Z. Zhang, *Angew. Chem., Int. Ed.* **2015**, *54*, 1832.
[173] Y. Liu, K. Ai, X. Ji, D. Askhatova, R. Du, L. Lu, J. Shi, *J. Am. Chem. Soc.* **2017**, *139*, 856.
[174] X. He, F. Zhang, J. Liu, G. Fang, S. Wang, *Nanoscale* **2017**, *9*, 18066.
[175] Q. Zhang, X. He, A. Han, Q. Tu, G. Fang, J. Liu, S. Wang, H. Li, *Nanoscale* **2016**, *8*, 16851.
[176] L. J. Prins, *Acc. Chem. Res.* **2015**, *48*, 1920.
[177] a) J. E. Mondloch, M. J. Katz, W. C. Isley Iii, P. Ghosh, P. Liao, W. Bury, G. W. Wagner, M. G. Hall, J. B. DeCoste, G. W. Peterson, R. Q. Snurr, C. J. Cramer, J. T. Hupp, O. K. Farha, *Nat. Mater.* **2015**, *14*, 512; b) E. López-Maya, C. Montoro, L. M. Rodríguez-Albelo, S. D. Aznar Cervantes, A. A. Lozano-Pérez, J. L. Cenís, E. Barea, J. A. R. Navarro, *Angew. Chem., Int. Ed.* **2015**, *54*, 6654; c) D. T. Lee, J. Zhao, G. W. Peterson, G. N. Parsons, *Chem. Mater.* **2017**, *29*, 4894.
[178] I. Nath, J. Chakraborty, F. Verpoort, *Chem. Soc. Rev.* **2016**, *45*, 4127.
[179] C. Xu, Y. Lin, J. Wang, L. Wu, W. Wei, J. Ren, X. Qu, *Adv. Healthcare Mater.* **2013**, *2*, 1591.
[180] N. Singh, M. A. Savanur, S. Srivastava, P. D'Silva, G. Mugesh, *Angew. Chem., Int. Ed.* **2017**, *56*, 14267.
[181] N. Gao, K. Dong, A. Zhao, H. Sun, Y. Wang, J. Ren, X. Qu, *Nano Res.* **2016**, *9*, 1079.
[182] C. Ge, G. Fang, X. Shen, Y. Chong, W. G. Wamer, X. Gao, Z. Chai, C. Chen, J.-J. Yin, *ACS Nano* **2016**, *10*, 10436.
[183] X. Xia, J. Zhang, N. Lu, M. J. Kim, K. Ghale, Y. Xu, E. McKenzie, J. Liu, H. Ye, *ACS Nano* **2015**, *9*, 9994.
[184] X. Zhou, S. Guo, J. Gao, J. Zhao, S. Xue, W. Xu, *Biosens. Bioelectron.* **2017**, *98*, 83.
[185] H. Cheng, L. Zhang, J. He, W. Guo, Z. Zhou, X. Zhang, S. Nie, H. Wei, *Anal. Chem.* **2016**, *88*, 5489.
[186] L. Hu, H. Liao, L. Feng, M. Wang, W. Fu, *Anal. Chem.* **2018**, *90*, 6247.
[187] C. Xu, Z. Liu, L. Wu, J. Ren, X. Qu, *Adv. Funct. Mater.* **2014**, *24*, 1624.
[188] U. Carmona, L. Zhang, L. Li, W. Münchgesang, E. Pippel, M. Knez, *Chem. Commun.* **2014**, *50*, 701.
[189] X. Wang, W. Cao, L. Qin, T. Lin, W. Chen, S. Lin, J. Yao, X. Zhao, M. Zhou, C. Hang, H. Wei, *Theranostics* **2017**, *7*, 2277.
[190] C. Xu, W. Bing, F. Wang, J. Ren, X. Qu, *ACS Nano* **2017**, *11*, 7770.
[191] C. Wang, Y. Shi, Y.-Y. Dan, X.-G. Nie, J. Li, X.-H. Xia, *Chem. - Eur. J.* **2017**, *23*, 6717.
[192] C. Li, Y. Wang, C. Li, S. Xu, X. Hou, P. Wu, *ACS Appl. Mater. Interfaces* **2019**, *11*, 20770.
[193] R. Wang, B. Li, Y. Xiao, X. Tao, X. Su, X. Dong, *J. Catal.* **2018**, *364*, 154.
[194] B. Liu, Z. Huang, J. Liu, *Nanoscale* **2016**, *8*, 13562.
[195] H. Wei, E. Wang, *Anal. Chem.* **2008**, *80*, 2250.
[196] L. Alili, M. Sack, A. S. Karakoti, S. Teuber, K. Puschmann, S. M. Hirst, C. M. Reilly, K. Zanger, W. Stahl, S. Das, S. Seal, P. Brenneisen, *Biomaterials* **2011**, *32*, 2918.
[197] C. Mandoli, F. Pagliari, S. Pagliari, G. Forte, P. Di Nardo, S. Licoccia, E. Traversa, *Adv. Funct. Mater.* **2010**, *20*, 1617.
[198] M. J. Hajipour, K. M. Fromm, A. A. Ashkarran, D. Jimenez de Aberasturi, I. R. de Larramendi, T. Rojo, V. Serpooshan, W. J. Parak, M. Mahmoudi, *Trends Biotechnol.* **2012**, *30*, 499.
[199] K. Qu, P. Shi, J. Ren, X. Qu, *Chem. - Eur. J.* **2014**, *20*, 7501.
[200] M. M. Masadeh, G. A. Karasneh, M. A. Al-Akhras, B. A. Albiss, K. M. Aljarah, S. I. Al-azzam, K. H. Alzoubi, *Cytotechnology* **2015**, *67*, 427.
[201] F. Natalio, R. André, A. F. Hartog, B. Stoll, K. P. Jochum, R. Wever, W. Tremel, *Nat. Nanotechnol.* **2012**, *7*, 530.
[202] L. Gao, Y. Liu, D. Kim, Y. Li, G. Hwang, P. C. Naha, D. P. Cormode, H. Koo, *Biomaterials* **2016**, *101*, 272.
[203] M. A. Maurer-Jones, I. L. Gunsolus, B. M. Meyer, C. J. Christenson, C. L. Haynes, *Anal. Chem.* **2013**, *85*, 5810.
[204] K. Zheng, M. I. Setyawati, D. T. Leong, J. Xie, *ACS Nano* **2017**, *11*, 6904.
[205] K. K. Dey, A. Sen, *J. Am. Chem. Soc.* **2017**, *139*, 7666.
[206] S. Sengupta, K. K. Dey, H. S. Muddana, T. Tabouillot, M. E. Ibele, P. J. Butler, A. Sen, *J. Am. Chem. Soc.* **2013**, *135*, 1406.
[207] K. K. Dey, *Angew. Chem., Int. Ed.* **2019**, *58*, 2208.
[208] K. K. Dey, S. Das, M. F. Poyton, S. Sengupta, P. J. Butler, P. S. Cremer, A. Sen, *ACS Nano* **2014**, *8*, 11941.
[209] S. Tang, F. Zhang, H. Gong, F. Wei, J. Zhuang, E. Karshalev, B. Esteban-Fernández de Ávila, C. Huang, Z. Zhou, Z. Li, L. Yin, H. Dong, R. H. Fang, X. Zhang, L. Zhang, J. Wang, *Sci. Rob.* **2020**, *5*, eaba6137.
[210] M. Liang, K. Fan, Y. Pan, H. Jiang, F. Wang, D. Yang, D. Lu, J. Feng, J. Zhao, L. Yang, X. Yan, *Anal. Chem.* **2013**, *85*, 308.
[211] S. Singh, P. Tripathi, N. Kumar, S. Nara, *Biosens. Bioelectron.* **2017**, *92*, 280.
[212] M. Khairy, H. A. Ayoub, C. E. Banks, *Food Chem.* **2018**, *255*, 104.
[213] N. Wang, L. Zhu, D. Wang, M. Wang, Z. Lin, H. Tang, *Ultrason. Sonochem.* **2010**, *17*, 526.
[214] W. Luo, L. Zhu, N. Wang, H. Tang, M. Cao, Y. She, *Environ. Sci. Technol.* **2010**, *44*, 1786.
[215] A. Zeb, X. Xie, A. B. Yousaf, M. Imran, T. Wen, Z. Wang, H.-L. Guo, Y.-F. Jiang, I. A. Qazi, A.-W. Xu, *ACS Appl. Mater. Interfaces* **2016**, *8*, 30126.
[216] Y. B. Feng, L. Hong, A. L. Liu, W. D. Chen, G. W. Li, W. Chen, X. H. Xia, *Int. J. Environ. Sci. Technol.* **2015**, *12*, 653.
[217] C. Peng, B. Jiang, Q. Liu, Z. Guo, Z. Xu, Q. Huang, H. Xu, R. Tai, C. Fan, *Energy Environ. Sci.* **2011**, *4*, 2035.
[218] Y. Ye, L. Xiao, H. Bin, Q. Zhang, T. Nie, X. Yang, D. Wu, H. Cheng, P. Li, Q. Wang, *J. Mater. Chem. B* **2017**, *5*, 1518.
[219] B. Liu, X. Han, J. Liu, *Nanoscale* **2016**, *8*, 13620.
[220] T. Xue, B. Peng, M. Xue, X. Zhong, C. Y. Chiu, S. Yang, Y. Qu, L. Ruan, S. Jiang, S. Dubin, R. B. Kaner, J. I. Zink, M. E. Meyerhoff, X. Duan, Y. Huang, *Nat. Commun.* **2014**, *5*, 3200.
[221] D. Son, J. Lee, D. J. Lee, R. Ghaffari, S. Yun, S. J. Kim, J. E. Lee, H. R. Cho, S. Yoon, S. Yang, S. Lee, S. Qiao, D. Ling, S. Shin, J.-K. Song, J. Kim, T. Kim, H. Lee, J. Kim, M. Soh, N. Lee, C. S. Hwang, S. Nam, N. Lu, T. Hyeon, S. H. Choi, D.-H. Kim, *ACS Nano* **2015**, *9*, 5937.

[222] A. Pratsinis, G. A. Kelesidis, S. Zuercher, F. Krumeich, S. Bolisetty, R. Mezzenga, J.-C. Leroux, G. A. Sotiriou, *ACS Nano* **2017**, *11*, 12210.
[223] L. Zhang, L. Han, P. Hu, L. Wang, S. Dong, *Chem. Commun.* **2013**, *49*, 10480.
[224] Q. Wang, X. Zhang, L. Huang, Z. Zhang, S. Dong, *Angew. Chem., Int. Ed.* **2017**, *56*, 16082.
[225] L. Deng, C. Chen, C. Zhu, S. Dong, H. Lu, *Biosens. Bioelectron.* **2014**, *52*, 324.
[226] D. Fan, C. Shang, W. Gu, E. Wang, S. Dong, *ACS Appl. Mater. Interfaces* **2017**, *9*, 25870.
[227] D. Duan, K. Fan, D. Zhang, S. Tan, M. Liang, Y. Liu, J. Zhang, P. Zhang, W. Liu, X. Qiu, G. P. Kobinger, G. Fu Gao, X. Yan, *Biosens. Bioelectron.* **2015**, *74*, 134.
[228] H.-H. Xu, H.-H. Deng, X.-Q. Lin, Y.-Y. Wu, X.-L. Lin, H.-P. Peng, A.-L. Liu, X.-H. Xia, W. Chen, *Microchim. Acta* **2017**, *184*, 3945.
[229] a) H. Su, D.-D. Liu, M. Zhao, W.-L. Hu, S.-S. Xue, Q. Cao, X.-Y. Le, L.-N. Ji, Z.-W. Mao, *ACS Appl. Mater. Interfaces* **2015**, *7*, 8233; b) T. Chen, H. Zou, X. Wu, C. Liu, B. Situ, L. Zheng, G. Yang, *ACS Appl. Mater. Interfaces* **2018**, *10*, 12453; c) L. Wang, Z. Wang, X. Li, Y. Zhang, M. Yin, J. Li, H. Song, J. Shi, D. Ling, L. Wang, N. Chen, C. Fan, *Nano Res.* **2018**, *11*, 2746.
[230] a) D. Oró, T. Yudina, G. Fernández-Varo, E. Casals, V. Reichenbach, G. Casals, B. González de la Presa, S. Sandalinas, S. Carvajal, V. Puntes, W. Jiménez, *J. Hepatol.* **2016**, *64*, 691.
[231] a) S. Cai, X. Jia, Q. Han, X. Yan, R. Yang, C. Wang, *Nano Res.* **2017**, *10*, 2056; b) S. Bukhari, D. Kim, Y. Liu, B. Karabucak, H. Koo, *J. Endod.* **2018**, *44*, 806.
[232] Z. Wang, Y. Zhang, E. Ju, Z. Liu, F. Cao, Z. Chen, J. Ren, X. Qu, *Nat. Commun.* **2018**, *9*, 3334.
[233] a) Y. Meng, W. Li, X. Pan, G. M. Gadd, *Environ. Sci.: Nano* **2020**, *7*, 1305; b) P. Hu, L. Han, S. Dong, *ACS Appl. Mater. Interfaces* **2014**, *6*, 500; c) Z. Zhang, J. Hao, W. Yang, B. Lu, X. Ke, B. Zhang, J. Tang, *ACS Appl. Mater. Interfaces* **2013**, *5*, 3809.
[234] R. André, F. Natálio, M. Humanes, J. Leppin, K. Heinze, R. Wever, H.-C. Schröder, W. E. G. Müller, W. Tremel, *Adv. Funct. Mater.* **2011**, *21*, 501.
[235] Y. Lin, C. Xu, J. Ren, X. Qu, *Angew. Chem., Int. Ed.* **2012**, *51*, 12579.
[236] C.-W. Lien, Y.-C. Chen, H.-T. Chang, C.-C. Huang, *Nanoscale* **2013**, *5*, 8227.
[237] E. Ju, K. Dong, Z. Wang, Y. Zhang, F. Cao, Z. Chen, F. Pu, J. Ren, X. Qu, *Chem. - Eur. J.* **2017**, *23*, 13518.
[238] J. Fan, N. He, Q. He, Y. Liu, Y. Ma, X. Fu, Y. Liu, P. Huang, X. Chen, *Nanoscale* **2015**, *7*, 20055.
[239] G. Y. Tonga, Y. Jeong, B. Duncan, T. Mizuhara, R. Mout, R. Das, S. T. Kim, Y.-C. Yeh, B. Yan, S. Hou, V. M. Rotello, *Nat. Chem.* **2015**, *7*, 597.
[240] a) D. Jiang, D. Ni, Z. T. Rosenkrans, P. Huang, X. Yan, W. Cai, *Chem. Soc. Rev.* **2019**, *48*, 368.
[241] Z. Zhang, Y. Liu, X. Zhang, J. Liu, *Nano Lett.* **2017**, *17*, 7926.
[242] P. Illien, X. Zhao, K. K. Dey, P. J. Butler, A. Sen, R. Golestanian, *Nano Lett.* **2017**, *17*, 4415.
[243] S. Sengupta, D. Patra, I. Ortiz-Rivera, A. Agrawal, S. Shklyaev, K. K. Dey, U. Córdova-Figueroa, T. E. Mallouk, A. Sen, *Nat. Chem.* **2014**, *6*, 415.
[244] X. Zhao, K. K. Dey, S. Jeganathan, P. J. Butler, U. M. Córdova-Figueroa, A. Sen, *Nano Lett.* **2017**, *17*, 4807.
[245] B. G. De Geest, R. E. Vandenbroucke, A. M. Guenther, G. B. Sukhorukov, W. E. Hennink, N. N. Sanders, J. Demeester, S. C. De Smedt, *Adv. Mater.* **2006**, *18*, 1005.
[246] O. Kreft, M. Prevot, H. Möhwald, G. B. Sukhorukov, *Angew. Chem., Int. Ed.* **2007**, *46*, 5605.
[247] S. Donatan, A. Yashchenok, N. Khan, B. Parakhonskiy, M. Cocquyt, B.-E. Pinchasik, D. Khalenkow, H. Möhwald, M. Konrad, A. Skirtach, *ACS Appl. Mater. Interfaces* **2016**, *8*, 14284.
[248] G. Begum, P. Swathi, A. K. Bandarapu, J. Nayak, R. K. Rana, *ACS Appl. Mater. Interfaces* **2020**, *12*, 45476.
[249] a) K. W. Pulsipher, D. A. Hammer, D. Lee, C. M. Sehgal, *Ultrasound Med. Biol.* **2018**, *44*, 2441; b) S. Zullino, M. Argenziano, I. Stura, C. Guiot, R. Cavalli, *Mol. Imaging* **2018**, *17*, 1536012118778216.
[250] a) H. Ai, *Adv. Drug Delivery Rev.* **2011**, *63*, 772; b) A. Lahooti, S. Sarkar, S. Laurent, S. Shanehsazzadeh, *Contrast Media Mol. Imaging* **2016**, *11*, 428; c) A. Kiani, A. Esquevin, N. Lepareur, P. Bourguet, F. Le Jeune, J. Gauvrit, *Contrast Media Mol. Imaging* **2016**, *11*, 92; d) N. Lee, S. H. Choi, T. Hyeon, *Adv. Mater.* **2013**, *25*, 2641; e) W. He, K. Ai, L. Lu, *Sci. China: Chem.* **2015**, *58*, 753; f) D. Pan, B. Kim, L. V. Wang, G. M. Lanza, *Wiley Interdiscip. Rev.: Nanomed. Nanobiotechnol.* **2013**, *5*, 517.
[251] K. Ferrara, R. Pollard, M. Borden, *Annu. Rev. Biomed. Eng.* **2007**, *9*, 415.
[252] S. Qin, C. F. Caskey, K. W. Ferrara, *Phys. Med. Biol.* **2009**, *54*, R27.
[253] R. Gramiak, P. M. Shah, *Invest. Radiol.* **1968**, *3*, 356.
[254] a) F. Cavalieri, A. El Hamassi, E. Chiessi, G. Paradossi, *Langmuir* **2005**, *21*, 8758; b) E. Kang, H. S. Min, J. Lee, M. H. Han, H. J. Ahn, I.-C. Yoon, K. Choi, K. Kim, K. Park, I. C. Kwon, *Angew. Chem., Int. Ed.* **2010**, *49*, 524; c) M. G. Shapiro, P. W. Goodwill, A. Neogy, M. Yin, F. S. Foster, D. V. Schaffer, S. M. Conolly, *Nat. Nanotechnol.* **2014**, *9*, 311; d) K. E. Hitchcock, D. N. Caudell, J. T. Sutton, M. E. Klegerman, D. Vela, G. J. Pyne-Geithman, T. Abruzzo, P. E. P. Cyr, Y.-J. Geng, D. D. McPherson, C. K. Holland, *J. Controlled Release* **2010**, *144*, 288.
[255] B. D. Butler, *J. Clin. Ultrasound* **1986**, *14*, 408.
[256] S. B. Feinstein, F. J. Ten Cate, W. Zwehl, K. Ong, G. Maurer, C. Tei, P. M. Shah, S. Meerbaum, E. Corday, *J. Am. Coll. Cardiol.* **1984**, *3*, 14.
[257] S. R. Sirsi, M. A. Borden, *Bubble Sci., Eng., Technol.* **2009**, *1*, 3.
[258] M. W. Keller, W. Glasheen, S. Kaul, *J. Am. Soc. Echocardiogr.* **1989**, *2*, 48.
[259] M. Ward, J. Wu, J. F. Chiu, *Ultrasound Med. Biol.* **2000**, *26*, 1169.
[260] D. G. Shchukin, K. Köhler, H. Möhwald, G. B. Sukhorukov, *Angew. Chem., Int. Ed.* **2005**, *44*, 3310.
[261] E. Donath, G. B. Sukhorukov, F. Caruso, S. A. Davis, H. Möhwald, *Angew. Chem., Int. Ed.* **1998**, *37*, 2201.
[262] S. V. German, D. N. Bratashov, N. A. Navolokin, A. A. Kozlova, M. V. Lomova, M. V. Novoselova, E. A. Burilova, V. V. Zyev, B. N. Khlebtsov, A. B. Bucharskaya, G. S. Terentyuk, R. R. Amirov, G. N. Maslyakova, G. B. Sukhorukov, D. A. Gorin, *Phys. Chem. Chem. Phys.* **2016**, *18*, 32238.
[263] A. A. Kozlova, S. V. German, V. S. Atkin, V. V. Zyev, M. A. Astle, D. N. Bratashov, Y. I. Svenskaya, D. A. Gorin, *Inorganics* **2020**, *8*, 11.
[264] M. V. N. M. D. Mokrousov, J. Nolan, W. Harrington, P. Rudakovskaya, D. N. Bratashov, E. I. Galanzha, J. P. Fuenzalida-Werner, B. P. Yakimov, G. Nazarikov, V. P. Drachev, E. A. Shirshin, V. Ntziachristos, A. C. Stiel, V. P. Zharov, D. A. Gorin, *Biomed. Opt. Express* **2019**, *10*, 14.
[265] M. V. Novoselova, D. V. Voronin, T. O. Abakumova, P. A. Demina, A. V. Petrov, V. V. Petrov, T. S. Zatsepin, G. B. Sukhorukov, D. A. Gorin, *Colloids Surf., B* **2019**, *181*, 680.
[266] A. M. Yashchenok, J. Jose, P. Trochet, G. B. Sukhorukov, D. A. Gorin, *J. Biophotonics* **2016**, *9*, 792.
[267] A. S. Timin, M. M. Litvak, D. A. Gorin, E. N. Atochina-Vasserman, D. N. Atochin, G. B. Sukhorukov, *Adv. Healthcare Mater.* **2018**, *7*, 1700818.
[268] J. E. Aldrich, *Crit. Care Med.* **2007**, *35*, S131.
[269] J. P. Lawrence, *Crit. Care Med.* **2007**, *35*, S314.
[270] D. Lieu, *Arch. Pathol. Lab. Med.* **2010**, *134*, 1541.
[271] P. N. T. Wells, *Phys. Med. Biol.* **2006**, *51*, R83.
[272] S. Satomura, *Jpn. J. Acoust. Soc.* **1959**, *15*, 151.
[273] I. Donald, J. Macvicar, T. G. Brown, *Lancet* **1958**, *1*, 1188.
[274] O. Couture, V. Hingot, B. Heiles, P. Muleki-Seya, M. Tanter, *IEEE Trans. Ultrason. Ferroelectr. Freq. Control* **2018**, *65*, 1304.

[275] J. Claron, V. Hingot, I. Rivals, L. Rahal, O. Couture, T. Deffieux, M. Tanter, S. Pezet, *PAIN* **2021**, *162*, 1047.
[276] O. Couture, M. Fink, M. Tanter, *IEEE Trans. Ultrason. Ferroelectr. Freq. Control* **2012**, *59*, 2676.
[277] C. Errico, J. Pierre, S. Pezet, Y. Desailly, Z. Lenkei, O. Couture, M. Tanter, *Nature* **2015**, *527*, 499.
[278] M. Tanter, M. Fink, *IEEE Trans. Ultrason. Ferroelectr. Freq. Control* **2014**, *61*, 102.
[279] T. Deffieux, C. Demene, M. Pernot, M. Tanter, *Curr. Opin. Neurobiol.* **2018**, *50*, 128.
[280] C. L. Bayer, G. P. Luke, S. Y. Emelianov, *Acoust. Today* **2012**, *8*, 15.
[281] P. Beard, *Interface Focus* **2011**, *1*, 602.
[282] F. Cavalieri, M. Ashokkumar, F. Grieser, F. Caruso, *Langmuir* **2008**, *24*, 10078.
[283] M. Zhou, F. Cavalieri, F. Caruso, M. Ashokkumar, *ACS Macro Lett.* **2012**, *1*, 853.
[284] L. Lee, F. Cavalieri, M. Ashokkumar, *Langmuir* **2019**, *35*, 9997.
[285] F. Vong, Y. Son, S. Bhuiyan, M. Zhou, F. Cavalieri, M. Ashokkumar, *Ultrason. Sonochem.* **2014**, *21*, 23.
[286] X. Ma, A. Bussonniere, Q. Liu, *Ultrason. Sonochem.* **2017**, *36*, 454.
[287] L. L. A. Adams, T. E. Kodger, S.-H. Kim, H. C. Shum, T. Franke, D. A. Weitz, *Soft Matter* **2012**, *8*, 10719.
[288] a) L. Capretto, S. Mazzitelli, C. Nastruzzi, *J. Controlled Release* **2012**, *160*, 409; b) Y. Zhao, H. C. Shum, H. Chen, L. L. A. Adams, Z. Gu, D. A. Weitz, *J. Am. Chem. Soc.* **2011**, *133*, 8790; c) S.-H. Kim, J. Nam, J. W. Kim, D.-H. Kim, S.-H. Han, D. A. Weitz, *Lab Chip* **2013**, *13*, 1351; d) E. Amstad, S.-H. Kim, D. A. Weitz, *Angew. Chem., Int. Ed.* **2012**, *51*, 12499; e) P. M. Valencia, O. C. Farokhzad, R. Karnik, R. Langer, *Nat. Nanotechnol.* **2012**, *7*, 623; f) D. Liu, B. Herranz-Blanco, E. Mäkilä, L. R. Arriaga, S. Mirza, D. A. Weitz, N. Sandler, J. Salonen, J. Hirvonen, H. A. Santos, *ACS Appl. Mater. Interfaces* **2013**, *5*, 12127.
[289] S. Yang, F. Guo, B. Kiraly, X. Mao, M. Lu, K. W. Leong, T. J. Huang, *Lab Chip* **2012**, *12*, 2097.
[290] A. Abbaspourrad, W. J. Duncanson, N. Lebedeva, S. H. Kim, A. P. Zhushma, S. S. Datta, P. A. Dayton, S. S. Sheiko, M. Rubinstein, D. A. Weitz, *Langmuir* **2013**, *29*, 12352.
[291] E. Stride, M. Edirisinghe, *Med. Biol. Eng. Comput.* **2009**, *47*, 883.
[292] K. Hettiarachchi, E. Talu, M. L. Longo, P. A. Dayton, A. P. Lee, *Lab Chip* **2007**, *7*, 463.
[293] a) K. Pancholi, E. Stride, M. Edirisinghe, *J. Drug Target* **2008**, *16*, 494; b) K. P. Pancholi, U. Farook, R. Moaleji, E. Stride, M. J. Edirisinghe, *Eur. Biophys. J.* **2008**, *37*, 515.
[294] M. Parhizkar, M. Edirisinghe, E. Stride, *RSC Adv.* **2015**, *5*, 10751.
[295] T. Segers, E. Gaud, G. Casqueiro, A. Lassus, M. Versluis, P. Frinking, *Appl. Phys. Lett.* **2020**, *116*, 173701.
[296] Y. W. Huang, F. A. Shaikh, V. M. Ugaz, *Angew. Chem., Int. Ed.* **2011**, *50*, 3739.
[297] a) U. Farook, E. Stride, M. J. Edirisinghe, R. Moaleji, *Med. Biol. Eng. Comput.* **2007**, *45*, 781; b) U. Farook, H. B. Zhang, M. J. Edirisinghe, E. Stride, N. Saffari, *Med. Eng. Phys.* **2007**, *29*, 749.
[298] S. Yang, F. Guo, B. Kiraly, X. Mao, M. Lu, K. W. Leong, T. J. Huang, *Lab Chip* **2012**, *12*, 2097.
[299] M. H. Lee, V. Prasad, D. Lee, *Langmuir* **2010**, *26*, 2227.
[300] L. L. A. Adams, D. Lee, Y. Mei, D. A. Weitz, A. A. Solovev, *Adv. Mater. Interfaces* **2020**, *7*, 1901583.
[301] F. E. Angilè, K. B. Vargo, C. M. Sehgal, D. A. Hammer, D. Lee, *Langmuir* **2014**, *30*, 12610.
[302] Z. Chen, K. W. Pulsipher, R. Chattaraj, D. A. Hammer, C. M. Sehgal, D. Lee, *Langmuir* **2019**, *35*, 10079.
[303] C. Zhou, C. Gao, Z. Lin, D. Wang, Y. Li, Y. Yuan, B. Zhu, Q. He, *Langmuir* **2020**, *36*, 7039.
[304] A. S. Timin, H. Gao, D. V. Voronin, D. A. Gorin, G. B. Sukhorukov, *Adv. Mater. Interfaces* **2017**, *4*, 1600338.
[305] M. V. Novoselova, D. N. Bratashov, M. Sarimollaoglu, D. A. Nedosekin, W. Harrington, A. Watts, M. Han, B. N. Khlebtsov, E. I. Galanzha, D. A. Gorin, V. P. Zharov, *J. Biophotonics* **2019**, *12*, e201800265.
[306] M. Ahmed, B. Gustafsson, S. Aldi, P. Dusart, G. Egri, L. M. Butler, D. Bone, L. Dähne, U. Hedin, K. Caidahl, *Cell. Mol. Bioeng.* **2019**, *12*, 15.
[307] S. V. German, M. V. Novoselova, D. N. Bratashov, P. A. Demina, V. S. Atkin, D. V. Voronin, B. N. Khlebtsov, B. V. Parakhonskiy, G. B. Sukhorukov, D. A. Gorin, *Sci. Rep.* **2018**, *8*, 17763.
[308] a) M. Lee, E. Y. Lee, D. Lee, B. J. Park, *Soft Matter* **2015**, *11*, 2067; b) S. A. Castleberry, W. Li, D. Deng, S. Mayner, P. T. Hammond, *ACS Nano* **2014**, *8*, 6580; c) Y.-W. Chang, P. He, S. M. Marquez, Z. Cheng, *Biomicrofluidics* **2012**, *6*, 024118; d) J. J. Richardson, D. Teng, M. Björnmalm, S. T. Gunawan, J. Guo, J. Cui, G. V. Franks, F. Caruso, *Langmuir* **2014**, *30*, 10028.
[309] C. Priest, A. Quinn, A. Postma, A. N. Zelikin, J. Ralston, F. Caruso, *Lab Chip* **2008**, *8*, 2182.
[310] C. Kantak, S. Beyer, D. Trau, in *Proc. of the 17th Int. Conf. on Miniaturized Systems for Chemistry and Life Sciences (MicroTAS)*, Chemical and Biological Microsystems Society (CBMS), San Diego, CA **2013**.
[311] S. Matosevic, B. M. Paegel, *Nat. Chem.* **2013**, *5*, 958.
[312] L. Y. a. D. T. S. Zhang, in *Proc. of the 12th Int. Conf. on Miniaturized Systems for Chemistry and Life Sciences (MicroTAS)*, Chemical and Biological Microsystems Society (CBMS), San Diego, CA, USA **2008**.
[313] C. Kantak, L. Yobas, T. Bansal, D. Trau, in *Proc. of the 14th Int. Conf. on Miniaturized Systems for Chemistry and Life Sciences (MicroTAS)*, Chemical and Biological Microsystems Society (CBMS), San Diego, CA, USA **2010**.
[314] R. D. Sochol, R. Ruelos, V. Chang, M. E. Dueck, L. P. Lee, L. Lin, in *Proc. of the 16th Int. Solid-State Sensors, Actuators and Microsystems Conf., Transducers'11*, IEEE, Piscataway, NJ, USA **2011**, pp. 1761–1764, https://doi.org/10.1109/TRANSDUCERS.2011.5969455.
[315] C. Kantak, S. Beyer, L. Yobas, T. Bansal, D. Trau, *Lab Chip* **2011**, *11*, 1030.
[316] M. Björnmalm, A. Roozmand, K. F. Noi, J. Guo, J. Cui, J. J. Richardson, F. Caruso, *Langmuir* **2015**, *31*, 9054.
[317] a) Y. Liu, J. C. Fanguy, J. M. Bledsoe, C. S. Henry, *Anal. Chem.* **2000**, *72*, 5939; b) W.-A. C. Bauer, M. Fischlechner, C. Abell, W. T. S. Huck, *Lab Chip* **2010**, *10*, 1814.
[318] M. A. Borden, M. L. Longo, *Langmuir* **2002**, *18*, 9225.
[319] M. A. Borden, G. Pu, G. J. Runner, M. L. Longo, *Colloids Surf., B* **2004**, *35*, 209.
[320] L. Hoff, P. C. Sontum, J. M. Hovem, *J. Acoust. Soc. Am.* **2000**, *107*, 2272.
[321] S. H. Bloch, M. Wan, P. A. Dayton, K. W. Ferrara, *Appl. Phys. Lett.* **2004**, *84*, 631.
[322] I. Eames, E. Stride, *Philos. Trans. R. Soc., A* **2008**, *366*, 2103.
[323] D. B. Khismatullin, *J. Acoust. Soc.* **2004**, *116*, 1463.
[324] N. A. Hosny, G. Mohamedi, P. Rademeyer, J. Owen, Y. Wu, M.-X. Tang, R. J. Eckersley, E. Stride, M. K. Kuimova, *Proc. Natl. Acad. Sci. USA* **2013**, *110*, 9225.
[325] S. K. Verma, A. Amoah, U. Schellhaas, M. Winterhalter, S. Springer, T. A. Kolesnikova, *Adv. Funct. Mater.* **2016**, *26*, 6015.
[326] T. A. Kolesnikova, G. Kiragosyan, T. H. N. Le, S. Springer, M. Winterhalter, *ACS Appl. Mater. Interfaces* **2017**, *9*, 11506.
[327] a) J. J. Richardson, M. Y. Choy, J. Guo, K. Liang, K. Alt, Y. Ping, J. Cui, L. S. Law, C. E. Hagemeyer, F. Caruso, *Adv. Mater.* **2016**, *28*, 7703; b) S. T. Gunawan, K. Kempe, T. Bonnard, J. Cui, K. Alt, L. S. Law, X. Wang, E. Westein, G. K. Such, K. Peter, C. E. Hagemeyer, F. Caruso, *Adv. Mater.* **2015**, *27*, 5153.
[328] a) S. M. Nimjee, C. P. Rusconi, B. A. Sullenger, *Annu. Rev. Med.* **2005**, *56*, 555; b) A. Z. Wang, O. C. Farokhzad, *J. Nucl. Med.* **2014**, *55*, 353.
[329] E. W. Ng, D. T. Shima, P. Calias, E. T. Cunningham Jr., D. R. Guyer, A. P. Adamis, *Nat. Rev. Drug Discovery* **2006**, *5*, 123.

[330] Y. Sultan, M. C. DeRosa, *Small* **2011**, *7*, 1219.
[331] Y. Sultan, R. Walsh, C. Monreal, M. C. DeRosa, *Biomacromolecules* **2009**, *10*, 1149.
[332] X. Zhang, D. Chabot, Y. Sultan, C. Monreal, M. C. DeRosa, *ACS Appl. Mater. Interfaces* **2013**, *5*, 5500.
[333] W.-C. Liao, C.-H. Lu, R. Hartmann, F. Wang, Y. S. Sohn, W. J. Parak, I. Willner, *ACS Nano* **2015**, *9*, 9078.
[334] T. M. Maul, D. D. Dudgeon, M. T. Beste, D. A. Hammer, J. S. Lazo, F. S. Villanueva, W. R. Wagner, *Biotechnol. Bioeng.* **2010**, *107*, 854.
[335] M. A. Nakatsuka, R. F. Mattrey, S. C. Esener, J. N. Cha, A. P. Goodwin, *Adv. Mater.* **2012**, *24*, 6010.
[336] M. A. Nakatsuka, M. J. Hsu, S. C. Esener, J. N. Cha, A. P. Goodwin, *Adv. Mater.* **2011**, *23*, 4908.
[337] A. Z. Wang, V. Bagalkot, C. C. Vasilliou, F. Gu, F. Alexis, L. Zhang, M. Shaikh, K. Yuet, M. J. Cima, R. Langer, P. W. Kantoff, N. H. Bander, S. Jon, O. C. Farokhzad, *Chem. Med. Chem.* **2008**, *3*, 1311.
[338] Z. Wang, S. Zong, Y. Wang, N. Li, L. Li, J. Lu, Z. Wang, B. Chen, Y. Cui, *Nanoscale* **2018**, *10*, 9053.
[339] a) E. S. Lander, L. M. Linton, B. Birren, C. Nusbaum, M. C. Zody, J. Baldwin, K. Devon, K. Dewar, M. Doyle, W. FitzHugh, R. Funke, D. Gage, K. Harris, A. Heaford, J. Howland, L. Kann, J. Lehoczky, R. LeVine, P. McEwan, K. McKernan, J. Meldrim, J. P. Mesirov, C. Miranda, W. Morris, J. Naylor, C. Raymond, M. Rosetti, R. Santos, A. Sheridan, C. Sougnez, et al., *Nature* **2001**, *409*, 860; b) H. K. Binz, P. Amstutz, A. Kohl, M. T. Stumpp, C. Briand, P. Forrer, M. G. Grütter, A. Plückthun, *Nat. Biotechnol.* **2004**, *22*, 575; c) M. T. Stumpp, H. K. Binz, P. Amstutz, *Drug Discovery Today* **2008**, *13*, 695.
[340] S. Deyev, G. Proshkina, A. Ryabova, F. Tavanti, M. C. Menziani, G. Eidelshtein, G. Avishai, A. Kotlyar, *Bioconjugate Chem.* **2017**, *28*, 2569.
[341] S. Deyev, G. Proshkina, O. Baryshnikova, A. Ryabova, G. Avishai, L. Katrivas, C. Giannini, Y. Levi-Kalisman, A. Kotlyar, *Eur. J. Pharm. Biopharm.* **2018**, *130*, 296.
[342] E. Sokolova, G. Proshkina, O. Kutova, O. Shilova, A. Ryabova, A. Schulga, O. Stremovskiy, T. Zdobnova, I. Balalaeva, S. Deyev, *J. Controlled Release* **2016**, *233*, 48.
[343] E. A. Sokolova, O. N. Shilova, D. V. Kiseleva, A. A. Schulga, I. V. Balalaeva, S. M. Deyev, *Int. J. Mol. Sci.* **2019**, *20*.
[344] V. O. Shipunova, I. V. Zelepukin, O. A. Stremovskiy, M. P. Nikitin, A. Care, A. Sunna, A. V. Zvyagin, S. M. Deyev, *ACS Appl. Mater. Interfaces* **2018**, *10*, 17437.
[345] V. O. Shipunova, P. A. Kotelnikova, U. F. Aghayeva, O. A. Stremovskiy, I. A. Novikov, A. A. Schulga, M. P. Nikitin, S. M. Deyev, *J. Magn. Magn. Mater.* **2019**, *469*, 450.
[346] M. D. G. Köse, F. Kiessling, *Nanomaterials* **2020**, 10.
[347] Å. Barrefelt, M. Saghafian, R. Kuiper, F. Ye, G. Egri, M. Klickermann, T. B. Brismar, P. Aspelin, M. Muhammed, L. Dähne, M. Hassan, *Int. J. Nanomed.* **2013**, *8*, 3241.
[348] S. Wan, G. Egri, L. Oddo, B. Cerroni, L. Dähne, G. Paradossi, A. Salvati, I. Lynch, K. A. Dawson, M. P. Monopoli, *Int. J. Biochem. Cell Biol.* **2016**, *75*, 232.
[349] B. Li, R. Aid-Launais, M. N. Labour, A. Zenych, M. Juenet, C. Choqueux, V. Ollivier, O. Couture, D. Letourneur, C. Chauvierre, *Biomater* **2019**, *194*, 139.
[350] J. M. Warram, A. G. Sorace, M. Mahoney, S. Samuel, B. Harbin, M. Joshi, A. Martin, L. Whitworth, K. Hoyt, K. R. Zinn, *J. Drug Target* **2014**, *22*, 387.
[351] A.-H. Liao, S.-Y. Wu, H.-E. Wang, C.-H. Weng, M.-F. Wu, P.-C. Li, *Ultrasonics* **2013**, *53*, 320.
[352] a) M. Smeenge, F. Tranquart, C. K. Mannaerts, T. M. de Reijke, M. J. van de Vijver, M. P. Laguna, S. Pochon, J. J. M. C. H. de la Rosette, H. Wijkstra, *Invest. Radiol.* **2017**, *52*, 419; b) H. Zhang, E. S. Ingham, M. K. J. Gagnon, L. M. Mahakian, J. Liu, J. L. Foiret, J. K. Willmann, K. W. Ferrara, *Biomaterials* **2017**, *118*, 63.
[353] B. Cerroni, R. Cicconi, L. Oddo, M. Scimeca, R. Bonfiglio, R. Bernardini, G. Palmieri, F. Domenici, E. Bonanno, M. Mattei, G. Paradossi, *Heliyon* **2018**, *4*, e00770.
[354] D. V. Voronin, O. A. Sindeeva, M. A. Kurochkin, O. Mayorova, I. V. Fedosov, O. Semyachkina-Glushkovskaya, D. A. Gorin, V. V. Tuchin, G. B. Sukhorukov, *ACS Appl. Mater. Interfaces* **2017**, *9*, 6885.
[355] G. S. Navolokin NA, A. B. Bucharskaya, O. S. Godage, V. V. Zuev, G. N. Maslyakova, N. A. Pyataev, P. S. Zamyshliaev, M. N. Zharkov, G. S. Terentyuk, D. A. Gorin, G. B. Sukhorukov, *Nanomaterials* **2018**, *8*, 812.
[356] O. Gusliakova, E. N. Atochina-Vasserman, O. Sindeeva, S. Sindeev, S. Pinyaev, N. Pyataev, V. Revin, G. B. Sukhorukov, D. Gorin, A. J. Gow, *Front. Pharmacol.* **2018**, *9*, 559.
[357] M. V. Novoselova, H. M. Loh, D. B. Trushina, A. Ketkar, T. O. Abakumova, T. S. Zatsepin, M. Kakran, A. M. Brzozowska, H. H. Lau, D. A. Gorin, M. N. Antipina, A. I. Brichkina, *ACS Appl. Mater. Interfaces* **2020**, *12*, 5610.
[358] C. Jiang, X. Li, F. Yan, Z. Wang, Q. Jin, F. Cai, M. Qian, X. Liu, L. Zhang, H. Zheng, *Micro Nano Lett.* **2011**, *6*, 417.
[359] H.-T. Liu, H. Wang, W.-B. Wei, H. Liu, L. Jiang, J.-H. Qin, *Small* **2018**, *14*, 1801095.
[360] a) J. B. Nielsen, R. L. Hanson, H. M. Almughamsi, C. Pang, T. R. Fish, A. T. Woolley, *Anal. Chem.* **2020**, *92*, 150; b) Y. Cheng, X. Luo, G. F. Payne, G. W. Rubloff, *J. Mater. Chem.* **2012**, *22*, 7659; c) P. Domachuk, K. Tsioris, F. G. Omenetto, D. L. Kaplan, *Adv. Mater.* **2010**, *22*, 249.
[361] Q. Chi, Z. Wang, F. Tian, J. You, S. Xu, *Micromachines* **2018**, *9*, 537.
[362] B. Esteban-Fernández de Ávila, P. Angsantikul, J. Li, W. Gao, L. Zhang, J. Wang, *Adv. Funct. Mater.* **2018**, *28*, 1705640.
[363] S. Keller, S. P. Teora, G. X. Hu, M. Nijemeisland, D. A. Wilson, *Angew. Chem., Int. Ed.* **2018**, *57*, 9814.
[364] a) Y. Cheng, H. Cheng, C. Jiang, X. Qiu, K. Wang, W. Huan, A. Yuan, J. Wu, Y. Hu, *Nat. Commun.* **2015**, *6*, 8785; b) C. McEwan, J. Owen, E. Stride, C. Fowley, H. Nesbitt, D. Cochrane, C. C. Coussios, M. Borden, N. Nomikou, A. P. McHale, J. F. Callan, *J. Controlled Release* **2015**, *203*, 51.
[365] J. T. Alander, I. Kaartinen, A. Laakso, T. Pätilä, T. Spillmann, V. V. Tuchin, M. Venermo, P. Välisuo, *Int. J. Biomed. Imaging* **2012**, *2012*, 940585.
[366] a) R. Akasov, T. Borodina, E. Zaytseva, A. Sumina, T. Bukreeva, S. Burov, E. Markvicheva, *ACS Appl. Mater. Interfaces* **2015**, *7*, 16581; b) E. P. Mironov, T. N. Borodina, D. G. Yurina, D. B. Trushina, T. V. Bukreeva, *Colloids Surf., B* **2019**, *184*, 110464.

Krishna Kanti Dey received his Ph.D. in nanotechnology from Indian Institute of Technology Guwahati, India. He did his postdoctoral research at The Pennsylvania State University, USA, and currently is working as an assistant professor in physics at the Indian Institute of Technology Gandhinagar, India. His research focuses on the collective and emergent dynamics of active biomolecules and harnessing their cooperative functions for useful applications.

Dmitry Gorin is a professor at the Center of Photonics and Quantum Materials at Skolkovo Institute of Science and Technology (Russian Federation). He received his C.Sc. in 2001 and his D.Sc. degree in physical chemistry in 2011 from Saratov State University (SSU). From 2005 till 2009, he visited Max Planck Institute of Colloids and Interfaces (MPICI). From 2009 till 2010, he worked at the MPICI (Prof. H. Moehwald's group). From 2011 till 2017, he held a professorship at SSU. He was promoter of 11 C.Sc. and 2 D.Sc. theses. His lab's interests are biophysics, biophotonics, and physics of colloids and interfaces.

Alexander A. Solovev holds a full professorship in the Department of Materials Science, Fudan University, Shanghai, P. R. China. He received his Ph.D. (in the group of Prof. Yongfeng Mei and Prof. Oliver Schmidt) from the Institute for Integrative Nanosciences, IFW Dresden, Germany, in 2012. He was a postdoctoral fellow at the University of Toronto (with Prof. Geoffrey Ozin) in 2015. He was a visiting scholar at the John Paulson School of Engineering and Applied Sciences at Harvard University (host Prof. David Weitz) in 2017. His lab's interests include inorganic nanomembranes, nanomachines, theranostics, clean water, air, and energy.

Yongfeng Mei received his B.S. and M.S. degrees in physics from Nanjing University and his Ph.D. in materials physics from City University of Hong Kong. He is a professor in materials physics and chemistry in the Department of Materials Science at Fudan University (China). Before that, he worked as a post-doctoral researcher at the Max Planck Institute for Solid State Research (Germany) and then led a research group at the Leibniz Institute for Solid State and Materials Research Dresden (Germany) as a staff scientist. His research interest focuses on micro/nanorobotics, flexible electronics/optoelectronics and nanophotonics.